Design of an Automatic Voltage Regulator With Limited Plant Information

A Thesis

Presented in Partial Fulfillment of the Requirements for the

Degree of Master of Science

with a

Major in Electrical Engineering

in the

College of Graduate Studies

University of Idaho

by

John Tacke

Major Professor: Dakota Roberson, Ph.D.

Committee Members: Robert Borrelli, Ph.D.; Joseph Law, Ph.D.

Department Administrator: Joseph Law, Ph.D.

December, 2020

Authorization to Submit Thesis

This thesis of John Tacke, submitted for the degree of Master of Science with a Major in Electrical Engineering and titled "Design of an Automatic Voltage Regulator With Limited Plant Information," has been reviewed in final form. Permission, as indicated by the signatures and dates below is now granted to submit final copies for the College of Graduate Studies for approval.

Advisor:	Dakota Roberson, Ph.D.	Date
Committee Members:	Robert Borrelli, Ph.D.	Date
	Joseph Law, Ph.D.	Date
Department Chair:	Joseph Law, Ph.D.	Date

Abstract

Maintaining system voltage is a primary concern for power system stability. Within the excitation system, the voltage is maintained at the set point by a compensator known as the Automatic Voltage Regulator (AVR). One popular compensator design in AVR and other applications is the Proportional Integral Derivative (PID). The PID controller is popular in modern control applications due to its simplicity and robustness. In recent years a large body of research has been conducted on the optimization of PID tuning parameters using heuristic techniques. While PID is popular, the low order limits the performance of this design. In this paper, a PID compensator is used to develop a high-order compensator for an AVR system. The performance of the system with the new compensator is shown to be superior to that of the default system. Compensator performance is tested using a high-fidelity model of a nuclear generating station.

Contents

List of Figures

List of Acronyms

AVR Automatic Voltage Regulator

PID Proportional Integral Derivative

FOPID Fractional Order Proportional Integral Derivative

MBO Modified Bode Optimal

ZN Zeigler-Nichols

SISO Single Input Single Output

PSS Power System Stabilizer

WSC Western Services Corporation

HMI Human Machine Interface

mgp2 MGP2Main Generator and Exciter Control

OEL Over Excitation Limiter

UEL Under Excitation Limiter

PWR Pressurized Water Reactor

BPS Bulk Power System

Chapter 1: Introduction

1.1 Overview

Electrical devices are designed to operate at specified voltage magnitudes and frequencies given by the nameplate rating of the device. Ensuring that the voltage magnitude supplied by synchronous generators remains constant is of critical importance to electrical utilities. This is accomplished through excitation control with a compensator known as the Automatic Voltage Regulator (AVR) [1]. The AVR is part of a feedback control structure that compares the terminal voltage of a generator to a desired reference voltage. The voltage difference or error is then used to vary the generator excitation voltage. Additional signals are included to improve stability characteristics. The exciter voltage determines the exciter current which controls the magnitude of the rotating magnetic field. The terminal voltage is proportional to the time rate of change of the magnetic field flux in the stator windings. For synchronous machines operating at rated speed the magnitude of the induced voltage is determined solely by the magnitude of the field flux. A well designed AVR will act to reduce the voltage error to zero as quickly as possible.

The most basic type of AVR compensator is the proportional controller. The proportional controller is simply a variable amplifier which adjusts the magnitude of the error signal for excitation control. Proportional controllers are favored for the low cost and simplicity. Better performance in regard to speed of response and regulation accuracy can be achieved by implementing more sophisticated compensators.

One type of compensator that has gained popularity over the years is the Proportional Integral Derivative (PID) controller. The PID compensator consists of a proportional gain, an integrator, and a differentiator which act on the error signal. The control signal is the sum of the three signals. The popularity of PID is due largely to the simplicity of the compensator and to the ease with which the system parameters can be developed. The most well-known method for tuning PID controllers is the Zeigler-Nichols (ZN) online tuning method first proposed by the engineers John Ziegler and Nathaniel Nichols in their seminal paper on PID control design [2]. This method has the advantage of being able to develop a stable controller without *a priori* information about system dynamics. Modern research on AVR controllers usually focuses on optimal tuning techniques for the PID gain constants; however, some research has also focused on variations of the traditional PID system model.

In this work, a novel control design technique based on a known PID model is used to develop a high-order compensator to maximize system performance. Using this technique, a PID controller is first

developed, and then the closed-loop system response is used to determine the characteristics of the plant near the crossover frequency. Based on the gain and frequency margins of the plant, pole-zero spacing techniques are applied to develop a fractional-order slope for several octaves near crossover [3]. The fractional-order slope of the modulus plot is related to the phase shift imposed by the compensator and thus frequency stability margin. By creating a fractional-order slope at frequencies near the system crossover frequency, stability can be guaranteed for a wide range of plant parameter variations. Additionally, the introduction of zeros at frequencies well below crossover allows the compensator gain to be maximized over the functional bandwidth. The advantages of this type of high order control system are faster dynamic response, faster settling time, and the elimination of steady-state error when compared with lower-order control systems. Additionally, the maximization of compensator gain over the functional bandwidth provides the system with improved reference tracking and disturbance rejection. A disadvantage of high-performance control systems is a large overshoot due to the aggressive response. This response can also be complicated by the presence of actuator limitations.

1.2 Literature Survey

The Zeigler-Nichols tuning technique is an example of a "classical control" technique where the controller is designed to maintain stability in the event of plant variations so long as the variations remain within a certain range anticipated by the control designer. Classical control techniques often require *a priori* knowledge of plant dynamics to guarantee system stability and to perform advanced loop shaping techniques. Modern control techniques use iterative algorithms and performance functionals to develop optimal gain values for the AVR compensator. Several tuning algorithms and performance functionals have been developed over the past few decades [2-11, 19, 21, 25]. In [4] a PID compensator for an AVR system is tuned using an Artificial Bee Colony algorithm. The parameters for a PID AVR system and a PSS system are tuned simultaneously using a Differential Evolution algorithm in [5]. In [6] a PID compensator for an AVR system is developed using a simplified version of the Particle Swarm Optimization algorithm known as the Multiple Optimizing Liaisons (MOL) algorithm. In [7] a technique is proposed for tuning of PID parameters using a hybrid algorithm between Particle Swarm Optimization (PSO) and Gravitational Search Algorithm (GSA). In [8] a Symbiotic Organism Search (SOS) algorithm is used to tune parameters for a PID controller in an AVR system. In [9] the AVR control problem is presented as an optimization problem for an LQR system where instead of finding a solution to the algebraic Riccati equation directly, an iterative solution using an actor-critic structured algorithm is presented to achieve online tuning without knowledge of the full system dynamics. In [10] a fuzzy logic algorithm is applied to tuning PID compensator gains independently of one another. In [11] a combined AVR-PSS system is

developed by modeling the IDA excitation controller as a port controlled Hamiltonian system and then developing a PID AVR controller with traditional techniques. In [12] a Teaching Learning Based Optimization algorithm is applied to the AVR tuning problem. In [13] A PID controller is developed using the TLBO algorithm and applied to the AVR problem with the inclusion of a first-order low pass filter. A tuning algorithm is proposed in [14] based on Ant Colony Optimization (ACO) with a cost function that includes both frequency and time domain characteristics. A modified PID controller is developed in [15] using PSO where a second-order derivative is added to reduce rise time. In [16] a sine-cosine based (SCB) algorithm is used for finding the optimum tuning parameters in a PID AVR compensator.

In addition to the work done on conventional PID otherwise known as Integer Order PID (IOPID) there has been significant work in the past few decades on Fractional Order (FO) controllers and in particular Fractional Order Proportional Integral Derivative (FOPID) [17–24]. FO controllers are attractive because of their excellent stability characteristics combined with high compensator gains allowing for excellent disturbance rejection. Unfortunately, true FO compensators are physically unrealizable. However, high-order compensators can mimic the properties of FO compensators over frequencies of interest [25]. FOPID controllers introduce two more parameters to be tuned (the fractional orders) over the conventional IOPID system. Due to the added complexity of the fractional-order, FOPID controllers are typically tuned using adaptive control techniques. In [17] a machine learning algorithm (genetic algorithm) is used to determine optimal fractional order and adaptive gains for a Model Reference Adaptive Controller using FOPID. In [18] a FOPID is implemented for an AVR system using both Genetic Algorithm and Ant Colony Optimization algorithms. In [24] a FOPID AVR system is tuned by way of multiple objective extremal optimizations where a set of extremal functions are optimized to tune the controller gains. In [21] a fractional-order compensator is developed using an algorithm called Cuckoo Search (CS) additionally, the authors address the challenge of implementing a fractional-order compensator through high order pole-zero spacing. In [22] a FOPID controller is designed using Chaotic Ant Swarm (CAS) and is implemented using Oustaloupâs technique of pole-zero spacing. A FOPID compensator is developed using NSGA II with multiple objective functions in [19]. The first published application of a FOPID controller for the AVR system was in [23] where the compensator was developed using PSO. A frequency-domain approach is used in [19] to develop an AVR FOPID controller using NSGA-II and multiple objective functions.

A large body of literature produced by industry also exists in regards to the study of excitation control systems. Over time there has developed a number of generally accepted metrics and minimum standards to judge excitation system performance and to guide excitation system design. Of principal concern

are terminal voltage response characteristics. In the time domain rise time, settling time, and overshoot describe the behavior of the excitation system. For high initial response systems (exciter response time less than .1s) large-signal response is completely described by the response time, ceiling voltage, and ceiling current [26]. HIR systems can produce a destabilizing effect for inter-area modes and so are typically operated with the inclusion of a power system stabilizer (PSS). As of Jan 2019, all new generating units built within the WECC are required to include a PSS so there is no reason to avoid HIR designs for AVR systems in the western interconnection [27]. Frequency domain analysis of both the open-loop and closed-loop system response is also of interest. In the open-loop system, gain and phase margins are used to gauge relative stability with recommended values being $> 6dB$ and $> 40°$ for gain and phase margins respectively [1, 26]. For the closed-loop system, the peak value of the system response is of greatest interest. Values larger than 1.6 indicate a low stability margin at the crossover and will result in highly oscillatory step response. Recommended values are from 1.1-1.6 [1, 26].

Most of the literature on AVR designs in the past few decades have used simple excitation system models for testing of AVR designs. The most common model used is the 4 block simplified structure presented in [1]. In this model the excitation control system is modeled as three blocks each consisting of a time constant and a gain in the forward path and a signal gain and time constant in the feedback path. These blocks represent the amplifier, exciter, and generator in the forward path, and the voltage transducer in the feedback path. For the amplifier and the exciter this model is reasonable for small signal analysis. A good voltage transducer will have a very small time constant, several orders of magnitude smaller than those associated with the other system components and will not contribute any appreciable gain to the system. Therefore, for most studies the effect of the voltage transducer can be neglected.

The generator model varies considerably depending on the loading conditions of the system. Many authors use use the more sophisticated generator model presented in [1] for stability surveys. While this more advanced model can provide a more accurate description of the system response it still fails to account for all aspects of a full generating system model. Of particular importance are nonlinearities presented by protective circuitry that apply to specific generating stations but are not described by more general models. For these reasons in this work the general design technique presented by [3] is used to develop an AVR for a specific generating station model described by a simulator for training system operators. The simulation was developed by Western Services Corporation and is a high fidelity model of the Wolf Creek Generating Station, a PWR type nuclear generating station located in Wolf Creek, Kansas. The simulator includes a full implementation of the protective equipment associated with the

generator excitation system, as well as a reduced scale model of the local distribution system. The results in this document were obtained through testing of the compensator designs using the WSC simulator under a variety of operating conditions.

1.3 Performance Criteria

In the study of excitation control systems the definition of performance lacks standardization. The difficulties in standardizing definitions for system performance is due largely to the wide range of generators used in distribution networks. Some generating systems have large inertia and long time constants. This makes these generators very resistant to frequency deviations, however their ability to respond to voltage instabilities is low. Conversely smaller generators can rapidly respond to changing voltage demands, however their smaller inertia means they struggle to respond to frequency disturbances. Renewable generators further complicate the problem as their voltage and frequency profiles are determined by power electronics instead of the principles of synchronous machinery. Combined, these factors lead to different requirements for excitation control systems depending on the generating unit and it's intended application. IEEE standards state explicitly: "The performance indices which are of primary importance depend on the individual application of each feedback control system, and no universally applicable 'best criteria' can be recommended in standards [26]". Due to this lack of standardization, a gap has developed between definitions of performance used in industry versus those used in research literature.

Despite the range of differences in machine specifications there are a number of performance metrics which are generally accepted for excitation control systems. Excitation control systems are described using feedback control theory and more generally linear system theory. Therefore, many of the same performance standards used to describe linear feedback control systems are appropriate for describing the behavior of Excitation Control Systems. In particular, time domain standards such as *rise time, settling time, percent overshoot*, and *steady state error* are referenced extensively in both research literature and industry standards. Additionally, a number of frequency domain performance metrics are referenced. These metrics include *phase margin, gain margin, low frequency gain*, and *functional bandwidth* in the open-loop case, and *crossover frequency* and *regeneration* in the closed loop sensitivity function [26]. Academic research tends to neglect the effects of nonlinearities in excitation system modelling, however industry standards do not. As such, industry specifies different performance metrics for small-signal and large-signal responses

Modern excitation control research is primarily concerned with the optimization of control design using machine learning techniques. Optimality is defined as the control law which minimizes the cost function associated with the specific performance metric of interest [28]. This technique is advantageous in that it provides a method for designing control systems, as well as a method for defining performance. A completed compensator design is one which by definition has the "best performance". Different design philosophies will often have different standards of performance. The different performance standards typically place importance on different signals within the model. Signals of interest are usually the error signal or the control signal. For situations where it is desirable to maximize efficiency it is often sufficient to minimize the control action integrated as a function of time. This metric is used in [19]. When high performance is desired minimizing the integral of the absolute value of the error signal will force the the system to operate at the defined set point by forcing the error to zero. This is method is used in [6, 14, 17, 23, 24]. Including a time dependent term in the integrand will improve dynamic response by penalizing errors more as the simulation time increases. This technique provides good performance while minimizing settling time but at the cost of significant overshoot. This method is used in [6–8, 10, 12, 17, 18]. Many researchers use performance functions which combine two or more performance metrics [8, 12–14, 16, 17, 21–24]. These designs tend to be more well-rounded but at the cost of increased computational effort.

In general, industry standards leave the performance of AVR systems to system manufacturers. Current standards are more concerned with modeling for stability studies than with the performance of individual units. NERC regulations require that generator owners maintain accurate system models to describe the performance of their excitation systems [29] for grid stability surveys. System models are furnished by the equipment manufacturers for new devices [30]. For older systems, the models can be determined through field testing or can be estimated with accepted industry standard models [30, 31]. All excitation system models must be periodically verified, updated, and furnished to the relevant balancing authorities [29, 30]. Recommended practices for model verification are presented in [30]. [1] includes a range of models to describe excitation systems commonly encountered in industrial applications. Many of these models are the same as those presented in IEEE standards [31].

NERC requires that system performance be evaluated during initial unit commissioning and periodically thereafter as part of a regular maintainance schedule [32]. Methods for meeting this standard are given by [30]. The standard guideline for excitation system modeling and performance evaluation is given by [26]. This guide presents standards for evaluating excitation system performance in in the

frequency domain as well as time domain for both large and small signals. Because of the inherent difficulties in online performance testing [26] recommends performing excitation system testing during regular maintenance while the generator is disconnected from the Bulk Power System (BPS). For offline model verification and commissioning tests IEEE recommends injecting voltage errors at either the generator terminals or the reference. To remain within the realm of small signal analysis the magnitude is recomended to be $\leq 2\%$ of nominal [26]. [30] Also recommends using logs of system response data during contingency events to evaluate system performance.

For this project it was decided to use a range of metrics to evaluate the performance of the compensator. Because the compensator design comes from a frequency domain based approach the metrics of most relevance would be the frequency domain metrics of phase margin, gain margin, and low frequency gain. Unfortunately, without a complete frequency domain description of the plant an accurate reporting of these metrics is not possible. The compensator was designed to provide 30° of phase margin and $10dB$ of gain margin, however, parameter variations and plant uncertainties mean that these are only an approximation. The performance functionals of the papers examined as part of the literature review provide a useful metric for iterative design techniques. These numbers have no direct physical meaning however and so are not useful for describing system performance in a practical sense. Therefore it was decided to describe system performance using the time domain metrics of [1] and [26]. These metrics are rise time, settling time, percent overshoot, and steady state error. These metrics are general of feedback control systems and have been used for decades to describe system performance in a meaningful and useful way. To maintain consistency with industry standard testing practices the system performance is tested by the injection of step changes to the voltage reference signal with the system disconnected from the BPS. To ensure robustness of the design the system is tested using the same step changes with the system connected to the BPS and delivering rated power. Finally, to take advantage of the model sophistication and to provide a description of system performance under more realistic contingency events, the system is subjected to a range of disturbances caused by changes in various active and reactive loads represented by the load object connected to the substation bus as in Figure 5.10.

Chapter 2: Excitation Systems

The excitation system of a synchronous generator is the component of the generator system responsible for regulating the flow of reactive power and the terminal voltage. It is comprised of a combination of sensors, transformers, amplifiers, rectifiers, and/or DC generators needed to measure and maintain the voltage of the power system at the terminals of the generator stator or some point beyond. The industry standard definition for a generator excitation system is given by IEEE standard 421.1 [33]. This standard also provides standard definitions for terminology related to excitation systems. The IEEE standard makes a distinction between the excitation system and the excitation control system. The *excitation system* consists of the voltage regulator and the exciter. The excitation control system is the closed loop control system containing the excitation system as well as the synchronous generator and voltage sensing equipment. The excitation control system model as described above is presented in Figure 2.1.

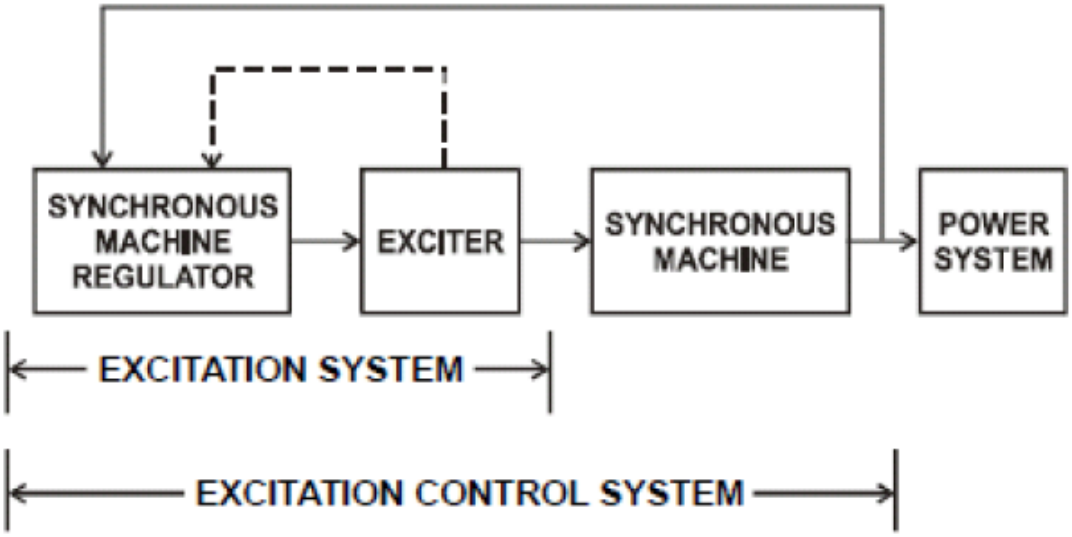

Figure 2.1: Basic structure of excitation control system

In this work, the component of greatest interest is the amplifier, also known as the Voltage Regulator or Automatic Voltage Regulator (AVR). The AVR is an example of a compensator in a feedback control system. Control systems in general will be discussed in more detail in Chapter 3. The voltage at the stator terminals of the generator is measured, typically with a voltage transducer. The voltage sensing equipment converts the high voltage AC signal by reducing and rectifying it to a DC signal suitable for use in signal processing. The DC signal is then compared to a reference signal. The difference between the measured signal and the reference signal is transferred through the Regulator and is known as the

"error" signal. The result is a DC voltage which is amplified and applied to the field windings of the exciter. This in turn increases the magnitude of the DC voltage produced by the exciter which is then applied to the field windings of the synchronous generator.

The system takes this form because of the large difference in the magnitudes of the voltage signals used in the power system and those used in signal processing. Generators produce voltages on the order of tens of thousands of volts while electronics systems deal with magnitudes on the order of several volts. Exciters are typically rated for outputs on the order of a few thousand volts. This is still too large to be fed directly by the signals produced by conventional electronics and so most systems use an additional intermediate amplifier. For older systems this is typically a type of rotating amplifier known as an Amplidyne. In many cases the Amplidyne possesses a variable gain setting. This variable gain acts as the compensator for the system and is used to adjust the excitation system response.

The excitation system has two modes of operation: Manual and Automatic. These modes are also referred to as DC and AC. The Automatic or AC mode of operation is the standard mode of operation. In this mode the Excitation system is controlled in response to the AC voltage of the generator as measured by the voltage transducer. In the Manual or DC mode of operation the voltage transducer is offline and the generator field voltage is controlled directly, irrespective of the generator terminal voltage. This mode of operation is called Manual or DC because the exciter voltage is a DC value and the system operator is "manually" controlling the system voltage by way of direct excitation voltage control. This mode of operation is typically used during startup and shutdown operations or occasionally when sensing equipment detects a potential malfunction of the AVR.

2.1 Background

In the early days of excitation systems, the exciter voltage was manually adjusted by the generator operator. When the systems were initially automated, the response was relatively slow and did little better than taking the role of an alert operator. In the 1920s it was realized that power system stability could be improved through the use of fast-acting regulators. By rapidly modulating the transfer of reactive power into the bulk power system The excitation system assists in damping voltage transient oscillations. As a result, during the middle part of the 20th century there was significant interest in the development of fast-acting voltage regulators. Ultimately the performance of these compensators was limited by the available electronics of the time. By the 1960s, despite the limitations of contemporary electronics, excitation systems had grown quite complex. Excitation systems began to include a number

of additional signals as inputs to the voltage regulator. Among these signals are those produced by supplemental compensators such as the Power System Stabilizer (PSS). They also include limiting signals like those from the generator volts/Hz limiter as well as the under/over excitation limiters.

Newer systems began to include regulators with multiple modes of operation. Typically these systems have settings for start-up, regular operation, and stressed operation. The sophistication of the compensators was still largely restricted by the electronics technology available at the time. During this time, Proportional Integral Derivative (PID) compensators became popular due to their relative simplicity, effectiveness, and ease of tuning. Supplementary control signals became standard in industry models in 1981 and many models were updated to include standard PID compensators in 2005 [31]. In recent years as computing technology has advanced there has been a renewed interest in advanced compensator designs. Due to the pervasive nature of PID systems much of the modern research related to voltage regulators deals with the optimization of PID parameters. Generally this is done by using machine learning techniques to optimize specific frequency or time domain performance metrics. In most of this work the system dynamics are known explicitly, and most often the compensator is the standard three term integer order PID. Most recently there has also been limited interest in developing fractional order compensators, as well as the development of compensators where system dynamics are not well known. [1]

2.2 System Components

Most excitation system models consist of five main system components. These components are: the exciter, the amplifier, the Sensor, the generator, and the regulator. The basic interconnection of these components is described in Figure 2.2. As mentioned above however most excitation systems also include additional components and signals to assist in system stability and equipment protection. This section will describe the most common excitation system components as well as the methods used to model them.

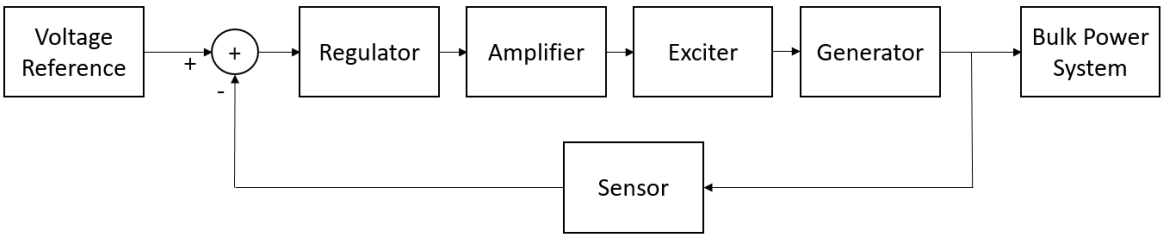

Figure 2.2: Primary components of excitation control system

Central to any excitation system is the exciter itself. IEEE standards define the exciter as the equipment that provides the field current for the excitation of a synchronous machine [33]. This definition is quite broad and can apply to a wide range of devices. IEEE utilizes a number of different models depending on the method of providing field current [31]. Most academic studies on voltage regulators tend to simplify the exciter model considerably [4–6, 8–10, 12–14, 16–24]. These studies assume that the exciter non-linearities and high frequency dynamics are negligible. They instead use a linearized model of the exciter which focuses on the most significant dynamics. This type of simplification is usually justifiable when concerned with grid stability studies. The exciter is therefore modeled with a transfer function of the following form:

$$G_{exciter}(s) = \frac{K_E}{1 + \tau_E s} \tag{2.1}$$

Where K_E and τ_E are the DC gain and the exciter dominant time constant respectively. Typically accepted values for these parameters are $1 \leq K_E \leq 10$ for per unit representations, $10 \leq K_E \leq 400$ for non-pu descriptions, and $0.4 \leq \tau_E \leq 1.0$.

Within the excitation system, the amplifier is the component responsible for controlling the amount of energy supplied to the exciter. The amplifier is not a controller but instead an intermediate component between the output if the AVR and the input to the exciter. Usually it is a rotating or solid state amplifier which converts the output of the regulator into the field current of the exciter. It can also be a rectifier controlled by the output of the regulator which controls the output of the exciter by way of pulse width modulation. In any case academic studies tend to simplify this component in a similar manner as the exciter [4–6, 8–10, 12–14, 16–24]:

$$G_{Amplifier}(s) = \frac{K_A}{1 + \tau_A s} \tag{2.2}$$

Similar to the exciter K_A is the DC gain of the amplifier and τ_A is the dominant time constant. However, unlike the exciter model typical values for K_A and τ_A are: $10 \leq K_A \leq 400$ and $0.02 \leq \tau_A \leq 0.1$. In industry models the amplifier depends on the type of excitation system and is often not identified explicitly. One notable exception to this is the case of systems with DC exciters. Often these systems use of a type of analog rotating amplifier known as an amplidyne. In older systems the system compensator was simply a variable gain setting on the amplidyne. These amplifiers are also represented as a simple gain and time constant, even within the standard IEEE models [31].

The sensor is a generic term which refers to any device can be used to determine the value of some system parameter of interest. The sensor in excitation systems is almost always a voltage transducer.

Older systems occasionally use transformers for sampling the power system voltage. Hence, in literature the terms sensor and transducer are often used interchangeably when referring to excitation systems. Academic surveys tend to only refer to the sensor while industrial standards and textbooks will use both. In traditional controls engineering the sensor refers to the entire system of devices necessary to refer the output value of the system back to the input of the compensator. This includes the voltage transducer/transformer as well as any rectifiers or load compensation. In regards to modelling, academia and industry generally agree that the Sensor can accurately be represented with a single time constant. This is represented by the transfer function below:

$$H_{Sensor}(s) = \frac{K_S}{1 + \tau_S s} \tag{2.3}$$

In general, it is desirable for the sensor to not contribute appreciable dynamics to the system. As such the sensor is designed to be 0dB with as small of a time constant as is practical [34]. Industry models will treat the gain constant K_S as unity [31], while academic papers take a more conservative approach with $0.9 \leq K_S \leq 1.1$. Industry does not describe typical values for τ_S [31]. Most academic studies use $0.001 \leq \tau_S \leq 0.06$. Because the sensor time constant is fast relative to the other time constants in the system many studies disregard the sensor dynamics entirely. IEEE standard 421.5 Agrees that this is justifiable for many systems as long as any dynamics due to load compensation are not neglected [31].

The generator is the system component which converts mechanical energy supplied by the prime mover to electrical energy. The generator is a highly non-linear system and it's response characteristics depend on the loading conditions at any given time. A number of models exist for describing the dynamics of synchronous generators. Kunder provides a number of models which are used in most power system stability studies [1,31]. Rather than specifying standard models for use in simulation, industry standards provide a number of guidelines for the development of models for synchronous generators [35]. NERC provides a a guideline for the development of generator models for use by generator owners to maintain regulatory compliance [30]. Due to the complexity of most generator models academic studies related to excitation systems seek to simplify them. Often they will use a first order approximation similar to that of the other system components. This results in a generator transfer function of the following form:

$$G_{Generator}(s) = \frac{K_G}{1 + \tau_G s} \tag{2.4}$$

The generator parameters will typically range as follows: $0.7 \leq K_G \leq 1$ and $1 \leq \tau_G \leq 2$. In the academic papers the researchers will develop their compensator based on initial generator parameters and then test

the robustness by varying the parameters over the expected range. Some studies use more sophisticated generator models which account for interactions with the power system [5, 17, 23]. With these models or with the models in [1] the generator cannot be described as a simple Single Input Single Output (SISO) transfer function. Rather, the generator is described by a complex series of signals and transfer functions relating to the loading condition of the machine.

The regulator is the component of the system responsible for determining the terminal voltage error and then issuing control signals to the amplifier. IEEE defines the voltage regulator as a synchronous machine regulator that functions to maintain the terminal voltage of a synchronous machine at a predetermined value, or to vary it according to a predetermined plan [31]. The regulator is the component of the system which the control engineer designs to improve the system performance. As such there is no standard model to describe the behavior of the regulator. Older systems typically did not have a sophisticated regulator or at most only had a variable gain, usually as a tap setting on an amplidyne. For such systems the regulator is simply represented by the gain:

$$C(s) = K \tag{2.5}$$

Another popular compensator design which has found wide spread adoption for voltage regulation is the PID architecture. This design is so common that many industry standards have begun to incorporate it into the standard excitation system models [31]. The basic form of the PID transfer function is given below:

$$C(s) = K_P + \frac{K_I}{s} + K_D s \tag{2.6}$$

Much of the modern research into excitation systems has been dedicated to optimization of the gain parameters in the PID architecture [4–10, 12–14, 16]. There has also been a growing interest in the design of alternative compensator architectures. Most popular is the Fractional Order Proportional Integral Derivative (FOPID) [17–24] which has the form:

$$C(s) = K_P + K_I s^{-\lambda} + K_D s^{\mu} \tag{2.7}$$

Other architectures have also been suggested such as the PIDD [15]. A more detailed analysis of the PID design is presented in Chapter 3. This paper uses a novel architecture known as the Modified Bode Optimal (MBO) controller which is described in detail in chapter 4.

2.3 Excitation System Models

Due to the large currents needed to produce the rotor magnetic field in grid scale generation systems, the excitation system requires a dedicated source of power. As a result the system model for any given excitation system depends on the exciter power source. There are three primary methods of supplying this excitation power. DC exciters use a direct current generator to supply excitation current. The magnitude is controlled by varying the field excitation of the DC generator. AC exciters use a combination of an alternator and rectifiers to supply DC excitation current. ST exciters are static excitation systems and do not rely on a rotating machine to provide excitation. This section will provide a brief description of these system models as described by IEEE standards [31].

When the generator is a DC generator the output is fed directly to the main generator field windings and the excitation system is called a direct current commutator exciter. DC exciters are typically older systems developed before the use of solid state amplifiers and rectifiers. Recently some of these systems have been upgraded with PID regulators. A model of one such system from [31] is given in Figure 2.3. The excitation current is controlled by varying the field current of the exciter directly. This current is typically fed directly by the output current of the regulator amplified by an amplidyne.

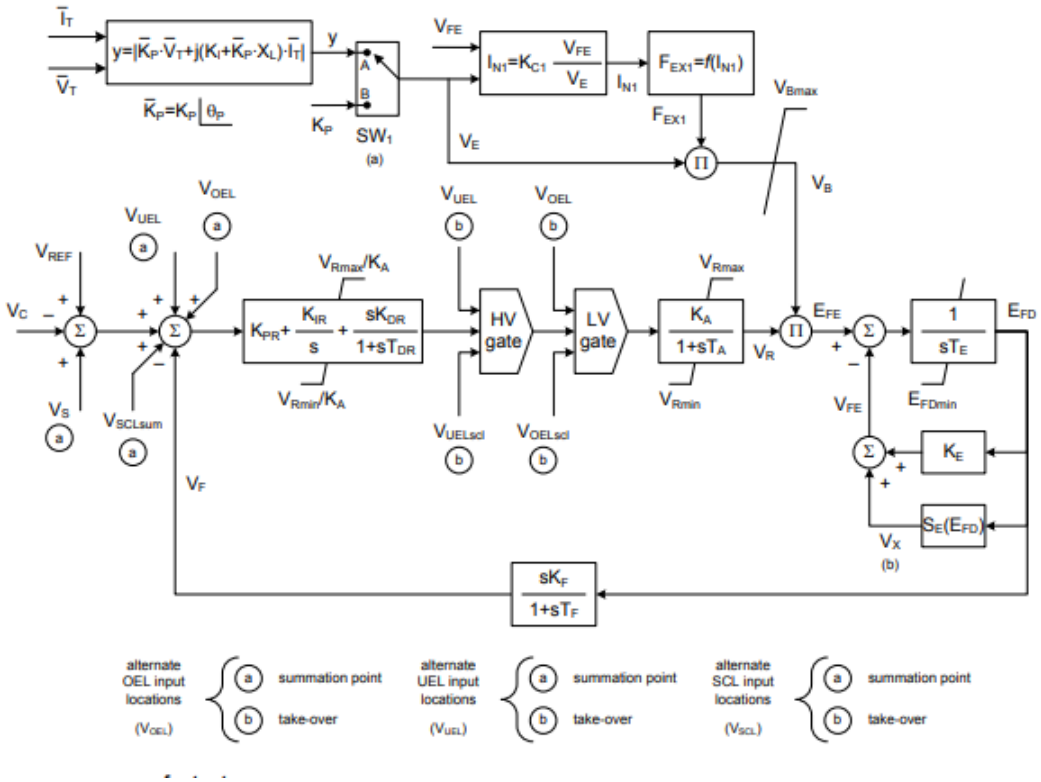

Figure 2.3: Example DC excitation system with PID regulator

Excitation systems which use an AC generator are called “alternator supplied rectifier excitation systems”. These systems have an advantage over DC systems in that the exciter does not require the use of a commutator. In AC systems the exciter output is passed through rectifiers to supply DC current to the generator field windings. These rectifiers can either be non-controlled or controlled. In the non-controlled case excitation voltage is controlled by controlling the the field current of the exciter, similar to the DC systems. with controlled rectifiers the excitation voltage is controlled by controlling the firing of a thyristor bridge. An example of a system where the exciter field power is derived from the output of the exciter is shown in Figure 2.4 [31].

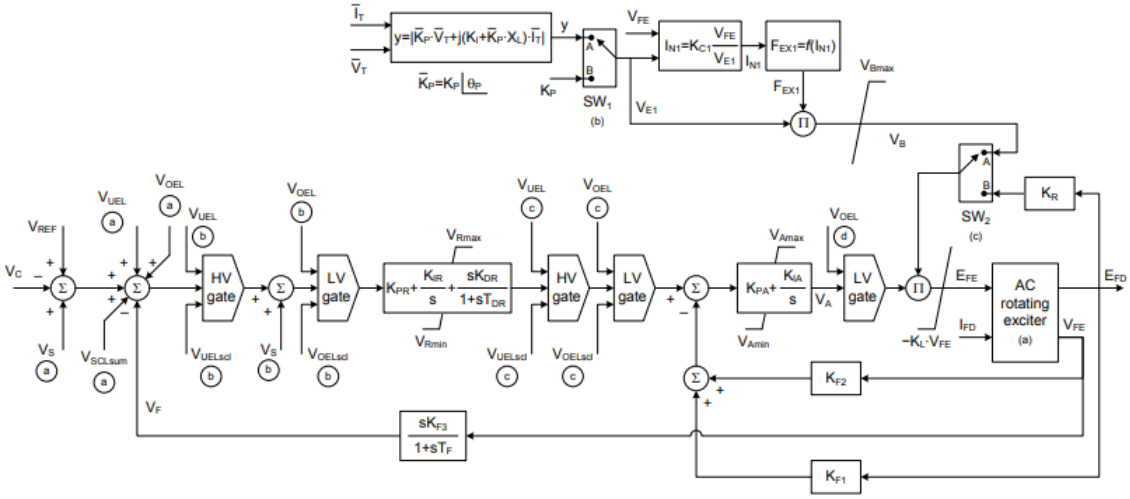

Figure 2.4: Example DC excitation system with PID regulator

Alternatively, the excitation current can be supplied directly by the power system itself. The generator field windings are connected through transformers and rectifiers usually to the generator substation bus. Such systems are called Potential Source or Static excitation systems. These exciters tend to be cheaper and simpler than rotating exciters. When system voltages are suppressed, however, the exciter ceiling voltage is also reduced making these systems more susceptible to voltage instabilities. An example of one such system employing a PI AVR is given in Figure 2.5 [31]. A PI controller is a special type of PID where the derivative gain is zero (i.e. there is no derivative action).

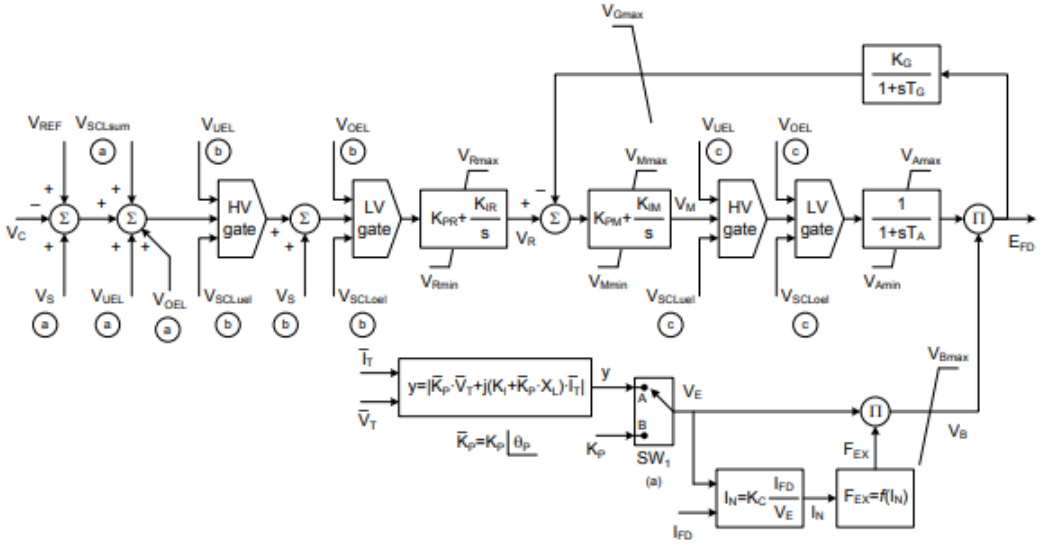

Figure 2.5: ST type excitation system

2.4 Protective Systems and Non-Linearities

The purpose of the generator excitation system is to maintain generator terminal voltage within the continuous capability of the generator and to respond to transient disturbances with field forcing consistent with the generator instantaneous and short-term capabilities [26]. Of primary concern is generator and exciter thermal limits during over-excitation events. The short term over-excitation thermal capacity and duration vary between generators but typical tolerances for over-excitation range from 15 to 60 seconds [1]. According to [32] excitation currents in the range of 140%-200% of rated current must be tolerated for at least 1 second and as much as 10 seconds while terminal voltage fluctuates above and below the AVR set point during fault clearing events. The greater the field forcing capability of the excitation system the more rapidly it can respond to voltage instabilities.

However, there are physical limitations to the excitation system equipment. Allowing the excitation system to operate outside of the nominal operating range for extended periods of time will result in mechanical failure of system components. As a result, a number of protective systems were developed for excitation systems. The additional components either modify the error signal to limit system action as in the case of the volts/hz limiter and PSS, or directly limit the value of the exciter current as in the case of the over/under excitation limiters. During regular operation, these systems do not operate and the systems behaves consistent with the models in the first part of this chapter. However, when these protective systems are active they alter the response of the system. As such, it is necessary to describe them here so that their potential effects on excitation system performance can be understood.

The purpose of the Volts/hertz limiter is is to protect the generator from damage which can occur as a result of excessive magnetizing flux [1]. Excessive flux results in overheating due to iron losses in the magnetic core if sustained. The flux within the core is not directly measurable, however it is proportional to the voltage and speed of rotation. These parameters are readily measurable and the ratio of their per unit values is knows ans the volts per hertz (V/Hz). This device injects an additional signal to the exciter when the ratio falls outside of a preset range.

The purpose of the PSS is to aid frequency stability in the Bulk Power System (BPS). This device modulates the output of the exciter to provide a signal in phase with rotor speed deviations. The goal of the PSS is to provide additional damping for power system oscillations which can arise as a result of stressed operation and may lead to destabilization of the BPS. Such events are known as small-signal instability events. These events are rare but can be incredibly disruptive. NERC standards now require

that all new generating stations operating in the western interconnection be equipped with a PSS [27]. The PSS provides an additional signal to the exciter which depends on various measured parameters from the BPS. Typically these signals are power, frequency, and shaft speed, although other signals may be used as well. For short duration events typically of interest to voltage stability, the system frequency is regarded as constant and the PSS does not contribute to the behavior of the excitation control system. PSS controllers are the subject of significant research in power systems and a full analysis of them is beyond the scope of this work.

The under/over excitation limiters are limiting circuits designed to protect the generator from damage which may result from operation with power factor outside of the nominal range of the generator. The under excitation limiter protects the generator from exceeding the stator core end-region heating limit. During under excitation the output of the limiter takes over from the output of the AVR and provides a constant level of excitation. The over excitation limiter protects the generator from excessive heating as a result of large excitation currents in the field windings. In most modelling applications both systems are can be described as gate limits acting on the output of either the exciter or the AVR

Chapter 3: Frequency-Domain Control

Controls engineering traces its origins to the early days of the industrial revolution. The first known application of feedback systems were in ancient greek float regulating devices [34]. The first patented feedback control structure was that of a self actuating valve for regulating the shaft speed of a steam engine [34]. The discipline became formalized in the late 19th and early 20th century when linear system theory was first applied to describe feedback structures. The resulting system behavior is described by differential equations. Before the age of digital computers it was difficult to solve differential equations for large systems or systems with significant nonlinearities. Therefore integral transforms were used to convert systems of differential equations into algebraic systems. The response of a system to a disturbance of at a given frequency can be found by evaluating the Laplace transform of the transfer function using the substitution $s = j\omega$ where s is the Laplace variable. Therefore, he complete response of a dynamical system can be determined by evaluating the transfer function over the range of frequencies of interest. The plot of the magnitude and phase of the complex function is the Bode plot of the system.

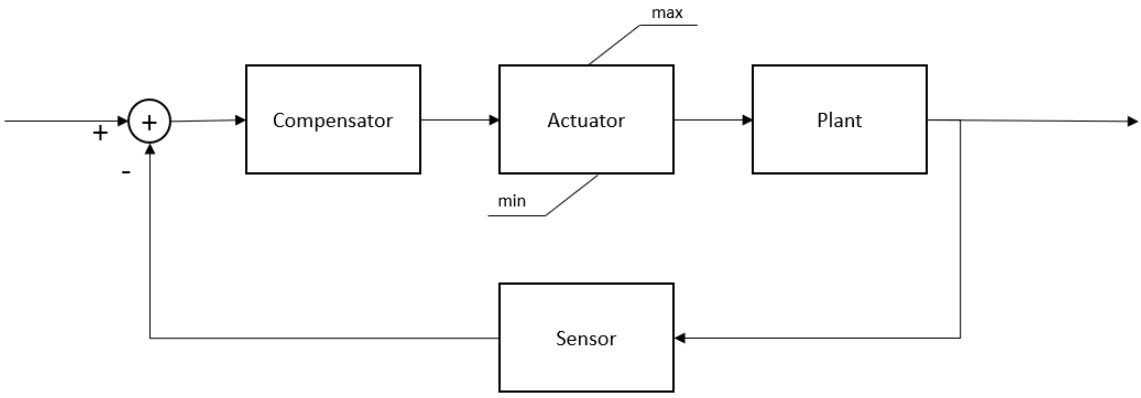

Figure 3.1: Basic feedback diagram

A typical feedback control system consists of four main components. The components are: the *plant*, the *actuator*, the *sensor*, and the *compensator*. A diagram of this basic structure is given in Figure 3.1. The *plant* describes the process being controlled and the name is a reference to the origins of control engineering in process control. The *actuator* is the controllable component of the system and often imposes limitations on the system performance. The *sensor* is the component of the system which measures the output to be compared to the reference signal. For well designed control systems the sensor does not contribute significantly to system dynamics and can be regarded as unity. For some systems the sensor dynamics are not negligible and must be accounted for to develop an accurate model. The

last component is the *compensator* which is also known as the *controller*. The *compensator* modifies the error signal to produce the control signal which is used to control the actuator.

3.1 Feedback

Consider the case where the sensor is disabled. In this instance there is no contribution to the error signal from the feedback path and the error signal is simply the command signal, This configuration is known as *open-loop*. When the system is in open-loop, the response of the system $Y(s)$ to an input $X(s)$ is given by the equation:

$$Y(s) = X(s)C(s)P(s) \tag{3.1}$$

where $C(s)$ and $P(s)$ are the transfer functions of the compensator and plant respectively. The ratio of functions:

$$\frac{Y(s)}{X(s)} = C(s)P(s) = T(s) \tag{3.2}$$

is the transfer function describing the response of the system in open loop and is also known as the *loop transmission function* or the *return ratio*. When a feedback path is added the output of the system is no longer a simple function of the input function $X(s)$ but is instead a function of the error signal:

$$Y(s) = e(s)C(s)P(s) \tag{3.3}$$

where:

$$e(s) = X(s) - H(s)Y(s) \tag{3.4}$$

The function $H(s)$ represents the dynamics of the sensor. Combining equations (3.3) and (3.4):

$$Y(s) = (X(s) - H(s)Y(s))C(s)P(s) \tag{3.5}$$

$$Y(s) = X(s)C(s)P(s) - H(s)Y(s)C(s)P(s) \tag{3.6}$$

$$Y(s)(1 + H(s)C(s)P(s)) = X(s)C(s)P(s) \tag{3.7}$$

$$\frac{Y(s)}{X(s)} = \frac{C(s)P(s)}{1 + H(s)C(s)P(s)} \tag{3.8}$$

This is the *closed loop transfer function*. The denominator of this transfer function is known as the *return difference*. The magnitude of the return difference is the *feedback* of the system. For most practical systems the sensor contributes no appreciable dynamics over the frequencies of interest. Thus, the return

difference can be approximated as:

$$F(s) = 1 + T(s) = 1 + C(s)P(s) \tag{3.9}$$

There are three different kinds of feedback described by the properties of the function $T(s)$. The range of frequencies for which $|T(s)| >> 1$ defines the region of *negative feedback*. In this region the response of the system to the reference signal is approximately unity and the response to disturbances and sensor noise is very small. *Negligible feedback* is defined by the range of frequencies where $|T(s)| << 1$. In this range the denominator of the closed loop transfer function is approximately 1. As such, the equation reduces to:

$$\frac{Y(s)}{X(s)} \approx C(s)P(s) \tag{3.10}$$

Which is the open-loop transfer function. The presence of the feedback path makes no appreciable contribution to the system response, hence why the feedback is called negligible. The range of frequencies where $T(s) \approx 1$ define the *positive feedback* of the system. In this region the phase of the loop transmission is of crucial importance. As the phase approaches 180°the feedback approaches zero and the response of the system over these frequencies becomes unbounded. Even in the best case where the phase is 0, the transfer function reduces to:

$$\frac{Y(s)}{X(s)} = \frac{1}{2} \tag{3.11}$$

In this region the response to disturbances is amplified. In other words, the sensitivity function is positive in this region, hence the term positive feedback.

The positive feedback range corresponds to the band of frequencies near the $0dB$ crossover region of the Bode plot of the open-loop transfer function. Because the phase of the system in this region is so important frequency domain performance is often described in terms of the phase and gain margins of the system. The phase margin of the system describes how far away from -180°the phase of the system is at the crossover frequency of the system. The gain margin describes how far the modulus of the system is from 0dB when the phase is -180°. because each pole in the system contributes a maximum of -90°of phase the gain margin is only applicable to systems of second order or greater.

3.2 Bode Phase-Gain relationship

For minimum phase systems the phase of the transfer function at any given frequency is related to the slope of the modulus at all frequencies. This relationship is known as the Bode phase-gain relationship

and is derived in [25]. The relationship itself is stated explicitly in Equation 3.12.

$$\phi(\omega_0) = \frac{1}{\pi}\int_{-\infty}^{\infty} \frac{dG}{du} ln\left(coth\frac{|u|}{2}\right) du \tag{3.12}$$

Because the core principle behind the Modified Bode Optimal (MBO) loop shape is based in this relationship it is worth taking the time to develop it here. In Equation 3.12 $\phi(\omega_0)$ is the phase of the system at the frequency ω_0. G is the modulus of the frequency response of the system and is a function of ω. u is a parameter which describes the logarithmic relationship between the frequency of interest ω_0 and all other frequencies. This relation is given by:

$$u = ln\left(\frac{\omega}{\omega_0}\right) \tag{3.13}$$

Consider a system with a constant slope of $-20\frac{dB}{dec}$ such as that of a system consisting of a single origin pole. $\frac{dG}{du} = -\frac{log(10)}{log(10)} = -1$ And therefore equation (3.12) can be expressed as:

$$\phi(\omega_0) = -\frac{1}{\pi}\int_{-\infty}^{\infty} ln\left(coth\frac{|u|}{2}\right) du \tag{3.14}$$

$$\int_{-\infty}^{\infty} ln\left(coth\frac{|u|}{2}\right) du \approx 4.93 \tag{3.15}$$

and therefore:

$$\phi(\omega_0) \approx -\frac{4.93}{\pi} = -1.57 \approx -\frac{\pi}{2} \tag{3.16}$$

Thus it can be seen that a single pole contributes $-\frac{\pi}{2}$ radians or -90° of phase beyond the pole frequency. For two poles the slope is $-40\frac{dB}{dec}$ which leads to the phase being equal to $-\pi$ or -180°. Therefore the phase can be approximated as $-90n^\circ$ where n is the number of poles minus the number of zeros preceding the frequency of interest.

To assess the phase at frequencies below the pole frequency it should be noted that according to equation (3.12) the phase at any frequency is related to the slope of the modulus plot at all frequencies. For a single pole the slope is $0\frac{dB}{dec}$ for frequencies below the pole frequency and $-20\frac{dB}{dec}$ beginning at the pole frequency. Again $\frac{dG}{du} = -\frac{log(10)}{log(10)} = -1$ for frequencies beyond the pole frequency. The slope of the modulus is not constant but rather varies as a function of the frequency. By using a straight line approximation the variation can be neglected and the integration can be done in 2 parts. Equation (3.12)

then becomes:

$$\phi(\omega_0) = \frac{1}{\pi}\int_{-\infty}^{ln(\frac{\omega_p}{\omega_0})}(0)ln\left(coth\frac{|u|}{2}\right)du + \frac{1}{\pi}\int_{ln(\frac{\omega_p}{\omega_0})}^{\infty}(-1)ln\left(coth\frac{|u|}{2}\right)du \tag{3.17}$$

Where ω_p is the frequency of the pole. Obviously, the first integral goes to zero and all that remains is the second integral. Taking advantage of the identity:

$$ln\left(coth\left(\frac{|u|}{2}\right)\right) = ln\left|\frac{1+\frac{\omega_0}{\omega}}{1-\frac{\omega_0}{\omega}}\right| \tag{3.18}$$

Equation (3.17) becomes:

$$\phi(\omega_0) = -\frac{1}{\pi}\int_{ln(\frac{\omega_p}{\omega_0})}^{\infty} ln\left|\frac{1+\frac{\omega_0}{\omega}}{1-\frac{\omega_0}{\omega}}\right|du \tag{3.19}$$

Noting that: $u = ln\left(\frac{\omega}{\omega_0}\right) = ln(\omega) - ln(\omega_0)$ leads to: $du = \frac{d\omega}{\omega}$ and therefore the integral becomes:

$$\phi(\omega_0) = -\frac{1}{\pi}\int_{\omega_p}^{\infty} ln\left|\frac{1+\frac{\omega_0}{\omega}}{1-\frac{\omega_0}{\omega}}\right|\frac{d\omega}{\omega} \tag{3.20}$$

$$\phi(\omega_0) = -\frac{1}{\pi}\int_{\omega_p}^{\infty}\left(ln\left|1+\frac{\omega_0}{\omega}\right| - ln\left|1-\frac{\omega_0}{\omega}\right|\right)\frac{d\omega}{\omega} \tag{3.21}$$

For frequencies well below the pole frequency ($\omega_0 << \omega_z$):

$$\left(ln\left|1+\frac{\omega_0}{\omega}\right| - ln\left|1-\frac{\omega_0}{\omega}\right|\right) \approx \left|\frac{2\omega_0}{\omega}\right| \tag{3.22}$$

Because we are only concerned with positive frequencies the integral becomes:

$$\phi(\omega_0) = -\frac{2\omega_0}{\pi}\int_{\omega_p}^{\infty}\frac{1}{\omega^2}d\omega = -\frac{2}{\pi}\frac{\omega_0}{\omega_z} \tag{3.23}$$

For multiple poles the slope is an integer multiple n of $-20\frac{dB}{dec}$ at high frequencies. The phase below the lowest frequency is therefore:

$$\phi(\omega_0) = -\frac{2n\omega_0}{\pi}\int_{\omega_p}^{\infty}\frac{1}{\omega^2}d\omega = -\frac{2n}{\pi}\frac{\omega_0}{\omega_z} \tag{3.24}$$

Through a similar development the phase contribution from poles is found to differ only in sign.

3.3 High Order Loop Shaping/Bode Optimal Loop Shape

Consider a system with a given functional bandwidth ω_1 and crossover frequency ω_2. For a first order system the slope of the modulus plot is $-20\frac{dB}{dec}$ after the functional bandwidth. This means the feedback applied over the functional bandwidth depends on the logarithmic spacing between the functional bandwidth and crossover frequency. For the case where the functional bandwidth and crossover frequency are separated by k decades ($\omega_2 = 10^k\omega_1$) the amount of feedback applied is $20k$ dB. By the Bode phase-gain relationship it is seen that the phase resulting from this slope at the crossover frequency is $-90°$. This results in a phase margin of $-(-180° - (-90°)) = 90°$. This is well above the Bode minimum of $30°$. While the system is stable it sacrifices potential performance.

Now consider a second order system with the same bandwidth and crossover. The slope at crossover is $-40\frac{dB}{dec}$. The maximum feedback which can be applied over the functional bandwidth is $40k$ dB, an additional factor of 10 per decade over the first order system. However, according to the Bode phase-gain relationship the phase of this system at crossover approaches $-180°$. This means that the phase margin of the system approaches 0. The positive feedback in the system is therefore clustered at the crossover frequency and the regeneration is excessive. Disturbances near this frequency are amplified and the compensator design is rendered useless.

From the above discussion it is clear that an ideal system would be a compromise between the stability of the first order system and the performance of the second order system. Consider the complex function given by [25]:

$$T_{des} = e^{log(A_0)+\frac{5}{3}log\theta(jf)} \tag{3.25}$$

with:

$$\theta(jf) = \frac{1}{\sqrt{1-f^2}+jf} \tag{3.26}$$

The modulus of this function has a flat response to the functional bandwidth. Afterwards it transitions to a constant slope of $-10\frac{dB}{oct}$ at all higher frequencies. The shape of the modulus of this function is given by Figure 3.2. By the Bode phase-gain relationship the phase caused by this modulus slope is $-150°$. This in turn leads to a phase margin of $30°$ for all frequencies beyond the functional break. This characteristic can be seen from the plot of the phase in Figure 3.3.

This loop shape demonstrates *ideal* phase characteristics for all possible crossover frequencies, however unfortunately such a function is physically unrealizable as it would be complex valued in the time-domain.

Transfer functions of real systems consist of either purely real poles and zeros or complex pole/zero pairs. Consider again the phase delay contributed by real poles. The phase is given by $-90n^\circ$ where n is the number of poles providing phase contribution. This is the relative degree of the transfer function. The relative degree of the transfer function required to realize the Bode optimal slope can be found by:

$$-150^\circ = -90n^\circ \tag{3.27}$$

$$n = \frac{5}{3} \tag{3.28}$$

Which implies a transfer function of the form:

$$\frac{Y(s)}{X(s)} = s^{-\frac{5}{3}} \tag{3.29}$$

From the derivative property of Laplace transformations it can be seen that this function describes a fractional order derivative operation somewhere between that of a first and second derivative. Such fractional order derivatives are a subject of much study and many different techniques exist for describing and approximating them. A number of approximations suitable for implementing such functions in practical applications are found in literature [3, 17–24]. The MBO compensator used in this project employs such a fractional order slope. The method used for approximating the slope is explained in detail in Chapter 6.

3.4 Proportional Integral Derivative Control

While Proportional Integral Derivative (PID) compensators are not inherently high-performance they are quite prevalent within modern excitation systems. Their relevance to the tuning technique used in [3] make necessary a more detailed analysis of this compensator design. As the name suggests the PID compensator consists of three terms. The general form of this compensator in the frequency domain is given by:

$$C_{PID}(s) = K_P + \frac{K_I}{s} + sK_D \tag{3.30}$$

To better understand the behavior of the PID compensator the PID transfer function is often rewritten in the following form:

$$C_{PID}(s) = K_D \frac{s^2 + \frac{K_P}{K_D}s + \frac{K_I}{K_D}}{s} \tag{3.31}$$

Rewritting the numerator:

$$s^2 + \frac{K_P}{K_D}s + \frac{K_I}{K_D} = s^2 + 2\zeta f_0 s + f_0^2 \tag{3.32}$$

where f_0 and ζ are the natural frequency and damping ratio respectively yields:

$$f_0 = \sqrt{\frac{K_I}{K_D}} \tag{3.33}$$

$$\zeta = \frac{K_P}{2\sqrt{K_I K_D}} \tag{3.34}$$

In this form it is readily seen that the PID structure consists of two finite zeros and an origin pole or integrator. From the Bode phase-gain relationship this means that the phase of this compensator is $-90°$ for low frequencies, and $+90°$ for high frequencies.

This compensator design was first introduced by the engineers John G. Zeigler and Nathaniel B. Nichols in 1942 [2]. Their work was an attempt to formalize the various types of analog compensators being implemented in control systems at the time as well as to propose a standardized method for tuning control systems to achieve optimal performance. The method they proposed has since become known as the Zeigler-Nichols (ZN) online tuning technique and is one of the best known methods for developing compensators without an in depth system identification study. In the ZN technique the control loop is first closed with a variable gain proportional controller. The gain of the controller is increased until a sustained oscillation is observed in the system output. This gain is recorded as well as the period of the resulting oscillation. These numbers are the critical gain and critical period of the closed loop oscillation and are denoted by K_u and t_u respectively. The numbers are then used to calculate the PID compensator gains. There have been many variations however, one of the most common sets of equations is given by the following:

$$K_P = 0.6K_u \tag{3.35}$$

$$K_I = 1.2\frac{K_u}{t_u} \tag{3.36}$$

$$K_D = 0.6\frac{K_u t_u}{8} \tag{3.37}$$

Due to the simplicity of this tuning method PID controllers are popular in many industrial applications. This design is so pervasive it has even become incorporated in many standard excitation system models [31]. It comes as no surprise then that much of the modern research into Automatic Voltage Regulator (AVR) design centers around the optimization of PID gains. The MBO design technique is also built upon the PID however, instead of optimizing the PID gains, the MBO compensator is a different compensator architecture entirely. A full discussion of the MBO compensator is given in Chapter 4.

A significant portion of literature dedicated to AVR research focuses on the development of something called a Fractional Order Proportional Integral Derivative (FOPID) controller [3, 17–24]. It is in this literature that much of the discussion about fractional order calculus and the approximation of fractional order slopes can be found. This is because the general form of the FOPID transfer function is given by the following:

$$C_{PID}(s) = K_P + K_I s^{-\lambda} + K_D s^{\mu} \tag{3.38}$$

where λ and μ are non-integer real numbers. In this case the fractional orders in the transfer function are treated as additional tunable parameters and are optimized along with the gains to achieve the desired results. From the discussion above of the Bode phase-gain relationship it can be inferred that this compensator architecture improves performance by altering the phase characteristics of the closed loop system near crossover by manipulating the slope to be fractional. while this additional flexibility represents a significant improvement over conventional PID tuning algorithms it still does not present enough flexibility in design to achieve the level of performance offered by high order loop shaping techniques.

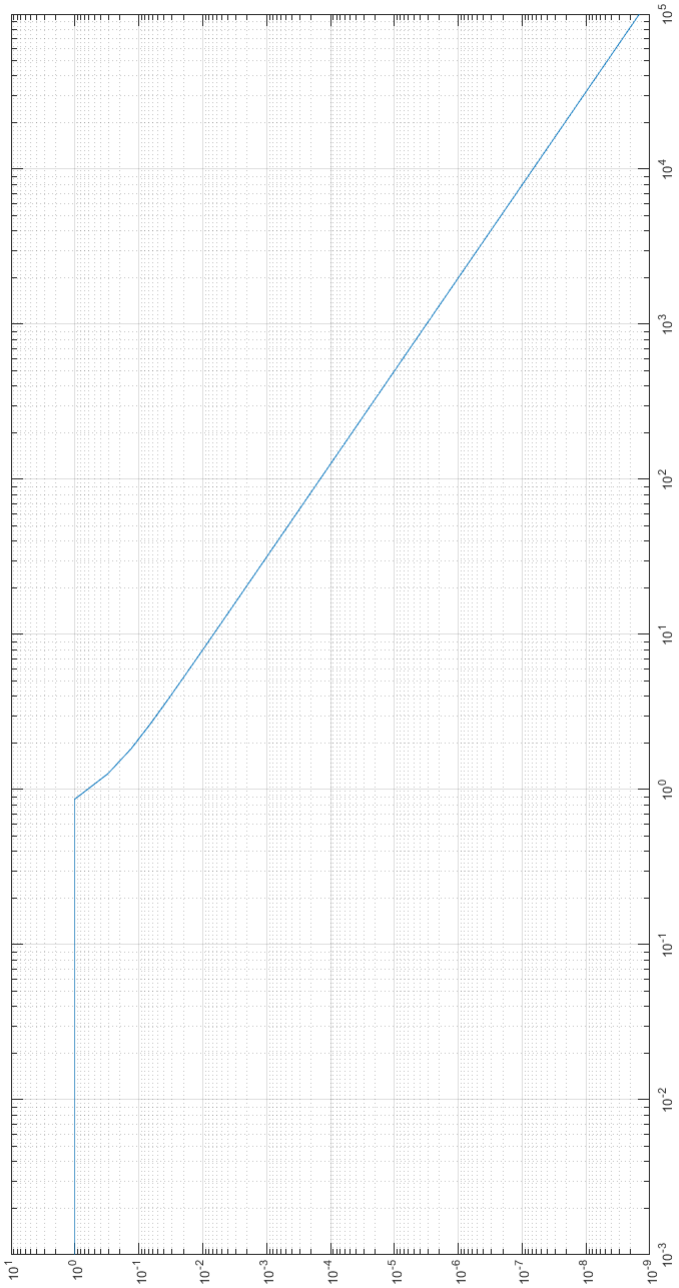

Figure 3.2: Bode optimal loop shape

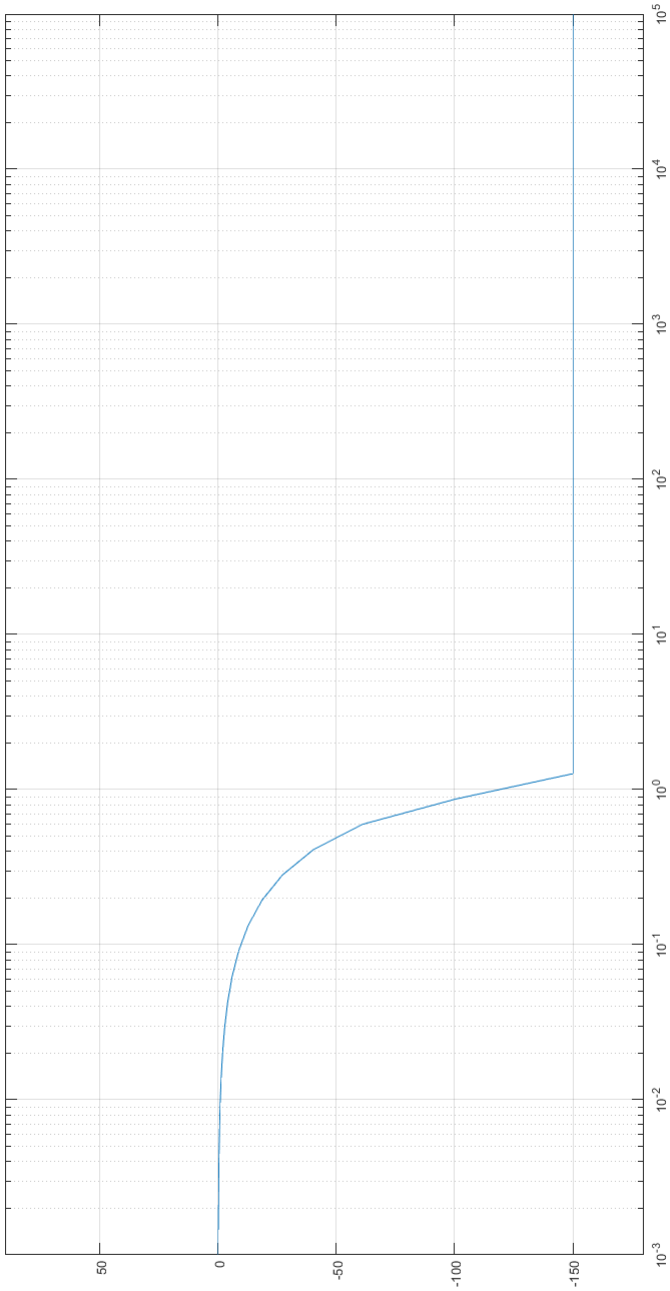

Figure 3.3: Phase plot of Bode optimal loop shape

Chapter 4: The Modified Bode Optimal Controller

The Modified Bode Optimal (MBO) is a controller design first presented in [3] by Robert L. Cloud and John F. O'brien. This compensator architecture achieves good performance through the optimization of frequency domain performance metrics. The performance measures in question are the crossover frequency, the functional bandwidth, the phase margin, gain margin, and low-frequency gain. The MBO compensator attempts to optimize these parameters through frequency domain techniques of loop shaping. Unlike conventional loop shaping techniques, the Cloud technique does not require detailed plant information.

The MBO synthesis technique draws inspiration from the Zeigler-Nichols (ZN) online tuning technique. In the ZN technique a higher order compensator is developed for an unidentified system by using a simpler compensator to determine plant information at a specific frequency of interest. The technique is to close the control loop with a variable gain proportional compensator and to increase the proportional gain until a sustained oscillation is observed. The presence of the sustained oscillation indicates that the phase of the system at this frequency is -180°and the gain is 0dB. The period of the oscillation is the inverse of the frequency. These values are then used in a series of equations to determine heuristically the gains for the Proportional, Integral, and Derivative blocks of the Proportional Integral Derivative (PID) compensator. In the MBO compensator the closed loop system response with a tuned PID compensator is used to determine frequency and damping for the placement of poles and zeros within a high order transfer function. The s-plane transfer function of the MBO compensator is given in Equation 4.1.

$$C_{MBO}(s) = K\frac{z_{s1}(s)z_{s2}(s)c_Z(s)c_{bsd}(s)}{c_0(s)c_p(s)c_{bsc}(s)} \tag{4.1}$$

The tuning algorithm presented by Cloud uses classical control theory and frequency domain design techniques as well as plant information inferred from the PID tuning process to populate the polynomials of the MBO compensator. An example of a system with an MBO loop shape is shown in Figure 4.1 The MBO loop shape consists of five regions. these regions are: the functional bandwidth, the low frequency high order roll-off, the Bode optimal slope, the Bode step, and the high frequency high order roll-off. The functional bandwidth is the frequency to which the magnitude of the modulus plot maintains a constant value. This magnitude is the low frequency gain and is one of the metrics of performance in frequency domain control. For many systems the functional bandwidth will be given as a design specification.

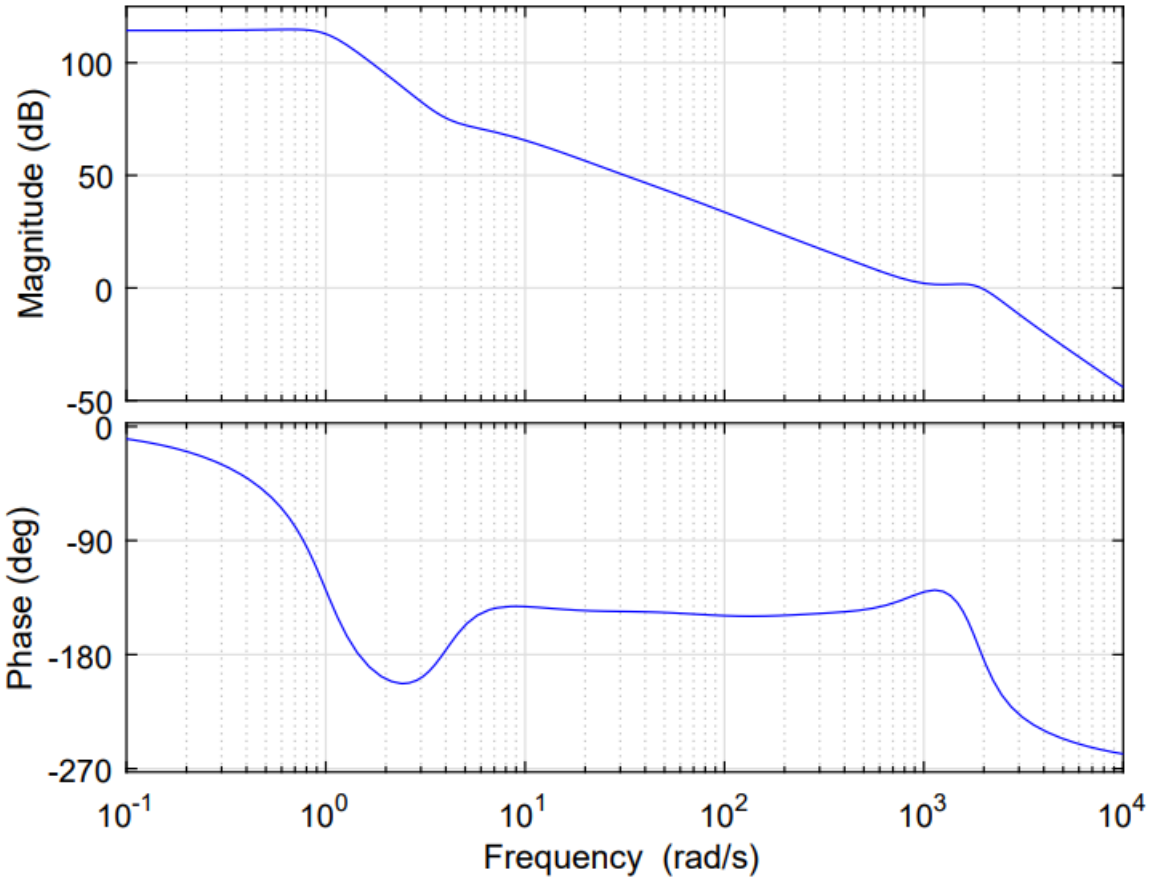

Figure 4.1: Example system with Modified Bode Optimal loop shape

Alternatively the functional bandwidth is determined by a desired low frequency gain and crossover frequency.

4.1 Compensator Development

The low frequency high order roll-off region is determined by the polynomial $c_0(s)$ in the denominator of the compensator transfer function. This polynomial is third order and consists of a pole at the break frequency ω_0 as well as a pair of partially damped poles at this same frequency. This results in a polynomial of the form:

$$c_0(s) = (s + \omega_0)(s^2 + 2\zeta_0\omega_0 s + \omega_0^2) \tag{4.2}$$

The damping of the complex poles is chosen to be between 0.4 and 0.6 so as to maintain a flat modulus to the break frequency while still providing a rapid phase advance. The purpose of this polynomial is to

maximize the low frequency gain by applying an aggressive slope at frequencies low enough that phase characteristics can be largely neglected. It is the inclusion of this portion of the compensator design which makes the compensator a *modified* Bode Optimal controller as opposed to standard Bode optimal controller.

The next polynomial is the numerator polynomial $z_{s1}(s)$. This polynomial is comprised of a pair of zeros at the frequency $\omega_{s1} > \omega_0$. This polynomial is of the form:

$$z_{s1}(s) = s^2 + 2\zeta_{s1}\omega_{s1}s + \omega_{s1}^2 \tag{4.3}$$

The choice of frequency ω_{s1} is dictated by the Bode optimal region of the system. For systems where the bandwidth is not predefined [3] recommends choosing $\omega_0 = \frac{1}{4}\omega_{s1}$.The purpose of this polynomial is to provide phase advance compensating for the delay of the poles at the break frequency. This reduces the slope of the modulus plot from third order to first order and marks the transition from the low frequency high order region to the Bode optimal region.

The Bode optimal region is defined by the polynomials $c_z(s)$ and $c_p(s)$ in the numerator and denominator, respectively. This region is the portion of the loop transmission where loop shaping is applied to obtain optimum frequency domain performance. Consider again the loop transmission given in Figure 3.2. As was explained in Chapter 3, this shape can be regarded as *optimal* because the phase margin is 30°for all frequencies beyond the functional bandwidth and the slope of the modulus plot is $-10\frac{dB}{oct}$. This characteristic provides for the application of significant feedback over the functional bandwidth while maintaining stability in the presence of parameter variations. According to the Bode phase gain relationship this slope corresponds to a function s^{-p} where p is a rational number. This function can be decomposed into a product of two functions:

$$s^{-p} = s^{-q}s^{-r} \tag{4.4}$$

In this expression r is an integer and q is a fraction between zero and one. By the Bode phase-gain relationship to achieve a slope of $-10\frac{dB}{oct}$ the value for p is found to be $p = \frac{5}{3}$. This leads to: $q = \frac{2}{3}$. To approximate this loop shape the polynomials $c_z(s)$ and $c_p(s)$ create a network function of poles and zeros spaced according to the relationship:

$$q = \frac{b}{a+b} \tag{4.5}$$

where a is the logarithmic octave spacing between zeros and poles and b is the logarithmic spacing between poles and zeros. With $q = \frac{2}{3}$ this yields:

$$q = \frac{2}{3} = \frac{b}{a+b} \tag{4.6}$$

with integer octave spacing this leads to $b = 2i$ and $a = i$ with $i \geq 1$. Consequently the minimum number of octaves to approximate the Bode Optimal slope is $a + b = 3(1) = 3$ and therefore:

$$\omega_{s1} \leq \frac{1}{2^{(a+b)}}\omega_b = \frac{1}{8}\omega_b \tag{4.7}$$

where ω_b is the crossover frequency. The choice of ω_{s1} therefore depends on the available bandwidth in the system.

The network function is populated with real poles and zeros according to the above discussion. The function is of the form:

$$\frac{c_z(s)}{c_p(s)} = \frac{(s-z_1)...(s-z_i)}{(s-p_1)...(s-p_j)} \tag{4.8}$$

The poles and zeros are computed as follows:

$$z_i = -\frac{1}{2}\frac{\omega_b}{2^{3(i-1)}} \tag{4.9}$$

$$p_j = -\frac{\omega_b}{2^{3(j-1)}} \tag{4.10}$$

Where $i = 1 : m$ and $j = 1 : m + 1$. the parameter m is found according to the following relation:

$$3m \leq log_2\frac{\omega_b}{\omega_0} \tag{4.11}$$

for the extreme case:

$$3m = log_2\frac{\omega_b}{\omega_0} \tag{4.12}$$

m describes a single 3 octave region between the system break frequency and the crossover frequency. In this extreme case the high order slope region has been completely omitted due to bandwidth restrictions. In this case the loop shape is the standard Bode optimal loop shape. A more practical relation is given by:

$$3m + 1 = log_2\frac{\omega_b}{\omega_{s1}} \tag{4.13}$$

This relation describes a Bode Optimal region of $3m+1$ octaves below crossover. The extra octave allows for the phase effects of the zeros at $\omega_s 1$ to take effect before the start of the Bode optimal slope.

Thus it is seen that there is no absolute method for determining the value of ω_{s1}. Indeed, the choice for this parameter when not dictated by bandwidth limitations is a question of engineering judgment. For a system with given ω_0 and ω_b the choice of m will determine ω_{s1}. Choosing a smaller value of m leads to more feedback applied over the functional bandwidth at the cost of robustness. Ultimately the choice should be determined by the level of certainty in the plant. The combination of the network function and the $-6\frac{dB}{oct}$ slope left over after the polynomial z_{s1} leads to the slope of $-10\frac{dB}{oct}$ for all frequencies $\omega_{s1} \leq \omega \leq \omega_b$.

Up until this point, plant dynamics have been ignored. The above polynomials create a loop shape that has ideal characteristics. The existence of the plant, however, alters this loop shape and yields undesirable response characteristics. As such, the polynomial $z_{s2}(s)$ is developed to account for the plant characteristics. In traditional loop shaping techniques a description of the plant dynamics is known and pole zero spacing is used to generate the desired loop shape taking advantage of the existing characteristics of the plant. In practice, to ensure stability only the plant characteristics near crossover need to be known.

The Cloud technique takes advantage of a tuned PID compensator to discern plant characteristics in much the same way Zeigler-Nichols takes advantage of a proportional compensator. It is assumed that the same characteristics which limit the bandwidth of the PID compensator also limit the bandwidth of the MBO compensator. As such, the crossover frequency for the MBO compensator is chosen to be the same as that for the PID compensator applied to the same plant. The crossover frequency is determined by noting the period of the closed loop step response of the system with a PID compensator. The Bode Sensitivity integral shows positive feedback is clustered near the crossover frequency. As such the period of the oscillation of the closed loop response will correspond closely to this frequency.

The PID architecture consists of an origin pole and two finite zeros. The origin pole provides -90°of phase at all frequencies. Each zero provides +90°of phase at frequencies well beyond the zero frequency. The phase advance becomes noticeable one decade below the zero frequency and increases to +45°at the zero frequency. Therefore, It can be seen that the PID compensator can only provide phase between +90°and -90°.

The Cloud technique uses a heuristic technique to estimate the plant phase at crossover. At the crossover frequency the loop transmission function modulus must have a negative slope. From the Bode

Phase-Gain relationship it can be inferred that for a negative slope the phase provided by the system must also be negative. For the closed loop system response to be stable there must be sufficient damping at crossover. Therefore, the phase of the system must be greater than -180°. As such the total phase of the loop transmission function must be between 0°and -180°. Since the phase characteristics of the PID compensator are already known, the phase of the plant can be estimated. For the sake of the approximation the plant dynamics are assumed to be far removed from the crossover frequency. Therefore it is assumed that the plant phase is a whole number multiple of -90°. If the phase provided by the PID compensator is negative the plant is assumed to be flat or first order and the phase is 0 or -90°. If the PID compensator phase is positive then the plant is assumed to be second order and the phase is -180°.

If the plant was estimated to be first order then the polynomial is of the form:

$$z_{s2}(s) = (s + \omega_{s2}) \tag{4.14}$$

And the frequency $\omega_{s2} \approx 0.5\omega_b$ is recomended by [3]. If the frequency were chosen to be $\omega_{s2} \approx 0.1\omega_b$, then the phase advance provided would be almost +90°at the crossover frequency. Conversely, if the frequency were chosen to be $\omega_{s2} \approx 10\omega_b$, then the phase advance provided would be negligible. The plant phase at this frequency is merely an estimate and in practice is not quite -90°due to the presence of dynamics near this frequency. In general the plant phase tends to be somewhere between -45°and -90°and so placing the compensator zero one or two decades before the crossover frequency will yield good results.

If the plant was estimated to be second order then the polynomial $z_{s2}(s)$ is of the form:

$$z_{s2}(s) = (s^2 + 2\zeta_{s2}\omega_{s2}s + \omega_{s2}^2) \tag{4.15}$$

Where again ω_{s2} is chosen to provide the desired phase characteristics. Similar to the case with the 1st order assumption the plant phase is generally more than -180°and so a good range of frequencies to try is:

$$0.1\omega_b > \omega_{s2} > \omega_b \tag{4.16}$$

The damping coefficient γ_{s2} affects the speed of the phase transition and can be reduced to provide rapid phase advance. Great care should be exercised when tuning the parameter however as decreasing it can reduce the gain of the system excessively at the zero frequency and introduce additional dynamics into the system. Cloud recommends using: $\gamma_{s2} = 0.8$. The system response is most sensitive to dynamics

in this frequency region and so multiple iterations of this polynomial may be necessary to achieve the desired results.

Next, polynomial $c_{bsd}(s)$ is developed to realize the Bode step. $c_{bsd}(s)$ consists of zeros at frequency ω_d which provide a phase advance to compensate for the high order roll-off at high frequencies. The compensator is designed such that the Bode optimal slop is carried through past the crossover frequency to the step transition frequency ω_d. Therefore the choice for ω_d depends on the choice of the Bode step depth. This in turn typically correlates to the desired gain margin of the system. For most high-performance systems the recommended gain margin is no less than $10dB$. Because the compensator has been designed to provide a slope of $-10\frac{dB}{oct}$ at the frequencies near crossover the frequency a gain margin of $10dB$ leads to:

$$\omega_d = 2\omega_b \tag{4.17}$$

The network function used to produce the Bode optimal slope is relative degree one. Including the uncompensated pole from the break frequency the total phase at the Bode step transition frequency should be $\approx -180°$. Therefore the polynomial $c_{bsd}(s)$ must be second order and is of the form:

$$c_{bsd}(s) = s^2 + 2\zeta_d\omega_d s + \omega_d^2 \tag{4.18}$$

Again, ζ_d is chosen to provide rapid phase transition without excessive loop gain reduction. Cloud recommends choosing $0.4 \leq \zeta_d \leq 0.6$ [3].

Next, the high-frequency roll-off is shaped. The last polynomial to be developed is $c_{bsc}(s)$. This polynomial provides poles at the frequency ω_c. It is desirable to reduce gain rapidly at frequencies beyond crossover so as to limit the potential destabilizing effects of unknown resonant modes at high frequencies. However, as was demonstrated by the Bode phase-gain relationship, poles at any frequency affect the phase of the system at all frequencies. Therefore, the Bode step exists to provide a separation between the crossover frequency and the high-order roll off so that the slope at high frequencies does not negatively impact the phase characteristics of the Bode optimal slope. Consider the phase provided from the Bode optimal slope. If this slope were to be continued indefinitely the phase at low frequencies contributed by this slope at frequencies above ω_d is given by:

$$\phi_{BO} \approx \frac{2}{\pi}(1+q)\frac{\omega}{\omega_d}, \omega << \omega_d \tag{4.19}$$

To ensure that the high-frequency roll off does not negatively impact the phase characteristics of the Bode optimal slope the transition frequency ω_c is found such that the phase contribution from the high-frequency roll off is equal to that which the Bode optimal slope would have provided anyway:

$$\phi_c = \frac{2}{\pi} n \frac{\omega}{\omega_C} + |B_n(\omega_c)| \frac{\omega}{\omega_c}, \omega << \omega_d \tag{4.20}$$

In the above equation the first term is the phase provided by the high frequency slope and the second term is any non-minimum phase present in the system and n is the order of the high-frequency slope. The frequency ω_c is therefore found by setting these equations equal to each other:.

$$\frac{2}{\pi} n \frac{\omega}{\omega_c} + |B_n(\omega_c)| \frac{\omega}{\omega_c} = \frac{2}{\pi}(1+q)\frac{\omega}{\omega_d} \tag{4.21}$$

Simplifying this equation yields:

$$\frac{\omega_c}{\omega_d} \approx \frac{n + \frac{\pi}{2}|B_n(\omega_c)|}{(1+q)} \tag{4.22}$$

For the common case where the high-frequency roll-off is second order, the Bode slope is $-10\frac{dB}{dec}$, and the system possesses no non-minimum phase the equation becomes:

$$\frac{\omega_c}{\omega_d} \approx \frac{2}{\frac{5}{3}} \tag{4.23}$$

$$\omega_c \approx \frac{6}{5}\omega_d \tag{4.24}$$

Similar to many of the other polynomials developed here the general form of the polynomial $c_{bsc}(s)$ is:

$$c_{bsc}(s) = s^2 + 2\zeta\omega_c s + \omega_c^2 \tag{4.25}$$

Again, ζ_c is chosen to provide a rapid transition without compromising the gain margin of the system. Consistent with other damping ratios Cloud recommends $0.4 \leq \zeta_c \leq 0.6$ [3].

Finally, with the compensator polynomials developed we now turn to the development of the compensator gain K. Recall that the crossover frequency was found according to the relationship:

$$1 = |C_{PID}(j\omega_b)P(j\omega_b)| \tag{4.26}$$

To maintain the same crossover frequency this relation must hold true for the MBO compensator:

$$1 = |C_{MBO}(j\omega_b)P(j\omega_b)| \tag{4.27}$$

To find K, we define: $C_{MBO}(s) = KC(s)$ where $C(s)$ is the combination of the numerator and denominator polynomials described above. This leads to:

$$|C_{PID}(j\omega_b)P(j\omega_b)| = 1 = K|C(j\omega_b)P(j\omega_b)| \tag{4.28}$$

$$\left|\frac{C_{PID}(j\omega_b)}{C(j\omega_b)}\right| = K \tag{4.29}$$

4.2 Variations from Standard Development

It should be noted that this technique does not guarantee that the compensator will be stable. The plant may contain unknown resonant dynamics at frequencies above or below the crossover frequency that cannot be accurately identified. Furthermore, a complete stability analysis cannot be performed and so performance metrics such as gain and phase margins *can only be estimated*. As a result, it is not uncommon for the design process to require several iterations and the adjustment of compensator parameters in accordance with sound engineering judgment.

One of the most common problems that can arise in compensator design are oscillations related to insufficiently damped modes or insufficient phase at crossover. A simple solution to these problems is to increase or decrease the loop gain K of the final compensator design. Increasing or decreasing the gain by a factor of two will shift the modulus plot by approximately 6 dB which can be sufficient to stabilize modes with unreasonably small or negative gain margins. Because the slope at crossover is $-10\frac{dB}{oct}$ changing the loop gain will also shift the crossover frequency of the system. This can have the benefit of changing the crossover from a frequency with a small phase margin to one with a better margin.

Ultimately, the MBO compensator is built around the frequency ω_b. This frequency is determined from the closed loop response of the PID compensator. The PID controller is generally a less aggressive design than the MBO compensator. Therefore in some cases the stable crossover frequency obtained from the PID design may result in unsatisfactory performance for the MBO design. As a result, it may sometimes be necessary to modify the crossover frequency to improve response. This is equivalent to altering the loop gain of the PID compensator to improve performance.

The polynomials $z_{s2}(s)$, $z_{s1}(s)$, and $c_0(s)$ play a significant role in determining the phase characteristics of the compensator. Specifically $z_{s1}(s)$ and $c_0(s)$ define the low frequency high-order slope region which maximizes the low frequency gain. In this region the phase delay exceeds $-180°$ and sufficiently deep modes can result in instabilities in this frequency range. The polynomial $z_{s2}(s)$ accounts for the plant phase near crossover. Changing the orders of these polynomials will change their phase contributions and may improve performance. Care must be taken to ensure the compensator design remains strictly proper (denominator order $\geq$ numerator order). Therefore, changing the order of any of these polynomials may require altering the order of subsequent polynomials as well.

The various alterations suggested here expand the applicability of the MBO algorithm to a wide range of systems. In practice, one or more of these adjustments will be necessary for any real system. This is because real systems almost always contain resonant modes. Ultimately the design depends on the decisions of the control engineer and there is always a trade-off between performance and relative stability. Great care should be taken to maximize performance while accounting for the stability requirements of the system. No design algorithm can replace sound engineering judgement.

Chapter 5: The WSC Simulator

5.1 Simulator Overview

For this project the compensator development technique presented in [3] is used to develop an Automatic Voltage Regulator (AVR) for a high fidelity model of a Pressurized Water Reactor (PWR) type commercial nuclear generating station. The reactor is a 3.5GW thermal reactor with two steam generation loops. The station has a single 1200MW electrical generator driven by a single shaft with one high pressure turbine and three low pressure turbines. The model is part of a training simulator developed by Western Services Corporation (WSC) for use in the training of generator operators. The system simulates the Human Machine Interface (HMI) pages available to a typical operator in a generating station. The simulation pages are populated with data generated by the modelling software. The modelling software is built using a C++ framework.

According to code comments found in several of the model object pages the earliest version of the simulator was developed in the late 1990s with various revisions throughout the 2000s. The simulation was primarily designed to model behaviors related to the reactor and associated subsystems. The electrical systems were modeled to a large degree of detail as well. The electrical componenets of the system described include the primary generator, the excitation system, the switchyard transformer, two secondary diesel generators, a simplified model of a local distribution network, as well as the various pumps and motors used throughout the plant. Based on the model of the local distribution network it was surmised that the simulation is an approximation of the Wolf Creek generating station in Burlington, Kansas.

HMI pages are purely graphical. They exist only to convey information to the users of the simulation and provide controls for operators to manipulate simulation parameters. The actual system behavior is described with *model* pages and *logic* pages. Model pages describe the interactions between various system components. They deal primarily with physical behavior such as fluid in a pipe, or current in a wire. As the name suggests, logic pages deal with logical computations. This consists of things like the status of a breaker or a valve. Both of these types of pages are developed on the same software and signals are passed between them freely. User interface controls usually affect parameters within logic pages, while gauges usually display values extracted from model pages. These distinctions hold true in general, however this is not an absolute rule. The modelling software makes no distinction between page types, and the same objects can be placed on either page type. Indeed, many model pages include logic

objects and occasionally logic pages will contain model objects. The distinction between page types is purely a convention used by the model developer.

The excitation system is described in the MGP2 (mgp2) HMI page. This page describes to the simulation user the functionality of the excitation system as well displaying relevant system parameters. The WSC simulator does not include documentation relating to the development of the system model, and the simulation pages are not extensively commented. This makes this system an excellent candidate for the application of the Cloud technique. For the purpose of developing the Modified Bode Optimal (MBO) compensator the specifics of the model development need not be known. Indeed, the primary advantage of the Cloud technique is that the compensator is developed without a detailed description of the plant model. So long as the compensator can be identified and a Proportional Integral Derivative (PID) can be tuned the MBO can be developed.

5.2 Excitation System

The simulator includes three model pages and one HMI page describing the behavior of the excitation system. The *ctrl* page describes the primary functionality of the excitation system. The *output* page describes the output of the exciter and updates the values in the generator object. The *misc* page contains various logical circuits used for different modes of operation as well as the calculation of additional signals for certain operating conditions. The excitation system model also uses several logic pages to track the values of various system breakers for the activation of protective systems. A detailed survey of these various logical operations is beyond the scope of this work. All of the calculations in the model are done using a per unit system with the exciter parameters used as the base. The rest of this section is dedicated to a more in depth analysis of each of the relevant model pages and their function in the simulator.

The excitation system HMI page is shown in Figure 5.1. The page is referred to by the simulator as MGP2. This page describes the structure of the excitation system used by the WSC simulator. Based on this description it can be seen that this is an Alternator-Rectifier type exciter employing controlled rectifiers. From the discussion in Chapter 2 we know that industry standards recommend modeling such systems in the way shown by Figure 2.4 [31]. This page consists of the excitation system operating parameters presented to the generator operator. It also contains the controls available to the operator which include: the AC and DC voltage set point controls, the substation bus breakers, and supplemental controls to adjust the turbine speed for power system synchronization.

Figure 5.2 is the model page titled *ctrl*. This page describes the core functionality of the regulator and the exciter. The WSC simulator uses an unconventional structure for the modelling of the exciter system. The sign on the summing junction where the terminal voltage is compared to the reference voltage is inverted. In other words, instead of the measured signal being subtracted from the reference signal the reference is instead subtracted from the measured signal. This representation is from an outdated convention. The result of this is that the error signal will have the opposite sign from that of the command signal.

It is in the ctrl page that the AVR can be found. In the WSC simulator the AVR is a simple proportional gain setting. Additionally, the simulator models the excitation system with a secondary signal being applied to the exciter which is not found in industry standard models. This secondary signal is a constant of magnitude 1pu. It likely represents a biasing signal, the effect of which is to reduce the steady state error of the proportional controller. Unfortunately the Simulator did not include documentation describing the development of the excitation system model so the function of this signal is purely speculative. The simulator compensates for the sign inversion on the error signal by subtracting the error from the bias signal. The ctrl page also contains the description of most of the protective features of the excitation system. As the page shows the WSC simulator models the exciter limits as limits on gating blocks.

The *output* model page, described by Figure 5.3, shows the output of the exciter. The model labels the output of the exciter as I despite the output of the previous page being a voltage. Indeed the parameter I is used in the section labelled Field Voltage as the pu value of the field voltage. This interchangeability in the model is justifiable given that the excitation system computations are done on a pu system where rated (1pu) field voltage produces rated (1pu) field current. The field current is converted to a pu value on the system base before being passed to the generator object. For a detailed description of the per unit system used in excitation system studies see [1]

Figure 5.4 is the *misc* page and describes a number of additional control features included in the excitation system. The main features of this model page are the exciter Status, the Manual Tracking Logic, and the Field Flashing Calc. The exciter Status is a logical operator which tracks the status of various protective devices to determine whether or not the excitation system is in a normal operating condition. The Manual Tracking Logic is a special feature which automatically adjusts the DC controller reference to track the exciter voltage when in AC regulating mode. The purpose of this feature is to avoid large system transients in the event of regulator malfunction forcing the system into manual operating mode. The Field Flashing Calc represents an additional current source applied to the exciter

field windings. The purpose of this signal is to assist with startup operation because the exciter is self excited and so is not active during loaded operation.

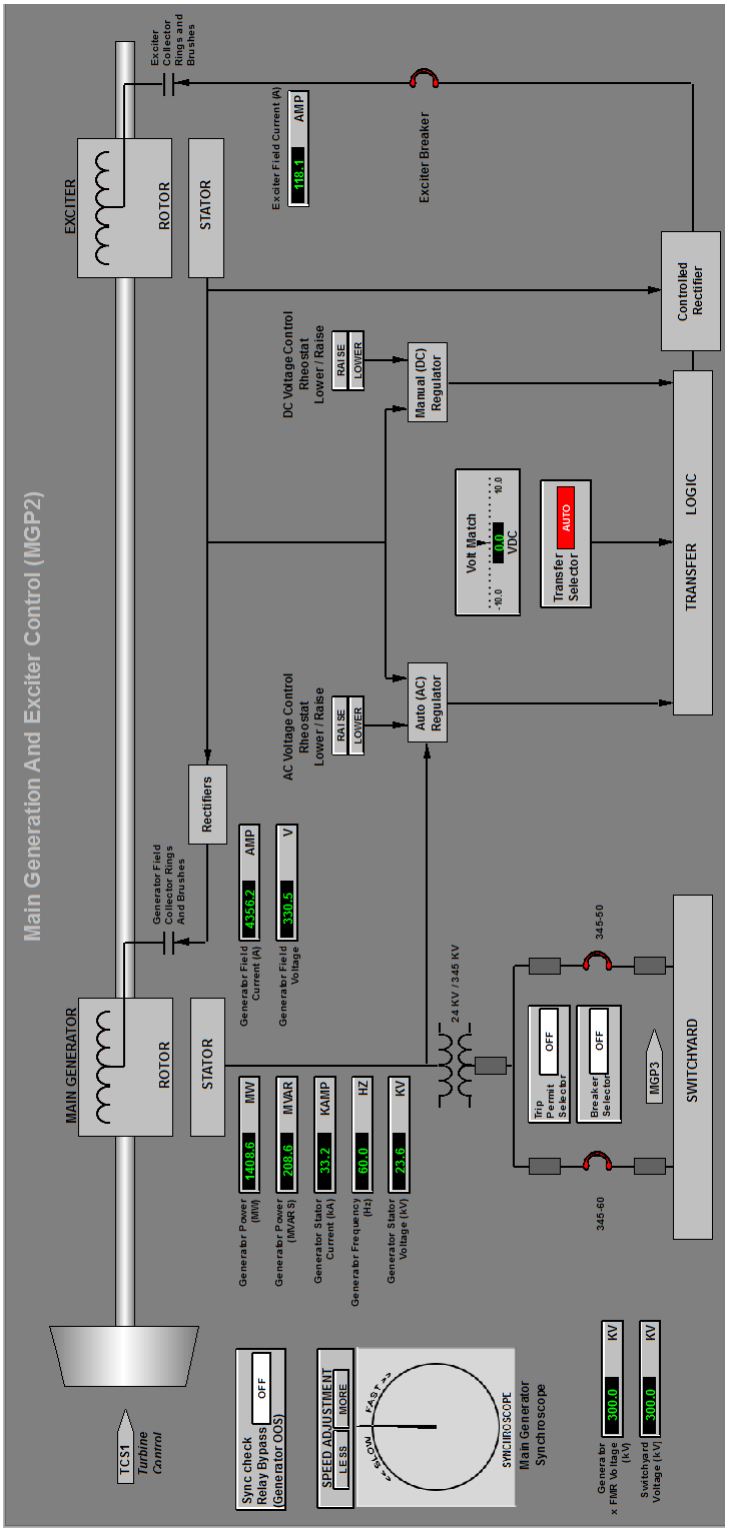

Figure 5.1: Exciter HMI page

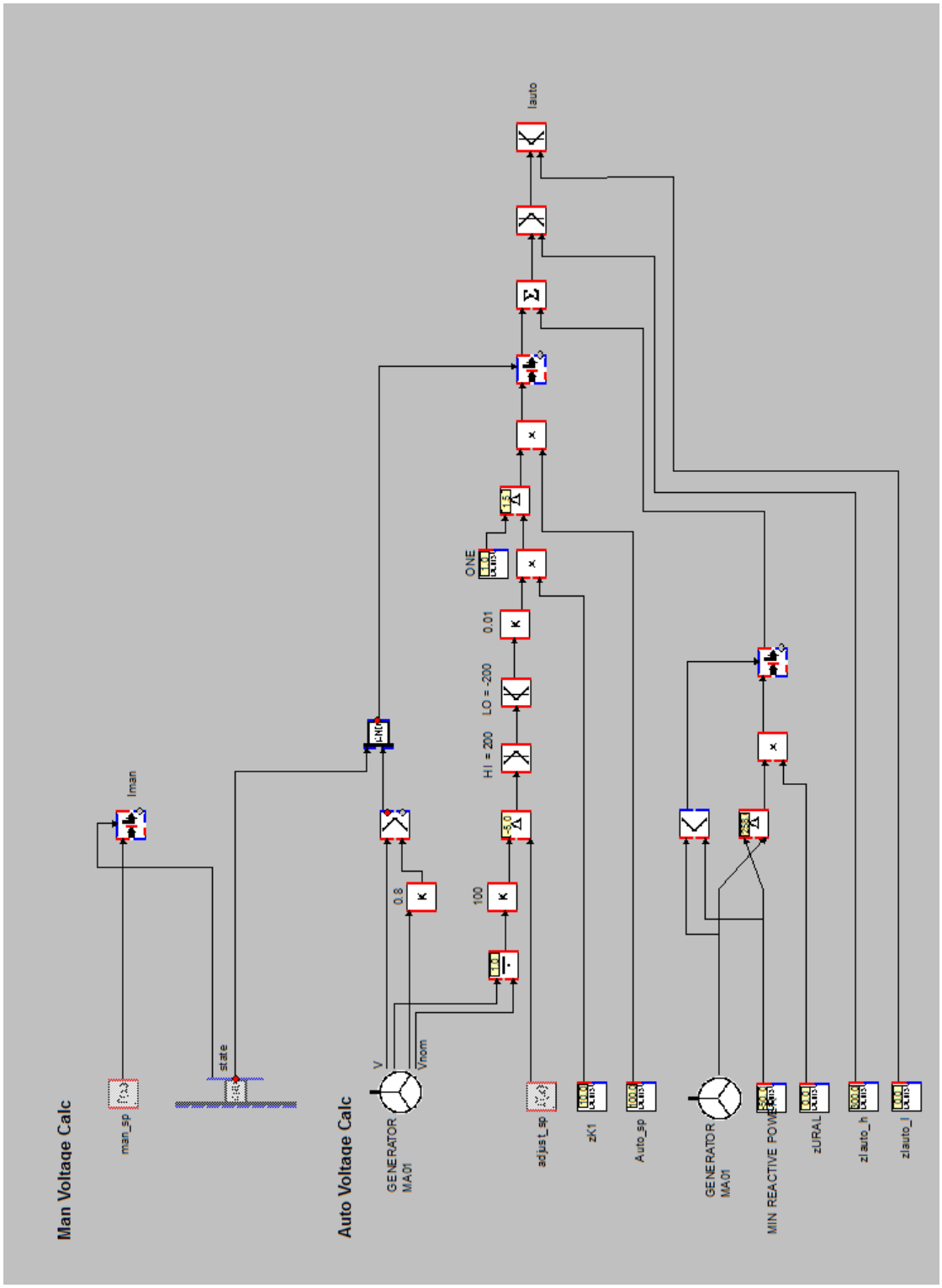

Figure 5.2: *ctrl* model page

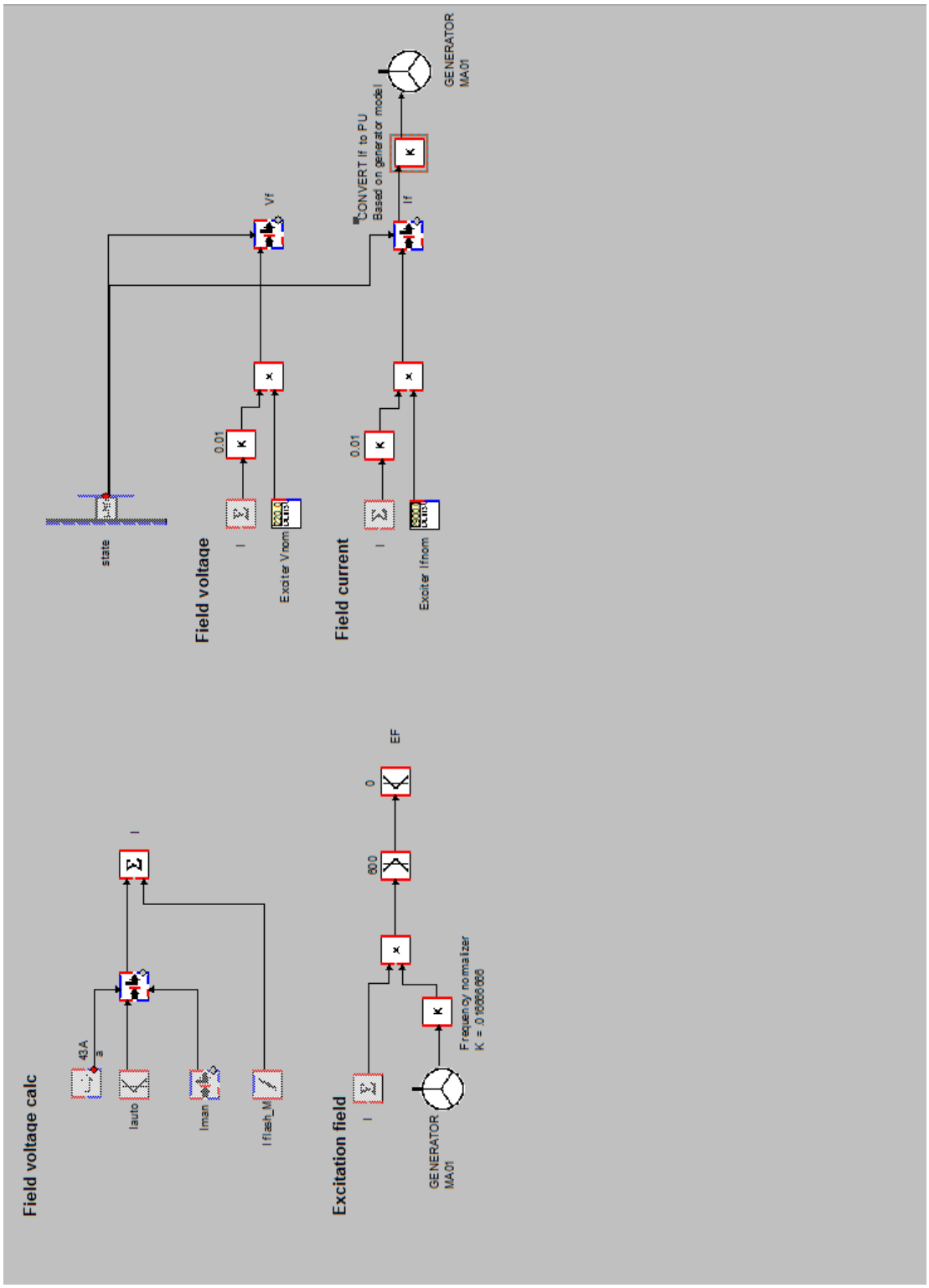

Figure 5.3: *Output* model page

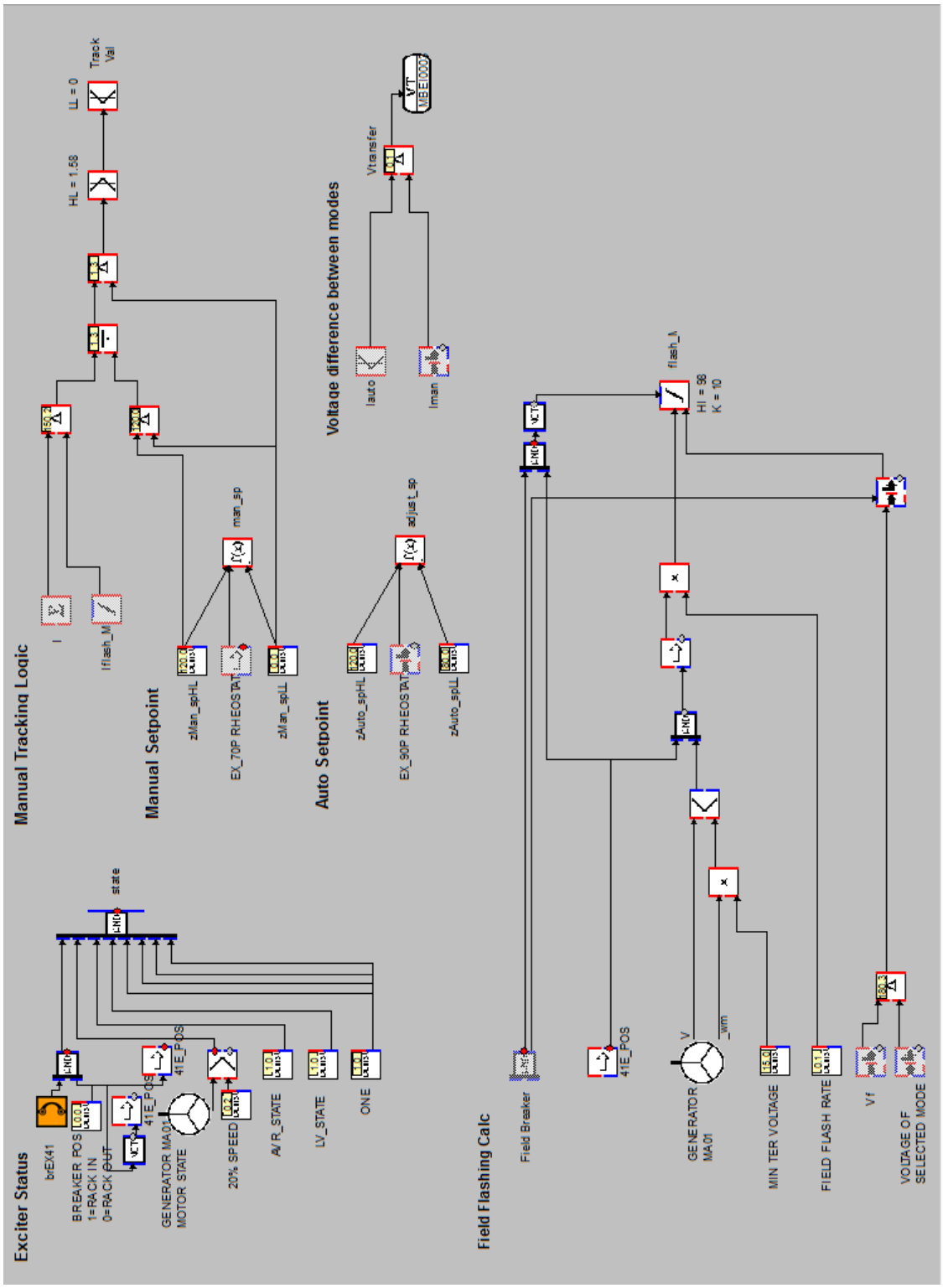

Figure 5.4: *Misc* model page

5.3 Distribution Network

One of the primary reasons the WSC simulator was chosen for this project was because of the moderately sized distribution network modelled by the system. The simulator includes this feature so that station operators can be trained on proper response procedures to grid side contingency events. Additonally, the simulator extensively models the internal electrical network of the generating station. The electrical systems controlling every pump, motor, and valve in the entire plant are modelled with great detail. The system also describes two supplemental diesel generators used during startup and emergencies. All of these components contribute to the generator dynamics as seen from the excitation system. A full description of the plant electrical system is beyond the scope of this work and would not contribute significantly to it. However, the inclusion of a reduced scale distribution system means that additional testing, beyond that of conventional studies of excitation systems, can be performed to verify AVR performance. This section is therefore dedicated to providing a brief functional descriptions of the simulator pages associated with modelling the wider power system. Figure 5.5 is the HMI page for the main generator output. Although the Bulk Power System (BPS) is modelled in the simulator there are no features of it directly controllable by a station operator and therefore no HMI pages represent it directly. Unlike many other HMI pages this one provides no controls for affecting simulation parameters. This page is, however, quite information dense. This page displays the operating parameters of the generator; terminal voltage, frequency, real and reactive power. In a sense this page shows the "final product" of the generating station. This page shows the substation transformer and is the closest to the BPS. This page also contains information about the thermal status of the distribution transformer, the primary generator, as well as the exciter.

The model page shown in 5.6 is the page responsible for describing the interaction of the generating station with the BPS. The distribution substation bus is designated ebXMA01 and is located in the top left corner of the page. This designation is important to note because it indicates the distribution system bus to which this generating station is connected. This page also has the electrical bus ebMA002 which is a local distribution bus that delivers power from the generator to various systems within generating station. The mathematical objects on this page are related to the thermal calculations for the different transformers.

Figure 5.7 describes the BPS in the immediate vicinity of the generating station. This page connects to the larger distribution station from the node labelled ebXMA02. It also possesses a bus labelled

OFFSITE. The name of this object in this page is a bit misleading because it connects back into the generating station and supplies power for cold starting from the grid. The large green object on the right side of the page is representative of the additional generation provided to the modelled loads. This object does not have set power characteristics and acts to balance the load flows under varying generator output. In other words it is treated as an infinite bus.

The regional transmission system is described by the model page shown in Figure 5.8. This page models the effects of distant distant generators and loads. These are represented by the two synchronous machine objects on the left hand side of the page. These objects are connected through series inductors which model the long transmission lines between the local power system and neighboring buses. As in the page described in Figure 5.7 these objects have no set power characteristics and exist for balancing line flows. Both bus ebXMA01 and ebXMA02 are shown on this page as well in the lower right of the model page. Recall from above that ebXMA01 is the distribution substation bus and ebXMA02 is the feeder to the local distribution network. The fact that these buses are only separated by a breaker confirms that Figure 5.8 is representative of the loads closest to the generating station.

5.4 Model Adjustments

While the model of the generating station is of extremely high fidelity, the excitation system is overly simplified in some aspects. Because the system was designed for use in the training of human operators system dynamics with small time constants were ignored in the original model development. This means that the amplifier time constant and the exciter time constant were both neglected. As a result the entire excitation system, when unloaded, is modeled as a first order system. Such systems do not contain enough phase delay to obtain resonance with proportional gain alone. This means that the Zeigler-Nichols technique is unsuitable for this plant [2].

So that the Cloud technique could be used it was decided to augment the system model to include the missing excitation system components. Without detailed knowledge of the plant upon which the simulator is based it was decided to approximate the components with values consistent with literature. The remainder of this chapter deals with the modifications that were made for the purpose of compensator development and testing. Because of the overall sophistication of the WSC simulator efforts were made to limit alteration of the model to only those aspects absolutely necessary to accurately implement and test the Cloud technique.

Figure 5.9 shows the modifications which were made to the output page of the exciter system. The components missing from the WSC model were the time constants and gains associated with the amplifier and the exciter as described in Chapter 2. Due to the lack of detailed information regarding the excitation system electrical parameters the simplest models were chosen. Thus, the amplifier and exciter are modelled as single pole systems. To maintain consistency with [31] and specifically the excitation system described by Figure 2.4 the amplifier lag block is placed at the output of the regulator after the Over Excitation Limiter (OEL) and Under Excitation Limiter (UEL) limiters. the placement of the exciter lag block was chosen to respect the fact that the field current must lag the applied voltage. Values were chosen consistent with the models used by papers in the literature review. These models describe a range of values for various excitation systems. The WSC simulator model is of a single large wattage generator so values were chosen for the time constants on the high range of the values found in literature [4–6, 8–10, 12–14, 16–24]. This decision is based on engineering judgement and the assumption that a larger machine would have longer time constants. Model fidelity could be further improved if the relevant parameters of the equipment used for the original development of the simulator were known.

Finally, to test the effect of sudden load rejections a simple load was added to the distribution substation bus on the generator output model page as shown in Figure 5.10. This load object can be used to describe sudden changes in both the active and reactive power flows at the distribution substation consistent with sudden load changes at arbitrary points within the distribution system. This block can be used to represent both positive and negative changes.

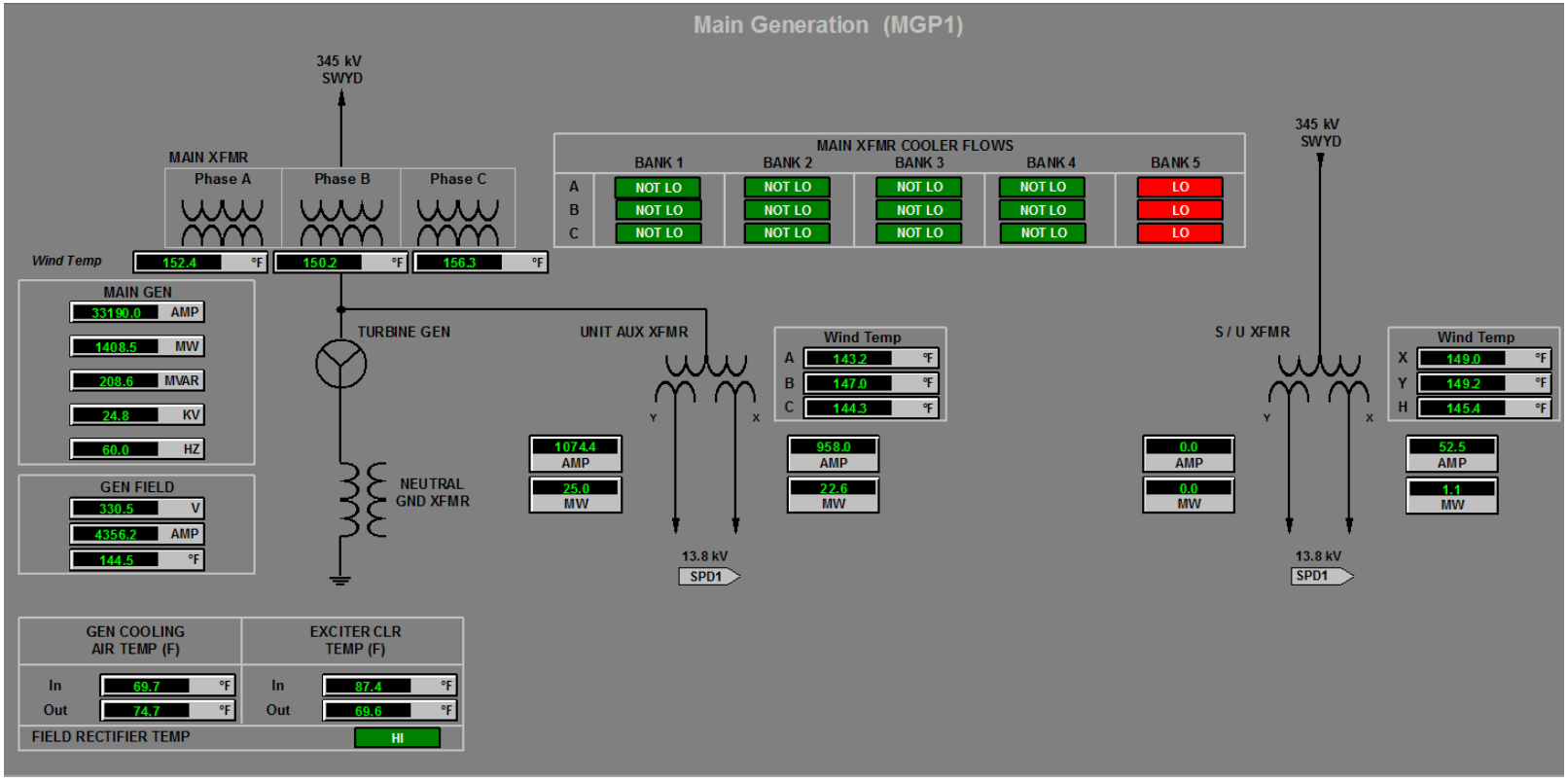

Figure 5.5: Distribution transformer HMI page

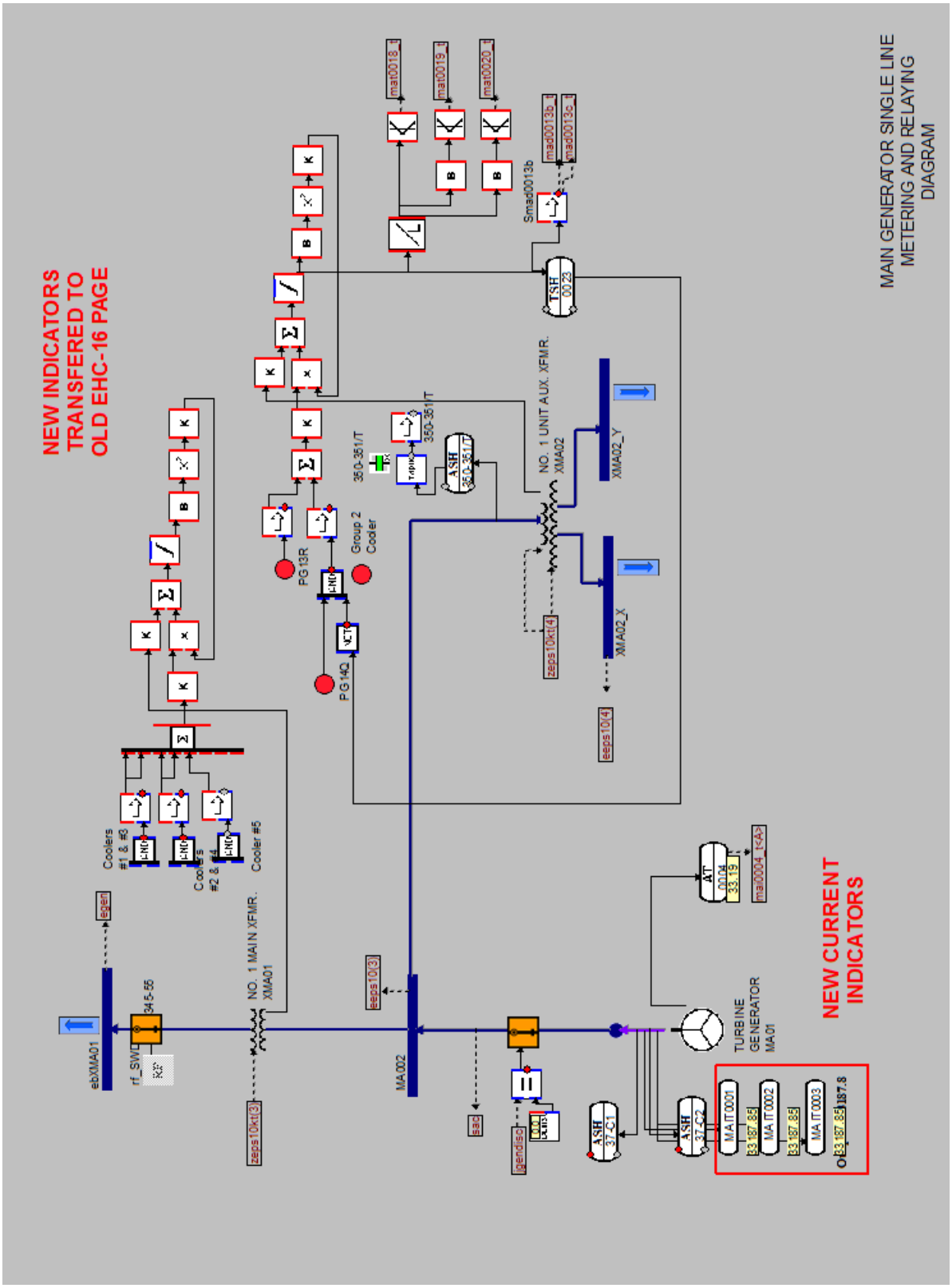

Figure 5.6: Model page of generator output and distribution transformer

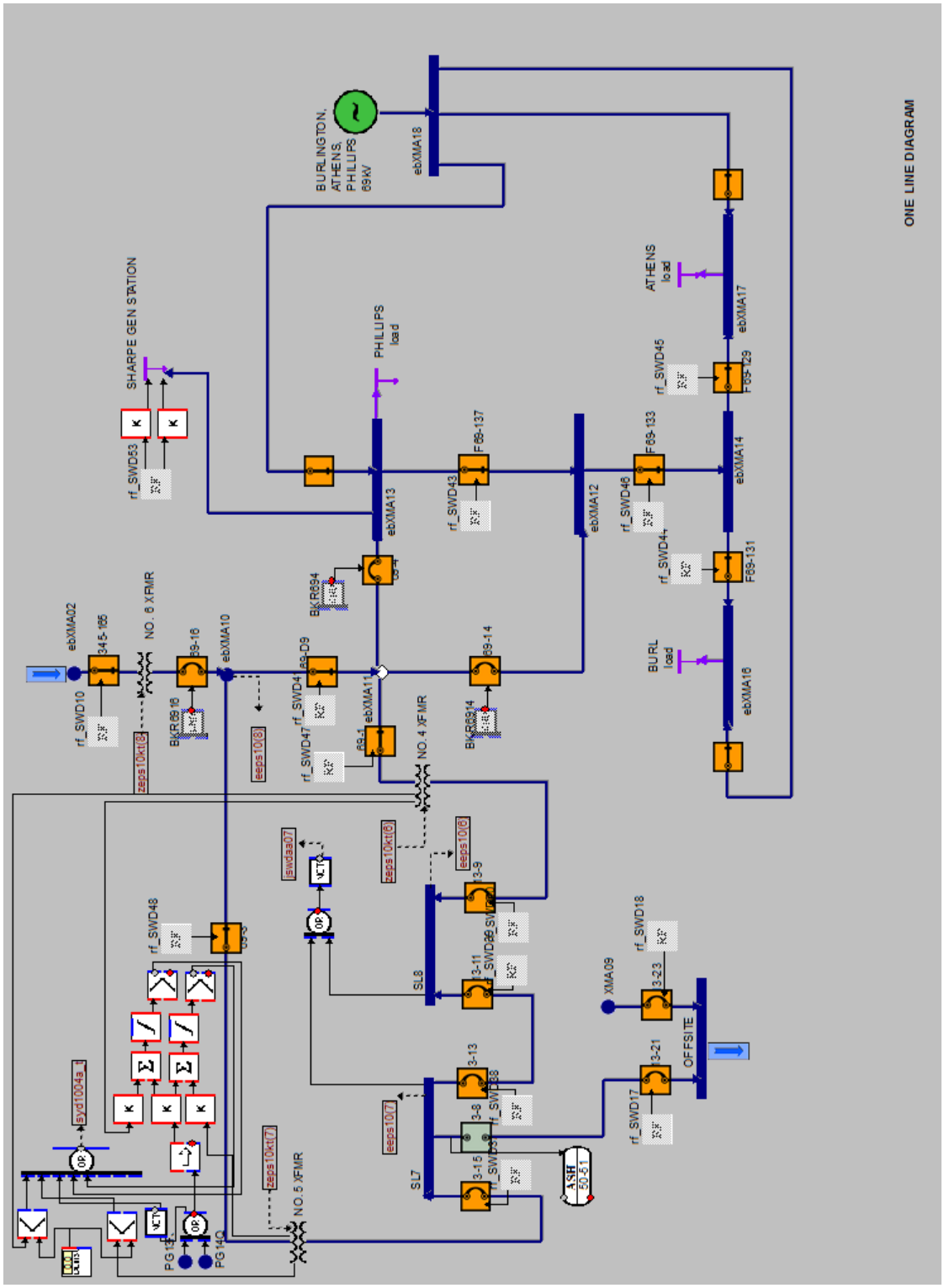

Figure 5.7: Model page of local distribution system

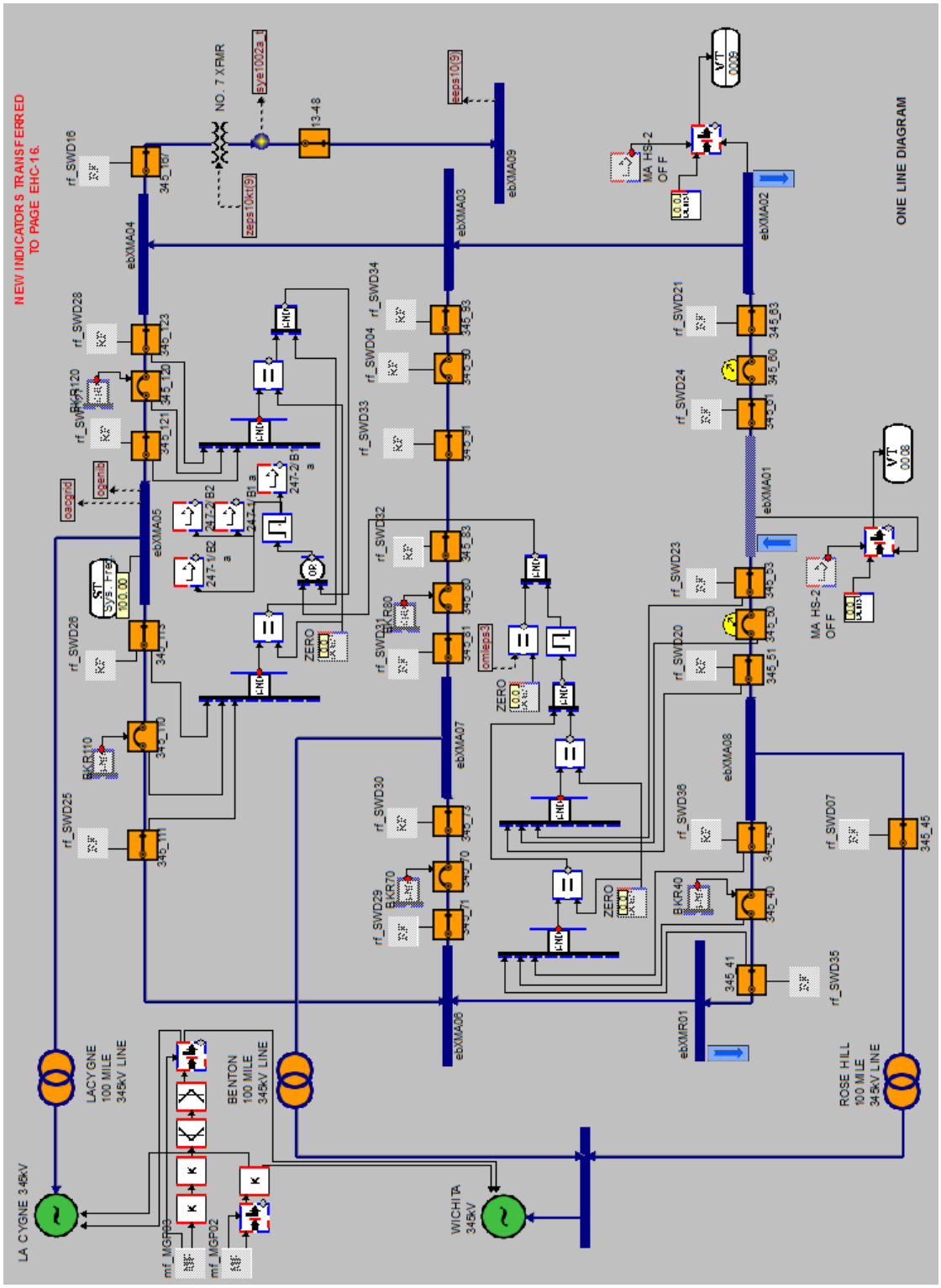

Figure 5.8: Model page of bulk power system

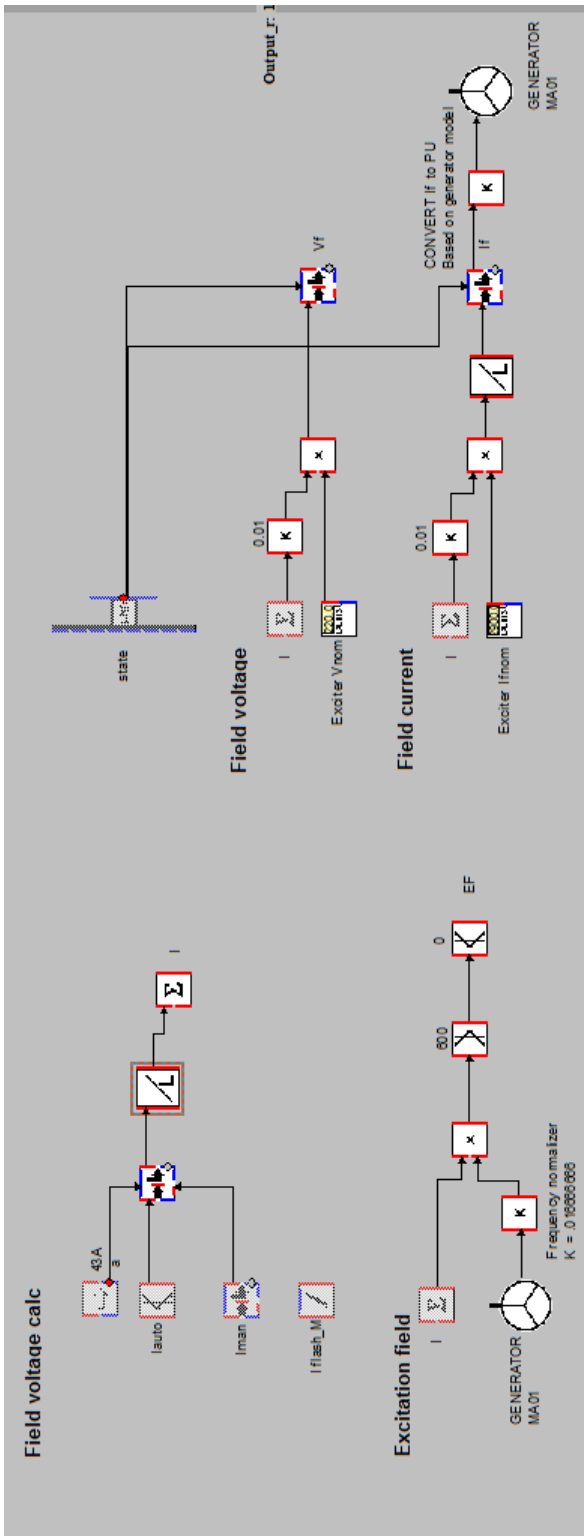

Figure 5.9: Modified exciter output

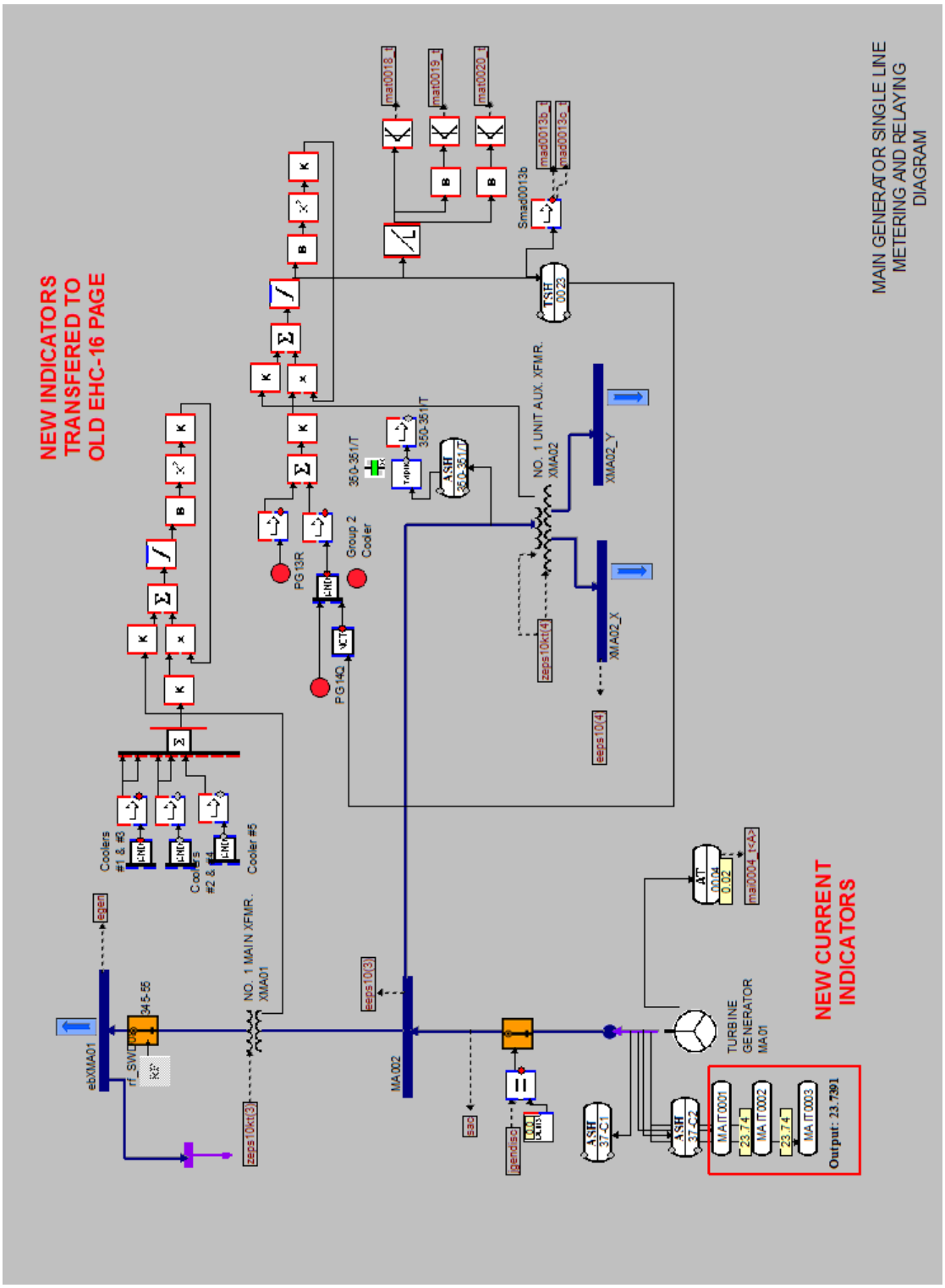

Figure 5.10: Modified generator output page with load on distribution transformer

Chapter 6: Compensator Development

With the basics of excitation system theory, frequency domain control, and the WSC system model explored, attention can now be turned to the development of the MBO compensator for the AVR. In this chapter the procedure by which the MBO compensator was developed and the method with which it was implemented in the WSC simulator are explored. This chapter differs from Chapter 4 in that this chapter describes the actual procedure that was followed for this specific application whereas Chapter 4 deals with the mathematical foundation for the MBO design. This chapter culminates with the full mathematical description of the completed compensator design as well as a discussion of the implementation of the compensator and any lingering concerns about model validity. Testing of the completed design and compensator adjustments are detailed in Chapter 7. A discussion of relative system performance is given in Chapter 8

6.1 Design Procedure

Recall from Chapter 4 that the first step in designing a MBO compensator is to develop a PID compensator for the system in question. Also recall from Chapter 3 and [2] that the PID compensator has the form:

$$C_{PID}(s) = K_P + \frac{K_I}{s} + K_D s \tag{6.1}$$

The WSC modelling software includes functionality for implementing proportional gains, integrators, and differentiators. Therefore it was decided to implement Equation 6.1 directly. This can be seen from the modified ctrl model page shown in Figure 6.1. The AVR output is the sum of the outputs from the three branches. Each block contains an adjustable gain setting for tuning of the PID parameters. The integrator path lacks a gain block because the WSC integrator block contains the proportional gain functionality internally. A proportional gain block was included in series with the AVR for adjusting the overall loop gain. This functionality provides a mechanism for gain stabilization of unstable modes as well as easy activation and deactivation of the PID compensator without the need to change tuned parameters. The location for the PID compensator was chosen to be after the gating block which limits the error signal and before the gates representing the excitation limiters to maintain consistency with the alternator-supplied controlled rectifier exciter model given in Figure 2.4.

According to the IEEE the system parameters of most interest to excitation system studies are the generator terminal voltage, the exciter voltage, and the exciter current [26]. In accordance with the Zeigler-Nichols (ZN) tuning method the PID is tuned by setting the integral and derivative gains to zero

and increasing the proportional gain until sustained oscillation is observed [2]. To avoid the injection of disturbances into the BPS NERC recommends tuning of AVR parameters with the system disconnected from the BPS [30]. Because of the coupling in the system the monitored parameters will oscillate out of phase, but at the same frequency. Therefore any one of the above three parameters can be used for determining the oscillation period. The critical gain of the system was found to be $K_U = 26$. The response of the system when the proportional gain was adjusted is shown in Figure 6.2 This oscillation was obtained without the need to introduce any disturbance but rather arose as a result of noise within the system. From this response it is observed that the oscillation period is $T_U \approx 1.960$ s. Combining these observations and applying the ZN technique yields the following gains [2, 3]:

$$K_P = 0.6k_U = 0.6(26) = 15.600 \tag{6.2}$$

$$K_I = 1.2\frac{K_U}{T_U} = 1.2\frac{(26)}{(1.960)} \approx 15.920 \tag{6.3}$$

$$K_D = 0.6\frac{K_U T_U}{8} = 0.6\frac{(26)(1.960)}{8} \approx 3.822 \tag{6.4}$$

The model was updated with the above compensator parameters and the response of the new system to a step change in the voltage reference was recorded. The magnitude of the step change was chosen to be large enough that a significant response could be observed, however not so large that the effect of system nonlinearities would distort the system response. This system response is presented in Figure 6.3. The crossover frequency of the system is determined by analyzing the period of the oscillatory response. The period of the response is estimated as $t_b \approx 2.667$ s. This in turn leads to:

$$\omega_b = \frac{2\pi}{t_b} = 2.356\frac{rad}{s} \tag{6.5}$$

The phase of the PID compensator is found as follows:

$$\theta_{PID} = arg(C_{PID}(j\omega_b)) \simeq 8.1986^\circ \tag{6.6}$$

This is greater than 0° and so the plant is assumed to be second order at crossover. For this compensator design the phase margin was chosen as 30°, the gain margin was chosen as $10dB$, and the roll-off was chosen as third order. This in turn leads to the selection of the MBO design parameters of $q = \frac{2}{3}$, $\omega_d = 2\omega_b = 4.712\frac{rad}{s}$ and $n = 3$. In the absence of additional information the plant is assumed to possess no appreciable non-minimum phase. Therefore, according to the method presented in Chapter 3

for determining the Bode step:

$$\omega_c = \omega_d \frac{n + \frac{\pi}{2}|B_n(\omega_c)|}{1+q} \tag{6.7}$$

$$\omega_c = (4.712)\frac{3+(0)}{1+(\frac{2}{3})} \simeq 8.482\frac{rad}{s} \tag{6.8}$$

No functional bandwidth is specified for excitation systems. The time constant of the generator is typically the largest so the low frequency characteristics are largely dictated by the loading condition. In general, robustness is the primary concern in the design of excitation systems due to the constant variation in the BPS. Therefore, it was decided to apply the Bode optimal slope for six octaves and the low-frequency high-order slope for two octaves. Choosing these parameters produces a compensator which emphasizes stability while still providing considerable feedback at low frequencies. This leads to the following parameter definitions:

$$m = 2 \tag{6.9}$$

$$\omega_{s1} = \frac{\omega_b}{2^{3(m)}} = 0.0184\frac{rad}{s} \tag{6.10}$$

$$\omega_0 = \frac{\omega_{s1}}{4} = 0.0046\frac{rad}{s} \tag{6.11}$$

Damping was chosen to be 0.4 for all polynomials to provide rapid phase transitions without threatening stability margins [3]. As a result, the constituent polynomials of the MBO compensator become:

$$c_0(s) = (s + 0.0046)(s^2 + 2(0.4)(0.0046)s + 0.0000212) \tag{6.12}$$

$$c_{bsc}(s) = (s^2 + 2(0.4)(8.482)s + 71.948) \tag{6.13}$$

$$z_{s1}(s) = (s^2 + 2(0.4)(0.0184)s + 0.000339) \tag{6.14}$$

$$z_{s2}(s) = (s^2 + 2(0.4)(1.1781)s + 1.388) \tag{6.15}$$

$$c_{bsd}(s) = (s^2 + 2(0.4)(4.7123)s + 22.206) \tag{6.16}$$

With the network function for approximating the Bode optimal slope being:

$$\frac{c_z(s)}{c_p(s)} = \frac{(s+1.176)((s+0.147))}{(s+2.36)(s+0.295)(s+0.0368)} \tag{6.17}$$

Substituting the polynomials into Equation 4.1 yields:

$$C_{MBO}(s) = K\frac{(s+1.176)((s+0.147))(s^2+2(0.4)(0.0184)s+0.000339)}{(s+2.36)(s+0.295)(s+0.0368)(s^2+2(0.4)(8.482)s+71.948)}\ldots \\ \ldots\frac{(s^2+2(0.4)(1.1781)s+1.388)(s^2+2(0.4)(4.7123)s+22.206)}{(s+0.0046)(s^2+2(0.4)(0.0046)s+0.0000212)} \quad (6.18)$$

Finally, the parameter K is calculated. The magnitude of the PID compensator response at crossover was found to be:

$$|C_{PID}(j\omega_b)| = 29.265 \quad (6.19)$$

The magnitude of the MBO compensator at crossover with $K = 1$ was found to be:

$$|C'_{MBO}(j\omega_b)| = 0.2651 \quad (6.20)$$

Therefore K is found to be:

$$K = \left|\frac{C_{PID}(j\omega_b)}{C'_{MBO}(j\omega_b)}\right| = \frac{29.265}{0.2651} = 110.390 \quad (6.21)$$

And the completed MBO compensator design is:

$$C_{MBO}(s) = 110.390\frac{(s+1.176)((s+0.147))(s^2+2(0.4)(0.0184)s+0.000339)}{(s+2.36)(s+0.295)(s+0.0368)(s^2+2(0.4)(8.482)s+71.948)}\ldots \\ \ldots\frac{(s^2+2(0.4)(1.1781)s+1.388)(s^2+2(0.4)(4.7123)s+22.206)}{(s+0.0046)(s^2+2(0.4)(0.0046)s+0.0000212)} \quad (6.22)$$

Cloud advises that the compensator is not guaranteed to be optimal or even stable [3]. As such, the design process is an iterative one. Cloud includes several suggestions regarding troubleshooting procedures and design alterations which may be employed to improve performance. To facilitate in the development of future MBO compensators much of the design process was automated using Matlab [36]. The Matlab code used for designing the compensators is included in appendix A

6.2 Implementation

With a completed transfer function for the MBO compensator the focus now turns to modelling the compensator within the WSC simulation software. To this end the form of the compensator transfer function was altered to be easier to implement with the available model objects. The MBO compensator includes several underdamped polynomials which must be modelled with complex pole/zero pairs. The simulation software includes simple lead-lag blocks which are sufficient for modeling real poles and zeros

but not complex ones. The transfer function could be rewritten to express the numerator as a network of parallel differentiators, however a similar treatment of the denominator was not possible. As a result, additional functionality was added to the simulation software for the modelling of complex poles. The code used to model this behavior is given in appendix B. Finally, because of the sheer number of model objects used to describe the AVR a new model page was added to describe it. This page needed to be incorporated into the existing model, and so the ctrl page was further modified as well.

The completed compensator design is given by the transfer function:

$$C_{MBO}(s) = 110.390\frac{(s+1.176)(s+0.147)(s^2+2(0.4)(0.0184)s+0.000339)}{(s+2.36)(s+0.295)(s+0.0368)(s^2+2(0.4)(8.482)s+71.948)}... \\ ...\frac{(s^2+2(0.4)(1.1781)s+1.388)(s^2+2(0.4)(4.7123)s+22.206)}{(s+0.0046)(s^2+2(0.4)(0.0046)s+0.0000212)} \quad (6.23)$$

While this representation is the most descriptive and mathematically accurate, it is not readily implemented using the WSC model software. Model objects available for the implementation of transfer functions include; proportional gains, integrators, differentiators, lead blocks, and lag blocks [37]. The lead and lag blocks are used to describe differential equations.

The lag block describes equations of the form [37]:

$$T_{lag}\frac{dY}{dt} + Y = X \quad (6.24)$$

Where X and Y are the block input and output respectively and T_{lag} is a user defined constant. Clearly this is a first order linear differential equation which can be expressed in the Laplace domain as follows:

$$(T_{lag}s+1)Y(s) - Y(0) = X(s) \quad (6.25)$$

With no inital conditions this reduces to the transfer function:

$$\frac{Y(s)}{X(s)} = \frac{1}{(T_{lag}s+1)} \quad (6.26)$$

This very closely resembles the real poles of the MBO transfer function and with slight alteration they

can be expressed in this form. By defining $T_{lag} = \frac{1}{\omega_p}$ the MBO compensator can be rewritten as follows:

$$C_{MBO}(s) = \frac{110.390}{(0.0046)(0.0368)(0.295)(2.36)}... \\ ...\frac{(s+1.176)(s+0.147)(s^2+2(0.4)(0.0184)s+0.000339)}{(0.424s+1)(3.390s+1)(27.174s+1)(217.390s+1)}... \\ ...\frac{(s^2+2(0.4)(1.1781)s+1.388)(s^2+2(0.4)(4.7123)s+22.206)}{(s^2+2(0.4)(8.482)s+71.948)(s^2+2(0.4)(0.0046)s+0.0000212)} \quad (6.27)$$

$$C_{MBO}(s) = 937000... \\ ...\frac{(s+1.176)(s+0.147)(s^2+2(0.4)(0.0184)s+0.000339)}{(0.424s+1)(3.390s+1)(27.174s+1)(217.390s+1)}... \\ ...\frac{(s^2+2(0.4)(1.1781)s+1.388)(s^2+2(0.4)(4.7123)s+22.206)}{(s^2+2(0.4)(8.482)s+71.948)(s^2+2(0.4)(0.0046)s+0.0000212)} \quad (6.28)$$

This leaves the modelling of the zeros, and the complex poles.

The lead block models equations of the form [37]:

$$T_{lag}\frac{dY}{dt} + Y = T_{lead}\frac{dX}{dt} \quad (6.29)$$

This can be expressed in the Laplace domain as follows:

$$(T_{lag}s+1)Y(s) - Y(0) = T_{lead}sX(s) - X(0) \quad (6.30)$$

assuming no initial conditions this reduces to the following transfer function:

$$\frac{Y(s)}{X(s)} = \frac{T_{lead}s}{(T_{lag}s+1)} \quad (6.31)$$

This function looks like that of Equation 6.26 with an added differentiator in the numerator. The goal is to model a real zero of the form:

$$\frac{Y(s)}{X(s)} = (s+\omega_z) \quad (6.32)$$

Clearly the lead block is unsuitable for modeling the zeros of the MBO compensator.

Consider again Equation 6.32. Converting this equation to the time domain yields:

$$Y = \frac{d}{dt}X + \omega_s X \tag{6.33}$$

This equation be implemented in the WSC simulator by passing the input separately through a gain block and a differentiator and then summing the outputs as in Figure 6.4. Now consider the following transfer function with arbitrary constants A and B:

$$\frac{Y(s)}{X(s)} = (s^2 + As + B) \tag{6.34}$$

In the time domain this can be expressed as:

$$Y = \frac{d}{dt}\frac{d}{dt}X + A\frac{d}{dt}X + BX \tag{6.35}$$

Similarly to 6.4 this can be implemented by treating each term as as a series calculation and then summing the outputs of each branch as in Figure 6.5. This approach is general and can be used to implement any transfer function of the form:

$$\frac{Y(s)}{X(s)} = A_n s^n + ... + A_1 s + A_0 \tag{6.36}$$

For this reason it was decided to implement the compensator zeros in this form. Therefore the MBO compensator now has the form:

$$\begin{aligned} C_{MBO}(s) = 937000... \\ ...\frac{(s^8 + 6.0524s^7 + 33.655s^6 + 63.453s^5 + 71.139s^4}{(0.424s+1)(3.390s+1)(27.174s+1)(217.390s+1)}... \\ ...\frac{+46.440s^3 + 6.039s^2 + 0.0941s + 0.00181)}{(s^2 + 2(0.4)(8.482)s + 71.948)(s^2 + 2(0.4)(0.0046)s + 0.0000212)} \end{aligned} \tag{6.37}$$

The only thing left is to implement the complex pole pairs of the lightly damped denominator polynomials. These polynomials convert to the time domain as second order differential equations. Unfortunately, the WSC simulator does not possess functionality for modeling second order differential equations [37]. One possible solution to this problem which was considered was to simply change the damping on the polynomials to $\zeta = 1$ so that they could be implemented as real pole pairs. This proved impractical as the compensator was no longer able to provide phase transitions rapidly enough to achieve satisfactory performance.

It was decided to augment the source code of the simulator modeling program to include functionality for the approximation of second order differential equations. The full development of this functionality is quite lengthy and so rather than being described here is presented in appendix B

Because of the sophisticated nature of the MBO compensator a considerable number of model objects were required to describe it. Therefore, it was necessary to create an entirely new model page for the AVR. To connect the new AVR page to the existing model it was necessary to make additional modifications to the ctrl page of the simulator. Figure 6.6 shows that the excitation system circuit was cut just prior to the proportional gain and just after the proportional block which converts the error signal to the pu system. The signal after the proportional block is transferred to the AVR model page, and the output from that page is brought back through the transfer object represented by the arrow. Additonally, summing blocks and constant blocks were added for the injection of signals at both the terminal voltage transducer and the terminal voltage reference. These locations were chosen in accordance with the recommended testing practices given in [26].

Finally, the full compensator is included within the WSC simulator. The newly created AVR model page is shown in Figure 6.7. This page includes essentially a single data path beginning with the transfer object feeding the error signal from the ctrl page and ending with the object that transfers the command signal back to it. The MBO numerator is implemented with the parallel cascade of differentiators as discussed above. This is then fed through the series of real and complex pole objects. Also included on this page is the same implementation of the PID compenator, as described in the Development section of this chapter. This is to provide for ease of switching between compensators for multiple design iterations. There is also a constant signal which can be added to the output. This is to eliminate the error prior to switching between compensators, because if a large error exists during switching it will trigger a significant transient response which may trigger protection devices.

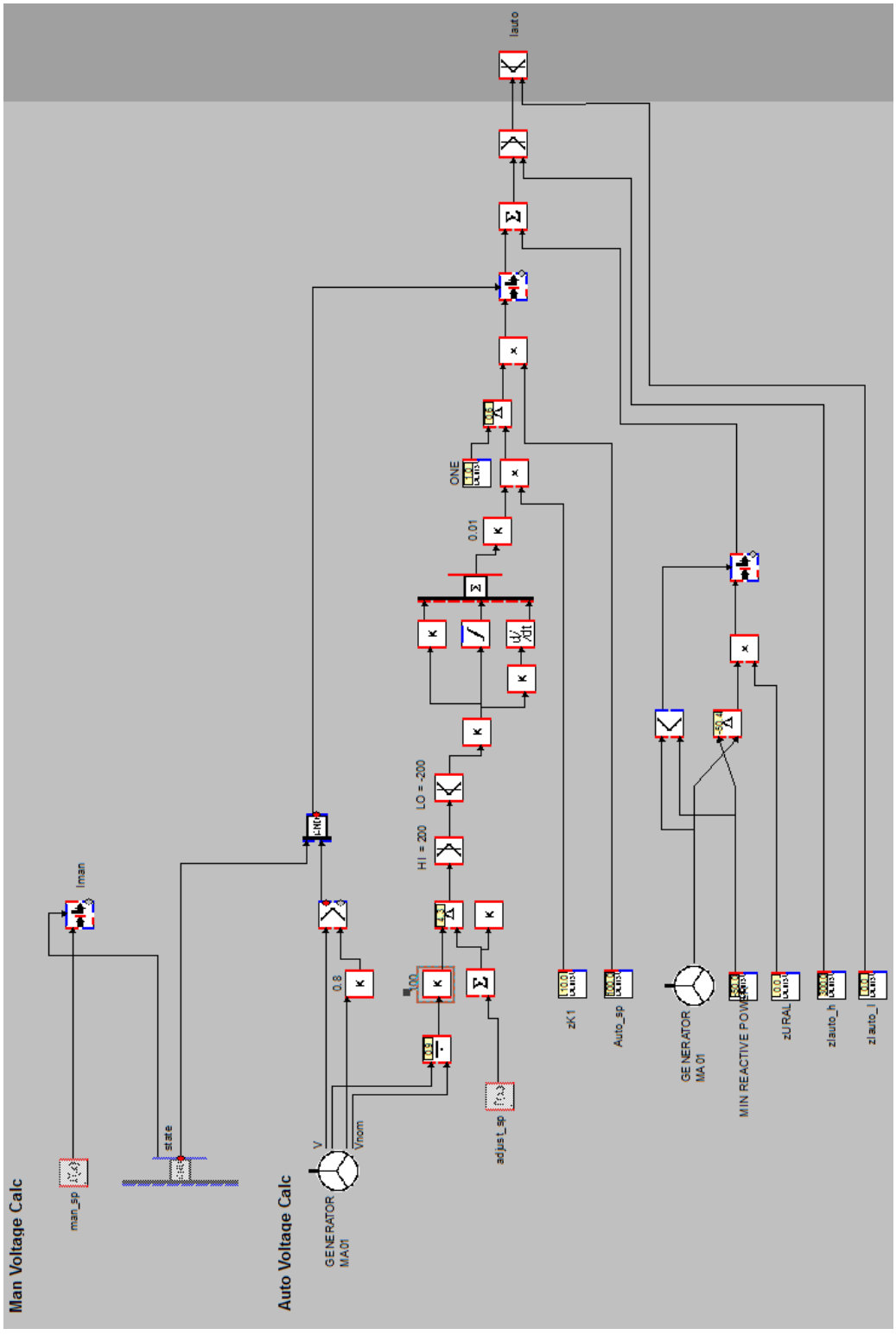

Figure 6.1: *ctrl* model page with PID compensator implemented

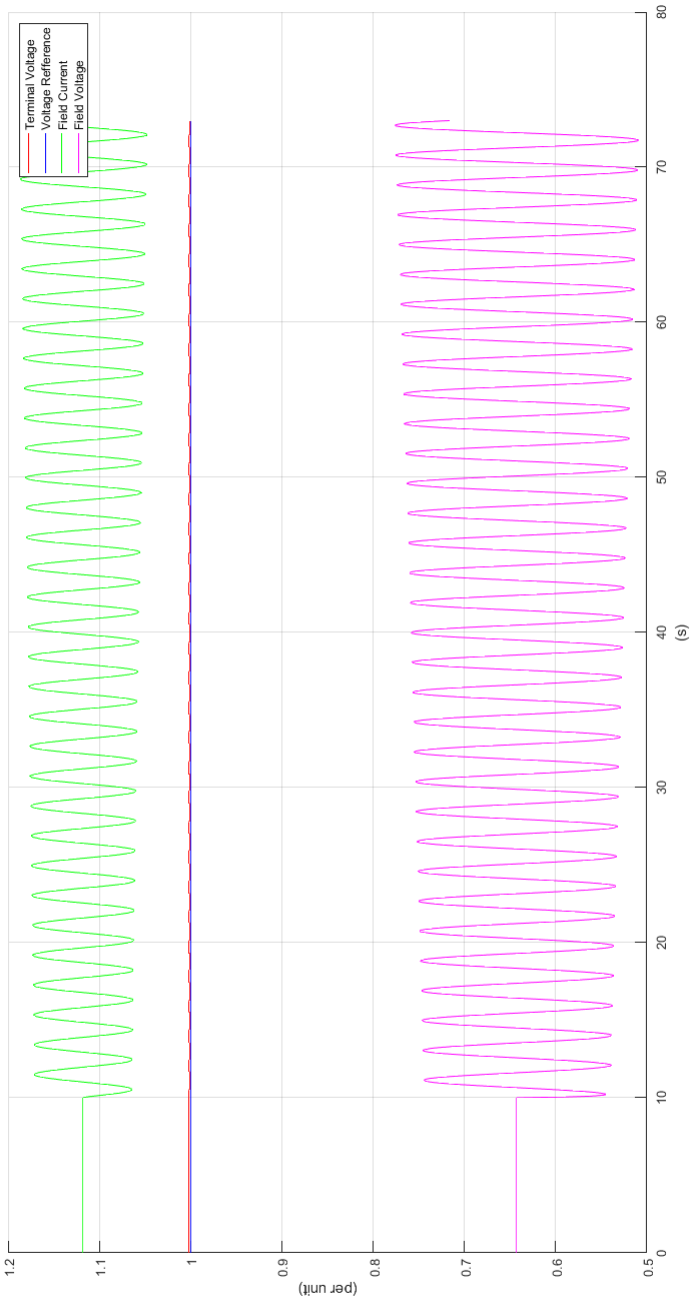

Figure 6.2: Sustained oscillation of exciter parameters under critical gain

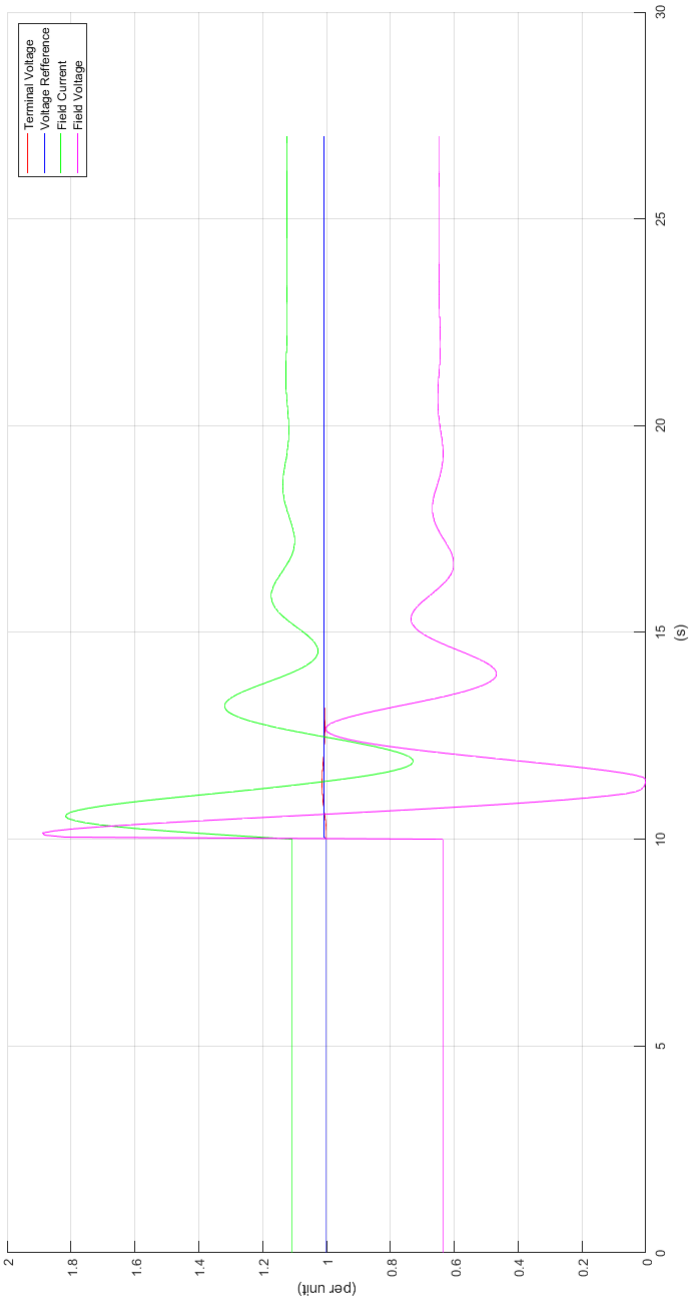

Figure 6.3: System response to 0.8% reference step command with PID compensator

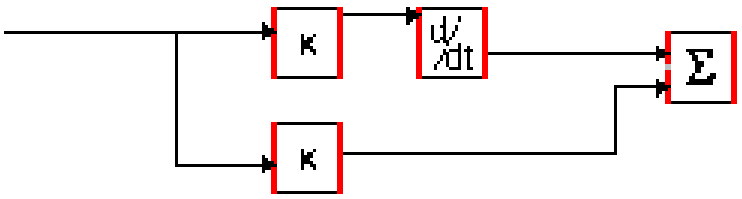

Figure 6.4: Real zero implemented in simulation

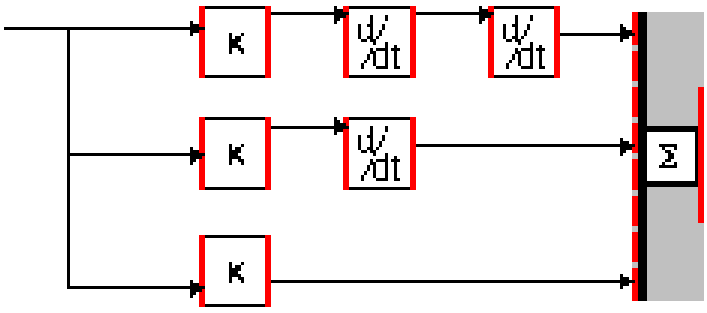

Figure 6.5: Two zeros implemented in expanded form

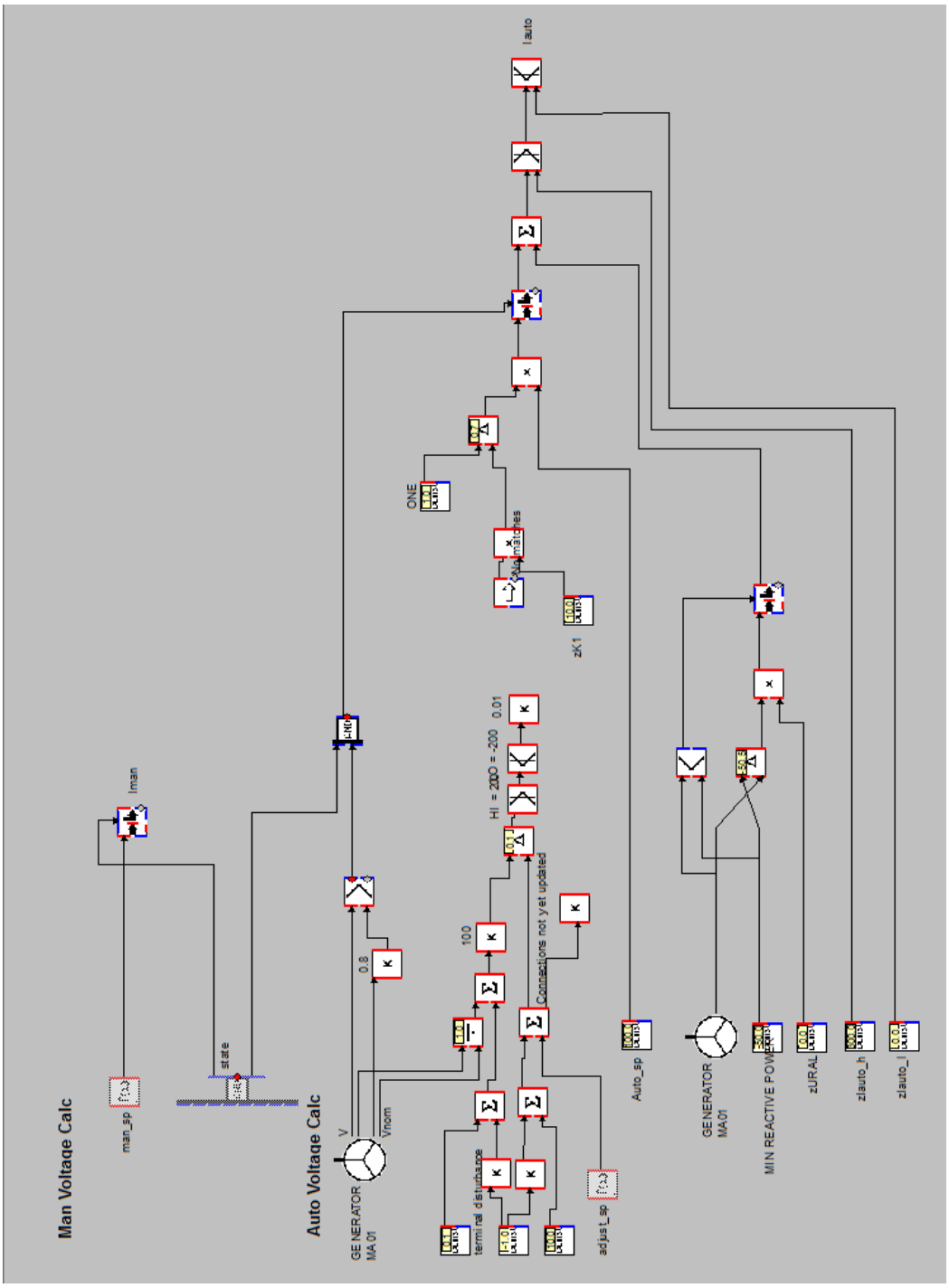

Figure 6.6: Modification to the simulator ctrl page

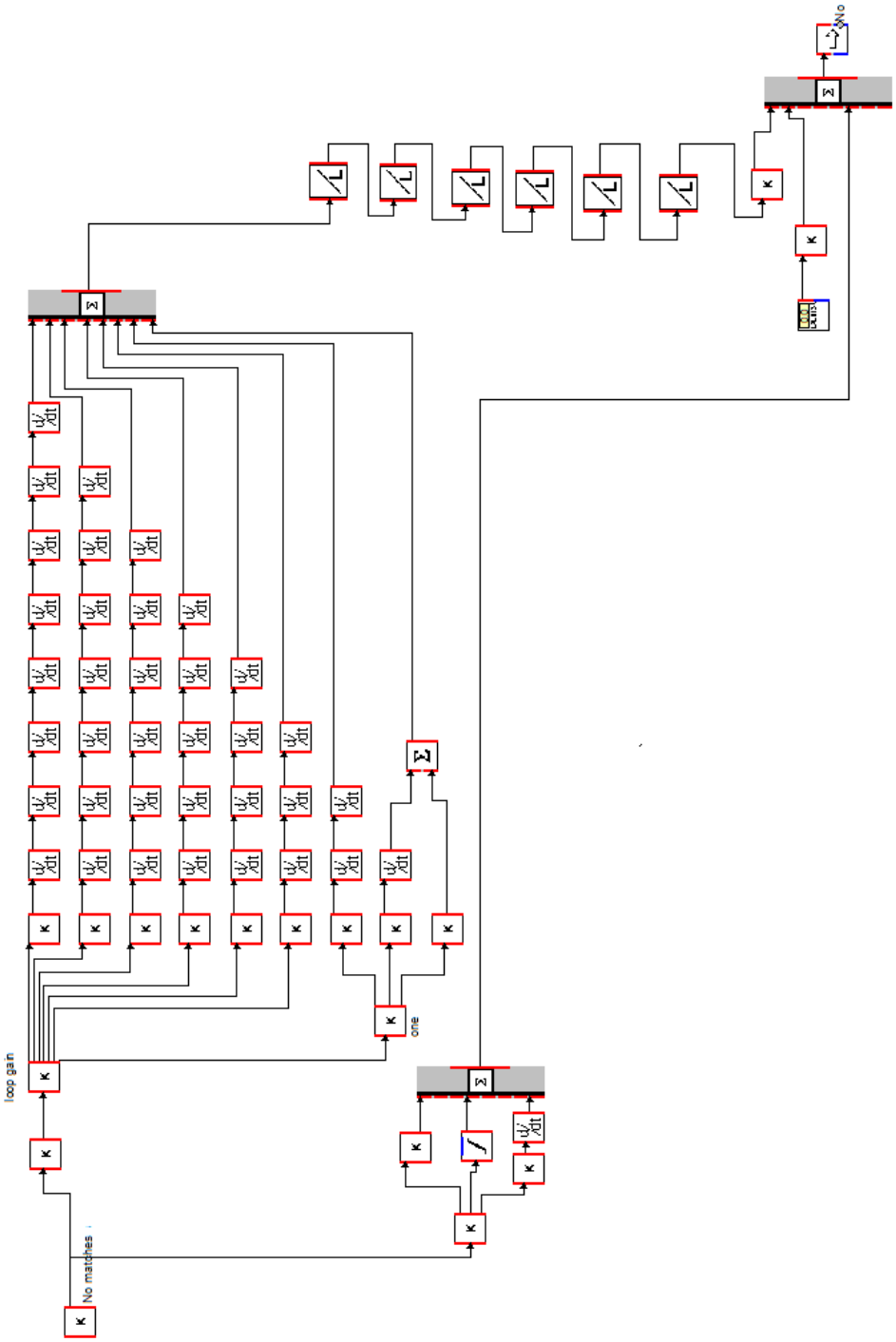

Figure 6.7: MBO AVR as implemented in the WSC simulator

Chapter 7: Simulation Results

With the Modified Bode Optimal (MBO) compensator fully realized within the Western Services Corporation (WSC) simulation model it is now possible to perform testing to assess the compensator performance. The sophistication and utility presented by the WSC simulator provides the opportunity to test the compensator under a variety of conditions. Additionally, the modelling of the local distribution network permits the testing of the excitation system performance during sudden load changes. In typical academic studies system models are not of sufficient fidelity to perform such tests. In industrial settings it is typically unfeasable to perform such testing due to the undesirable effects on the wider Bulk Power System (BPS).

Before testing it is first necessary to discuss the relevant metrics for assessing performance. A survey of the various performance standards used in industry and academia was presented in Chapter 1. There is no consensus between researchers and industry professionals on the definition of "performance" for an excitation control system. Academic literature tends to use integral based performance metrics as these lend themselves readily to use with optimization algorithms. Industry standards tend to focus on more traditional methods of gauging performance for feedback systems, which include both time and frequency domain metrics.

Typically, step responses are used for assessing system behavior in the time domain. In the frequency domain, Bode plots and Root-locus plots are used for describing system characteristics. This work was conducted without the benefit of detailed knowledge regarding the frequency response characteristics of the plant. Therefore, describing the performance of the system using frequency domain characteristics is impossible. At best, certain frequency domain characteristics can be estimated based on the system step response. Therefore, it was decided to characterize system performance consistent with the time domain step response metrics as outlined in IEEE standards [26, 33].

7.1 Initial Testing

To establish a reference for comparison purposes the excitation system as originally implemented in the WSC simulator was tested. In the WSC simulator the field flashing circuit provides a constant excitation signal when the generator is not connected to the BPS. To ensure the excitation system remains within the linear operating range this signal was disabled for no-load testing. System performance is described by the terminal voltage response profile. For the response to be considered "small signal", the testing must maintain the exciter field current and voltage within the bounds of the operating limits imposed by the excitation system protective devices [26]. The system was subjected to a step change in the voltage reference and the response is given by Figure 7.1. The exciter field current and voltage are described by Figure 7.2. The field voltage is described in the exciter per unit system while the field current is given in per unit on the system base (see [1, 26, 33]).

The response of the system with the new MBO Automatic Voltage Regulator (AVR) design was then tested subject to the same disturbance as the default excitation system. This system response is given by Figure 7.3. The response of the exciter parameters is given in Figure 7.4.

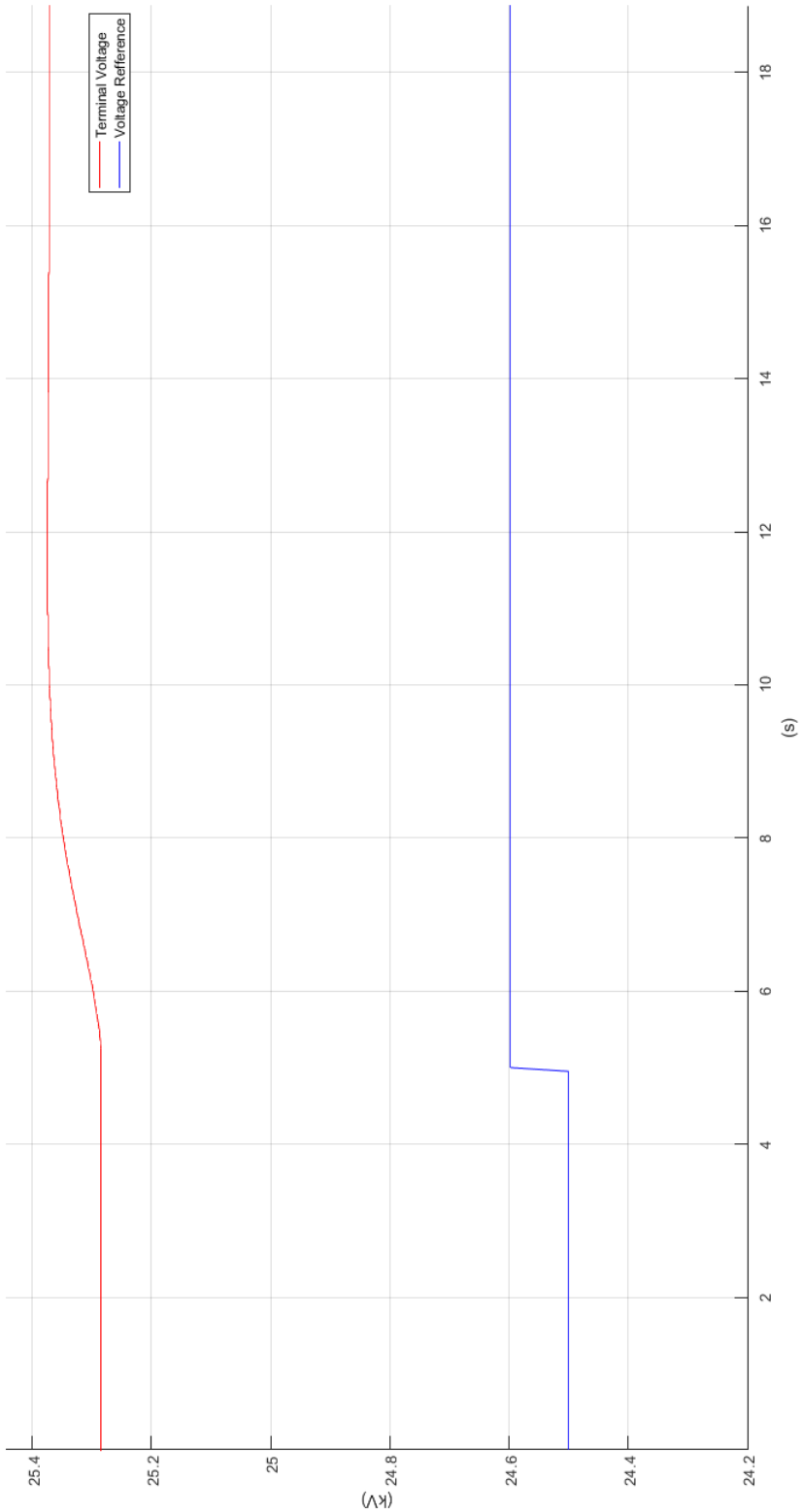

Figure 7.1: Terminal voltage response, default AVR, no load.

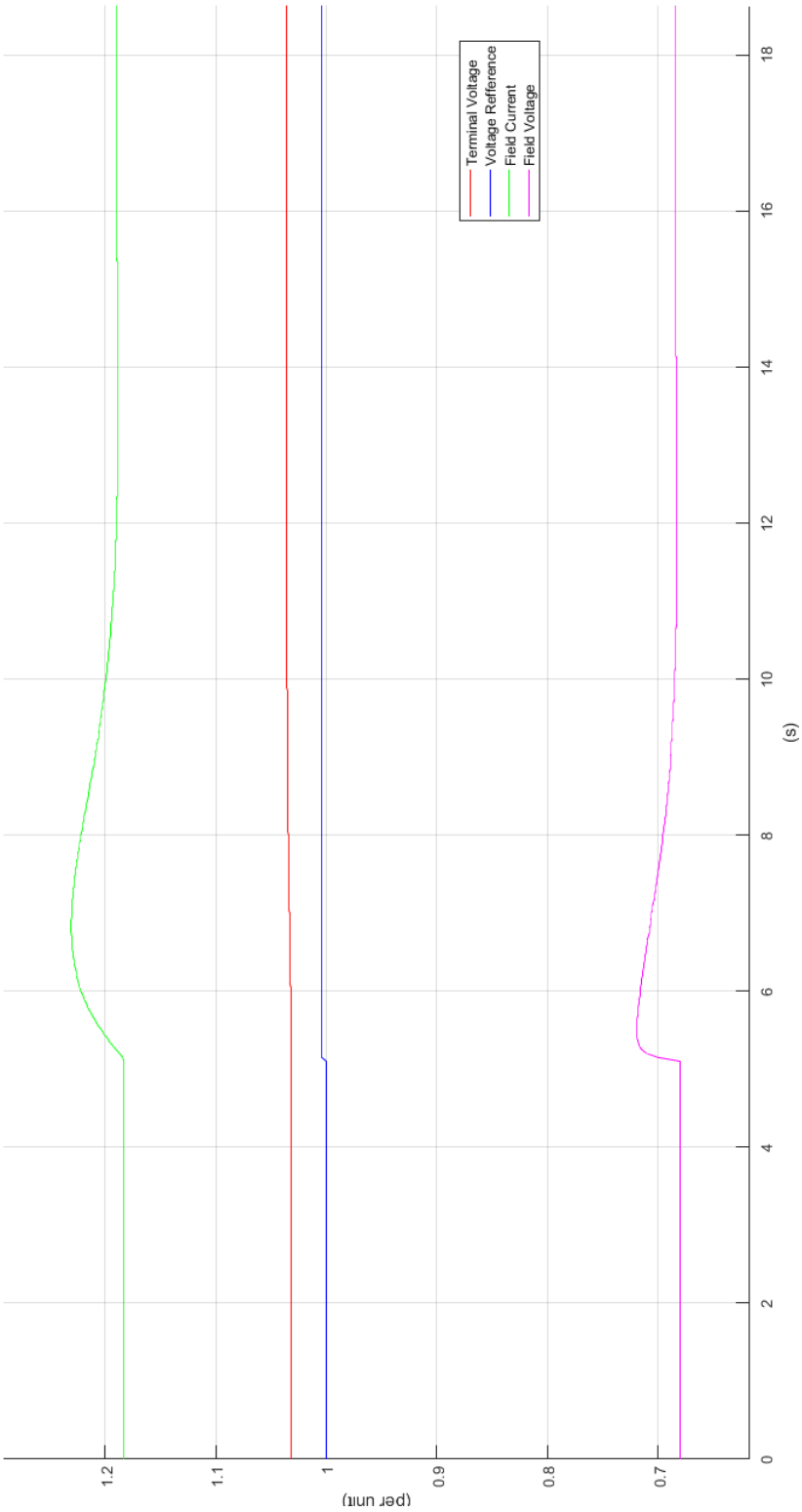

Figure 7.2: Excitation system response, default AVR, no load

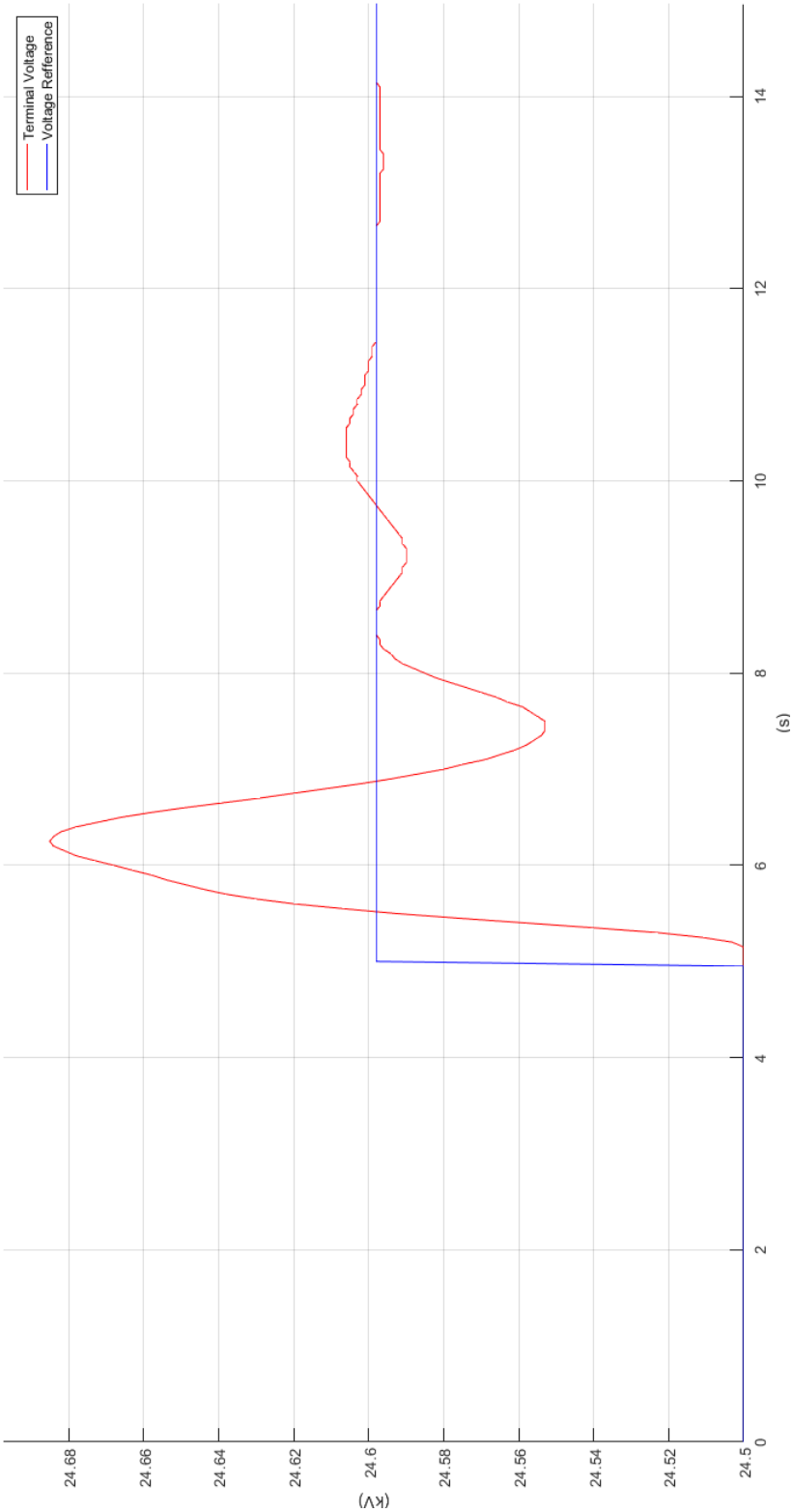

Figure 7.3: Response to 0.4% reference step with MBO compensator (no load)

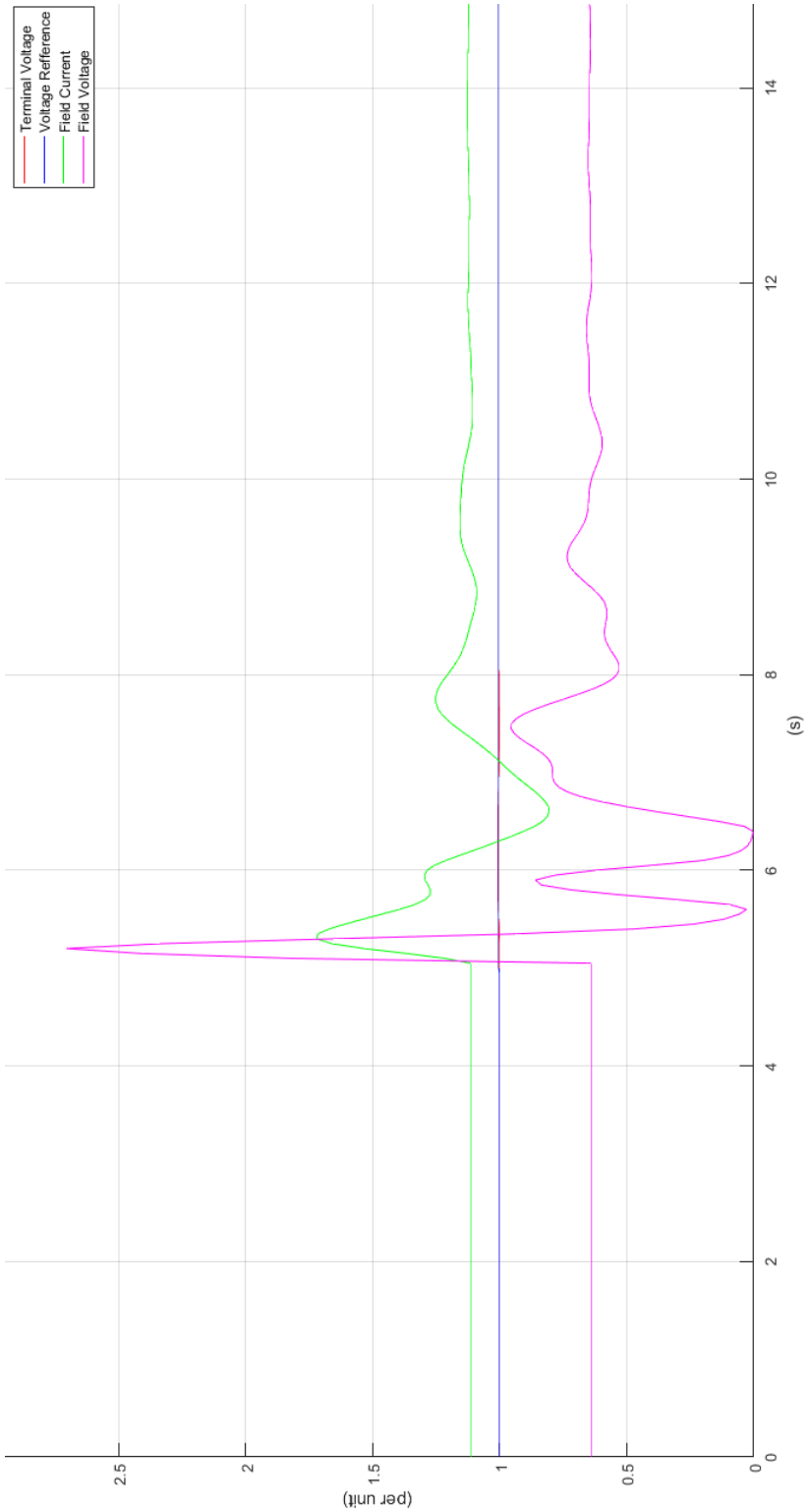

Figure 7.4: Response to 0.4% reference step with MBO compensator (no load)

7.2 Compensator Revisions

The stability of the design was verified by testing the system response when operating under nominal conditions. The simulation was modified to reflect the generating station delivering rated load from the generator terminals. The field flashing circuit was re enabled for the loaded condition although it provides no signal during regular operation. Testing of the MBO compensator under loaded condition reveals the presence of an unstable oscillation. The moment the compensator is switched into service an oscillation begins to build in the excitation system parameters. This response is shown in Figure 7.5.

The period of the unbounded oscillation is 5.5 s. This indicates the system possesses an insufficient phase margin at 0.18 Hz or $1.1\frac{rad}{s}$ which is below the crossover frequency for which the system was designed. The system was stabilized by increasing loop gain $6dB$. This behavior strongly implies the oscillation is due to a resonant mode in the power system which is insufficiently damped at this frequency. The pressence of the instability renders the initial compensator design invalid. The solution to this problem is to apply additional feedback at the modal frequency. The fact that the response is stable with the increased gain implies there is room to increase the crossover frequency upon which the design is built (ω_b). Because the slope of the response is $-10\frac{dB}{oct}$ at frequencies near crossover, doubling the crossover frequency will apply an additional $10dB$ of feedback at the modal frequency. The new compensator is given by the following:

$$c_0'(s) = (s + 0.0092)(s^2 + 2(0.4)(0.0092)s + 0.0000846) \tag{7.1}$$

$$c_{bsc}'(s) = (s^2 + 2(0.4)(16.964)s + 287.791) \tag{7.2}$$

$$z_{s1}'(s) = (s^2 + 2(0.4)(0.0368)s + 0.0014) \tag{7.3}$$

$$z_{s2}'(s) = (s^2 + 2(0.4)(2.3562)s + 5.552) \tag{7.4}$$

$$c_{bsd}'(s) = (s^2 + 2(0.4)(9.4247)s + 88.8242) \tag{7.5}$$

$$\frac{c_z'(s)}{c_p'(s)} = \frac{(s + 2.356)(s + 0.2945)}{(s + 4.712)(s + 0.589)(s + 0.0736)} \tag{7.6}$$

And the new compensator is:

$$C'_{MBO}(s) = 80.673\frac{(s+2.36)(s+0.295)(s^2+2(0.4)(0.0368)s+0.00135)}{(s+4.71)(s+0.589)(s+0.0736)(s^2+2(0.4)(17)s+289)}\cdots \\ \cdots\frac{(s^2+2(0.4)(2.36)s+5.569)(s^2+2(0.4)(9.42)s+88.736)}{(s+0.0092)(s^2+2(0.4)(0.0092)s+0.0000846)} \quad (7.7)$$

With the implemented form:

$$C'_{MBO}(s) = 42946... \\ \cdots\frac{(s^8+12.1s^7+134.6s^6+507.6s^5+1138s^4}{(0.212s+1)(1.698s+1)(13.587s+1)(108.7s+1)}\cdots \\ \cdots\frac{+1486s^3+386.5s^2+12.05s+0.4638)}{(s^2+2(0.4)(0.0092)s+0.0000846)(s^2+2(0.4)(17)s+289)} \quad (7.8)$$

Applying this compensator design results in an unstable oscillation corresponding to the crossover frequency of the system. Attempts to gain stabilize this oscillation succeed only in changing the frequency of the oscillation. This behavior implies that the phase delay in the neighborhood of the new crossover frequency is excessive. The crossover frequency derived from the Proportional Integral Derivative (PID) compensator is therefore assumed to be an absolute limit. Therefore, the algorithm is reset back to the original crossover frequency. To compensate for the unstable 0.18 Hz mode, the natural frequency of polynomial $z_{s2}(s)$ is reduced by one octave. This provides additional phase at the frequencies just below crossover without compromising the phase margin. The revised compensator is:

$$C'_{MBO}(s) = 57.598\frac{(s+1.178)(s+0.1473)(s^2+0.01473s+0.0003388)}{(s+2.356)(s+0.2945)(s+0.03682)(s+0.004602)}\cdots \\ \cdots\frac{(s^2+0.4712s+0.347)(s^2+3.77s+22.21)}{(s^2+0.003682s+2.118*10^{-05})(s^2+6.786s+71.95)} \quad (7.9)$$

And the implemented form is:

$$C'_{MBO}(s) = 489912\frac{s^8+5.581s^7+30.21s^6+45.2s^5+28.2s^4}{(0.424s+1)(3.396s+1)(27.16s+1)(217.3s+1)}\cdots \\ \cdots\frac{+12.67s^3+1.526s^2+0.02384s+0.0004529}{(s^2+2(.4)(0.0046)s+2.118*10^{-5})(s^2+2(0.4)(8.48)s+71.95)} \quad (7.10)$$

This compensator has much better performance under load, however there is still a slowly building oscillation at 0.1 Hz. This implies that although the phase margin has been improved considerably the phase delay at frequencies just below crossover is still excessive. The damping in polynomial z_{s2} is 0.4

which provides for a rapid phase transition at the natural frequency. To improve the phase characteristics of the system below crossover the damping of polynomial $z_{s2}(s)$ is increased to distribute the phase advance over a wider range of frequencies near the natural frequency. This adjustment results in the following compensator:

$$C'_{MBO}(s) = 57.234\frac{(s+1.178)(s+0.1473)(s^2+0.01473s+0.0003388)}{(s+2.356)(s+0.2945)(s+0.03682)(s+0.004602)}\cdots \\ \cdots\frac{(s^2+0.7068s+0.347)(s^2+3.77s+22.21)}{(s^2+0.003682s+2.118*10^{-5})(s^2+6.786s+71.95)} \quad (7.11)$$

Which is implemented as:

$$C'_{MBO}(s) = 486800\frac{s^8+5.817s^7+31.41s^6+51.67s^5+35.38s^4}{(0.424s+1)(3.396s+1)(27.16s+1)(217.3s+1)}\cdots \\ \cdots\frac{+13.69s^3+1.542s^2+0.02414s+0.0004529}{(s^2+2(.4)(0.0046)s+2.118*10^{-5})(s^2+2(0.4)(8.48)s+71.95)} \quad (7.12)$$

This variation results in a stable compensator in loaded condition, however when tested under no load the compensator is unstable. Again the unstable frequency is observed to be 0.1 Hz. The compensator is stabilized for the unloaded condition by doubling the compensator gain. The resonant frequency for $z_{s2}(s)$ is reduced by additional octave, and the factor of 2 in the gain is retained. This compensator is designed to provide 40° phase margin, 10 dB gain margin, with 120 dB of feedback at low frequencies and 20 dB of feedback at the problematic 0.1 Hz frequency. This compensator is of the form:

$$C'_{MBO}(s) = 114.1\frac{(s+1.178)(s+0.1473)(s^2+0.01473s+0.0003388)}{(s+2.356)(s+0.2945)(s+0.03682)(s+0.004602)}\cdots \\ \cdots\frac{(s^2+0.3534s+0.08674)(s^2+3.77s+22.21)}{(s^2+0.003682s+2.118*10^{-5})(s^2+6.786s+71.95)} \quad (7.13)$$

And is implemented in the simulation as:

$$C'_{MBO}(s) = 970500\frac{s^8+5.463s^7+29.34s^6+40.63s^5+17.46s^4}{(0.424s+1)(3.396s+1)(27.16s+1)(217.3s+1)}\cdots \\ \cdots\frac{+4.233s^3+0.3984s^2+0.006267s+0.0001132}{(s^2+2(.4)(0.0046)s+2.118*10^{-5})(s^2+2(0.4)(8.48)s+71.95)} \quad (7.14)$$

This compensator is stable for both loaded and unloaded conditions.

7.3 Testing Revisited

Once the stable compensator was found the response was tested for the loaded condition. The system remains within the linear region of operation for a step change in the reference signal of 0.8%. This system response is given by Figure 7.6. The excitation voltage and field current are shown in Figure 7.7.

For comparison the compensator was again disconnected and the response of the default excitation system to the same disturbance was tested. The terminal response profile is given by Figure 7.8. This excitation system response is given by Figure 7.9.

To evaluate the no-load response, the simulation was reset to the no-load condition and the revised MBO design was reenabled. The system response was again tested for a terminal voltage reference step change of 0.8%. This response is given by Figure 7.10. The response of the excitater parameters is given by Figure 7.11.

Because the final MBO design was tested for a reference step change of 0.8% instead of the 0.4% step change used for the first design the default system no-load response must be retested with the same signal to make an accurate comparison. The voltage response profile is given by Figure 7.12. The response of the excitater parameters is given by Figure 7.13.

The above information is sufficient to quantify compensator performance in terms of parameters consistent with those used in literature as well as those standard in industry specifications. However, these results do not provide an intuitive sense of the system performance during practical contingency events which affect regular operation of power system devices. The BPS is a complex system with active and reactive loads constantly being switched in and out of service at various points throughout the system. These changes present to the generating station as spontaneous changes in active at reactive power demand at the generator substation [1]. The magnitude of these load changes depends on the magnitude of the load as well as the location of the load relative to the generator substation. Due to the simplified version of the BPS used by the WSC simulator, it was decided to model these changing loading conditions by a simple load consuming varying active and reactive power connected directly to the generator substation bus.

During this testing the generator power setpoint is unaltered and the additional load demand is ultimately supplied by the synchronous machine objects described in Figure 5.8 representing the wider transmission system. The purpose of this test is to demonstrate the ability of the AVR to maintain terminal voltage during the subsequent transient event as the BPS settles into the new operating point. The active load is switched into service at $t = 5$ s. Once the system returns to steady state, the load is removed. The parameters of principle interest are the total time for the system to return to the original operating condition, and the degree of voltage regulation during the event.

First, the generator response to changes in active loads was tested. These loads are representative of any load which consumes active power. The sudden introduction of a large active power demand also mimics the loss of a source of active power somewhere within the BPS such as a generator trip or the loss of an interarea transmission line. The system response was tested for a range of active power changes including the insertion and removal of active loads ranging from 10MW to 1000MW. The response of the generator power output to the insertion and subsequent removal of a 1000Mw load at the distribution substation is given by Figure 7.14. The corresponding voltage profile is given by Figure 7.15. The exciter response is characterized by Figure 7.16

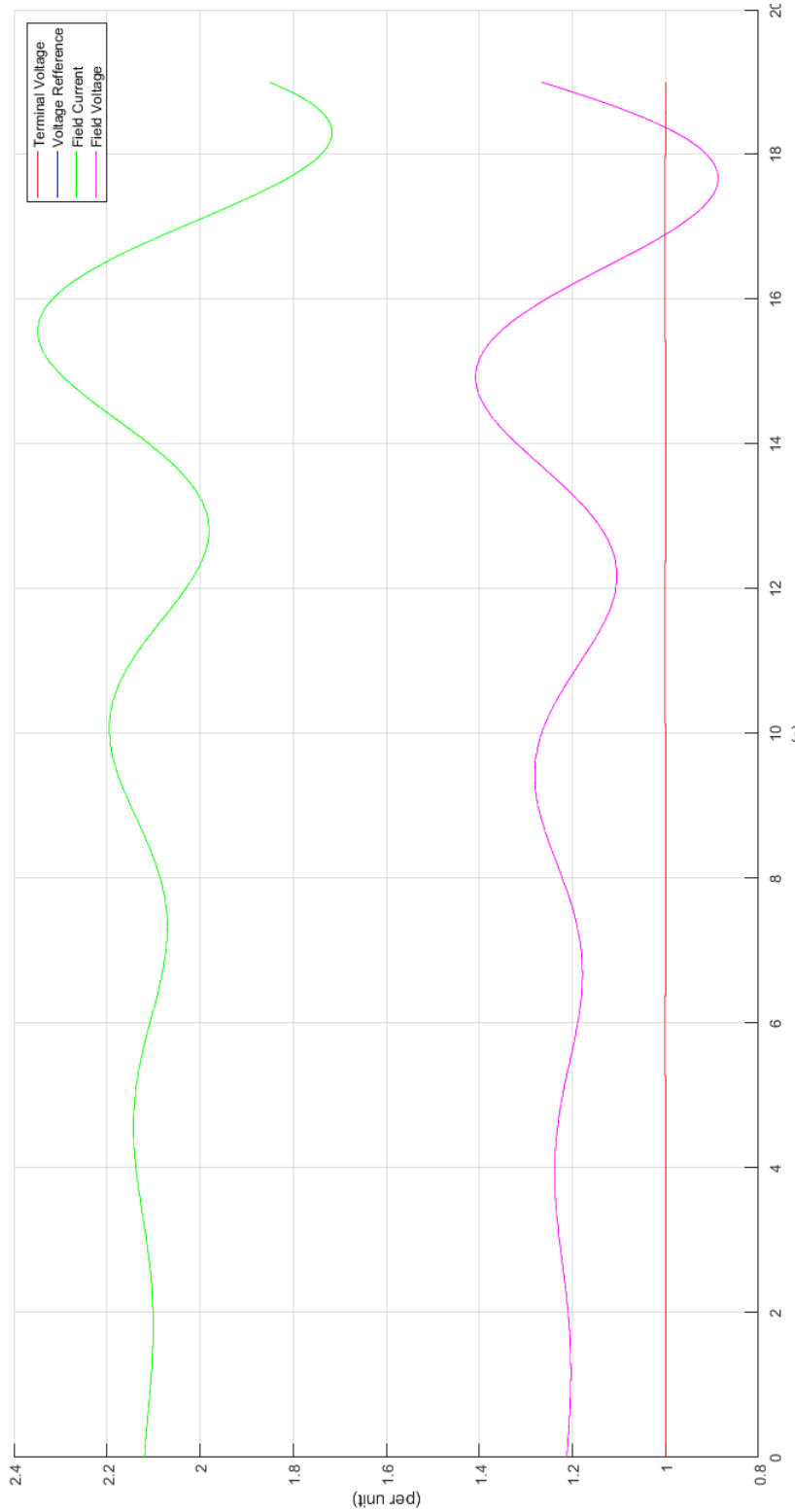

Figure 7.5: Unstable system response under load

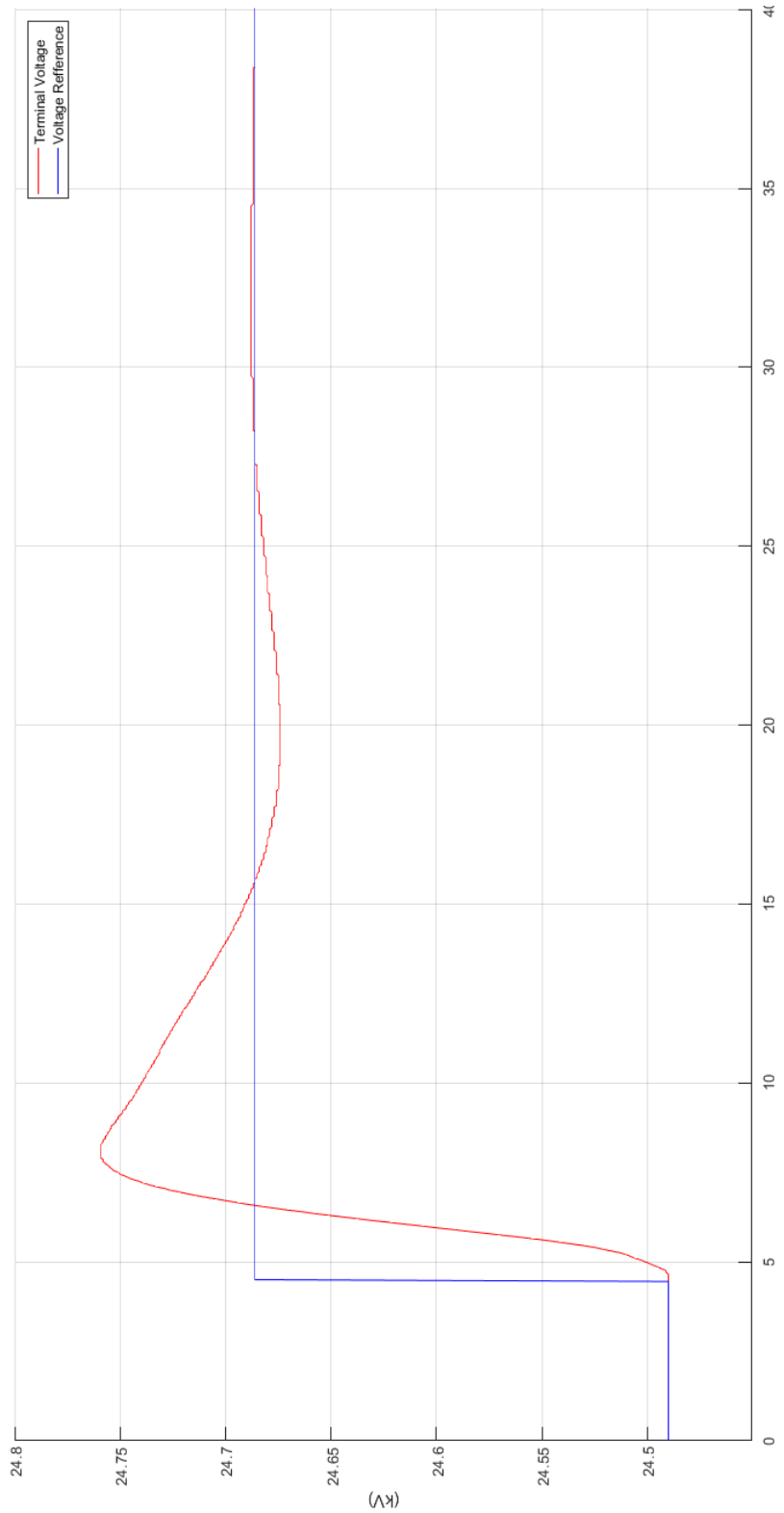

Figure 7.6: Terminal voltage response with MBO AVR (nominal load, 0.8% reference step)

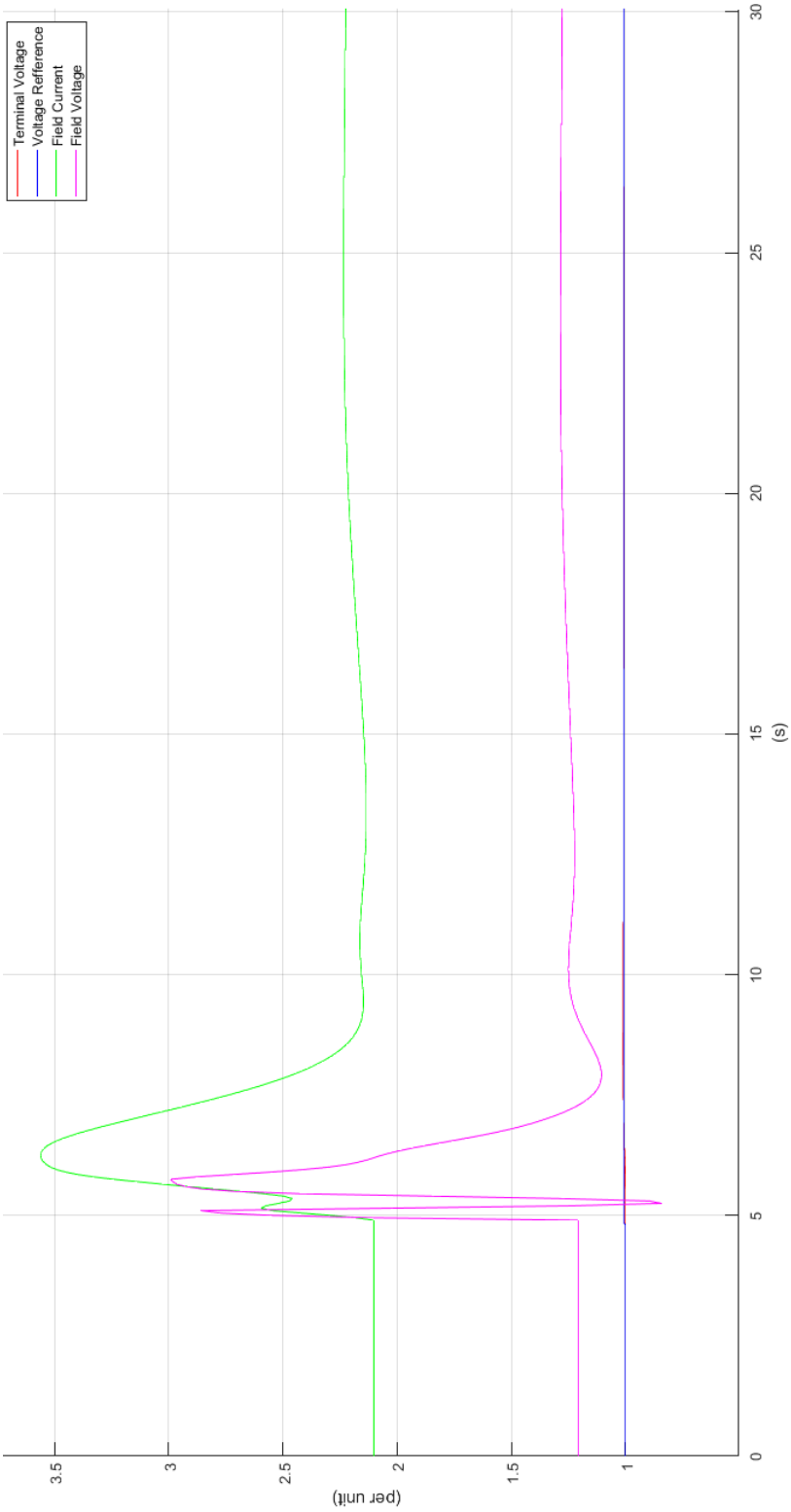

Figure 7.7: Excitation system response with MBO AVR (nominal load, 0.8% reference step)

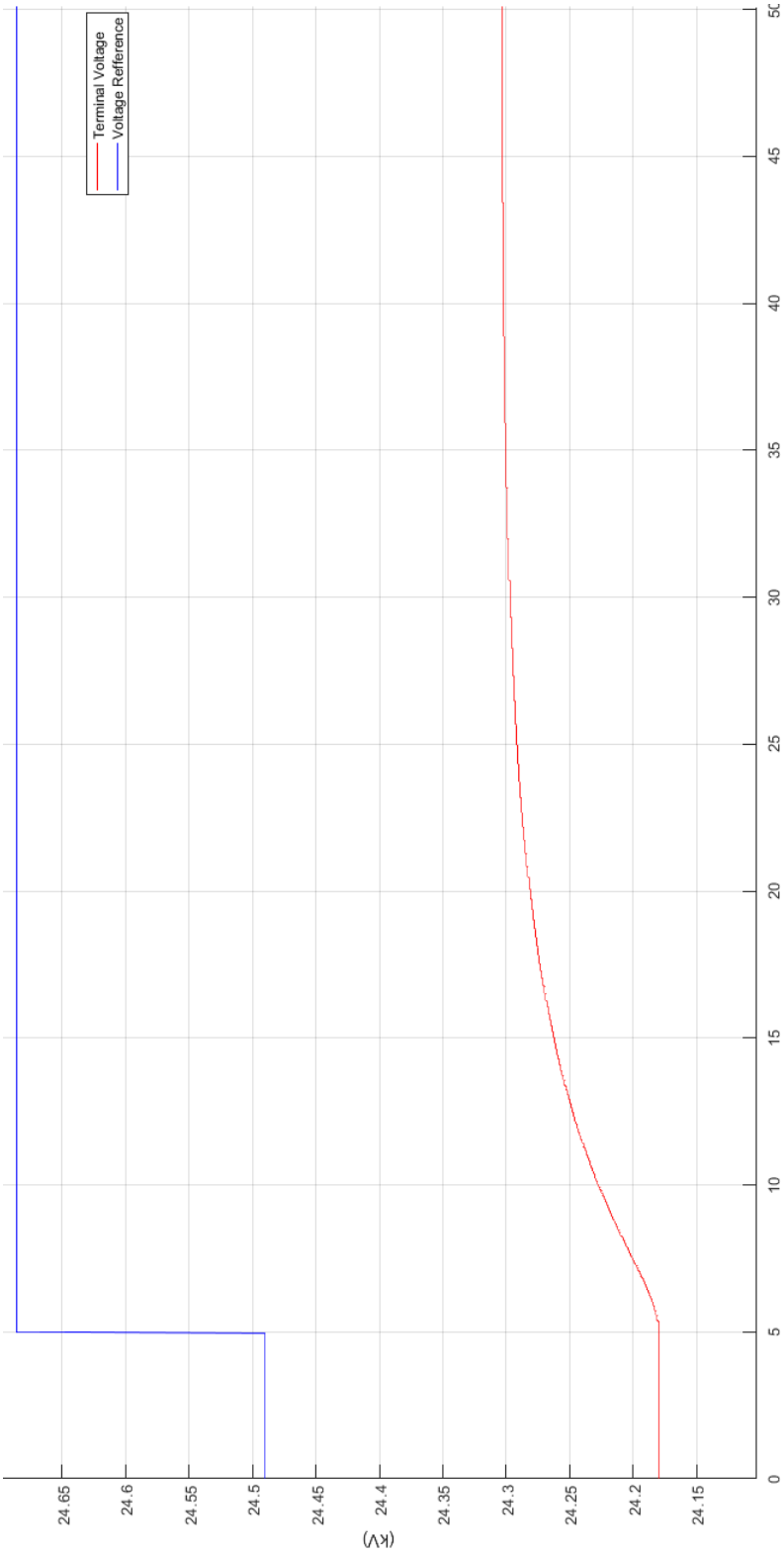

Figure 7.8: Terminal voltage response with default AVR (nominal load, 0.8% reference step change)

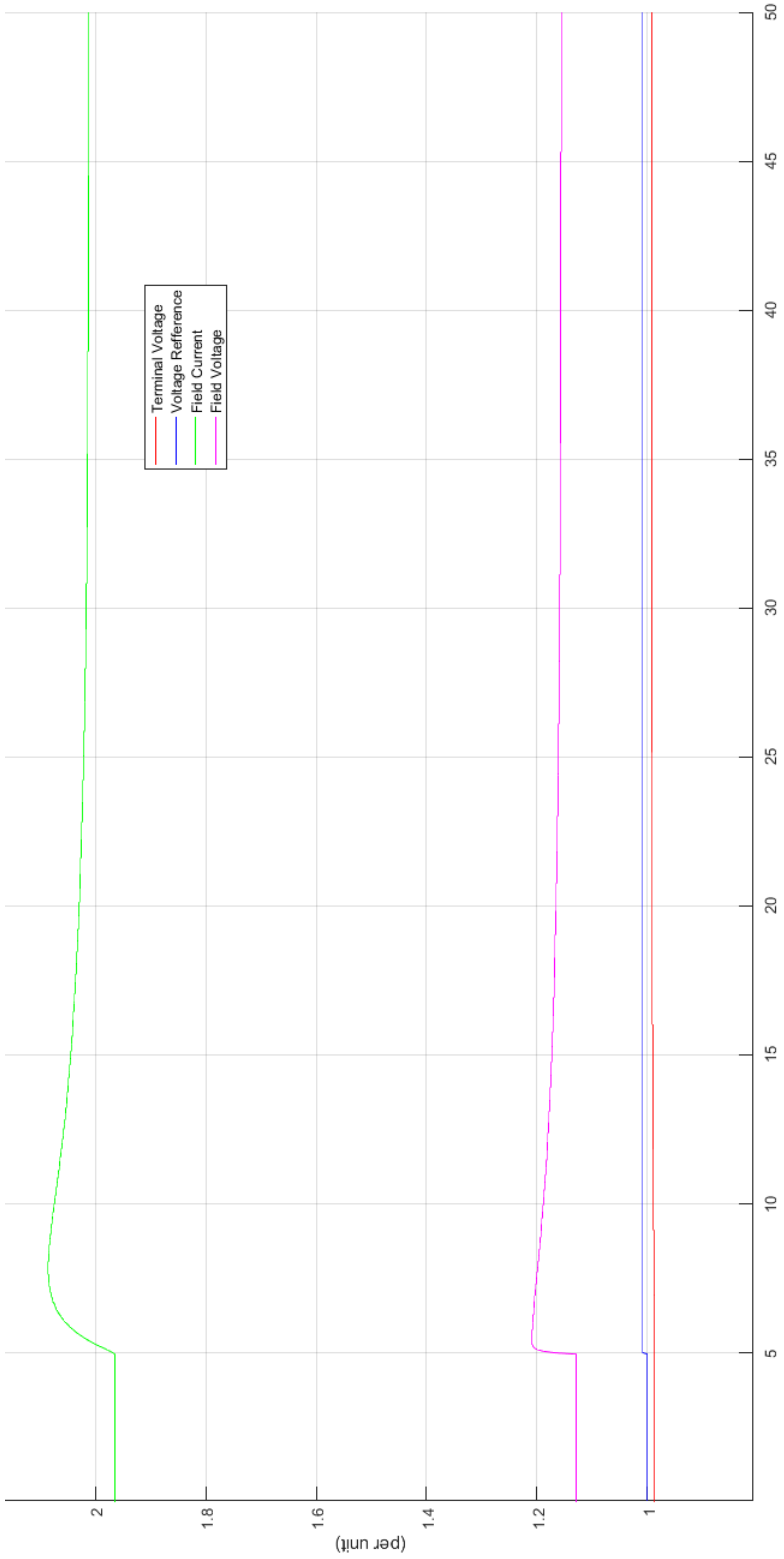

Figure 7.9: Excitation system response with default AVR (nominal load, 0.8% reference step change)

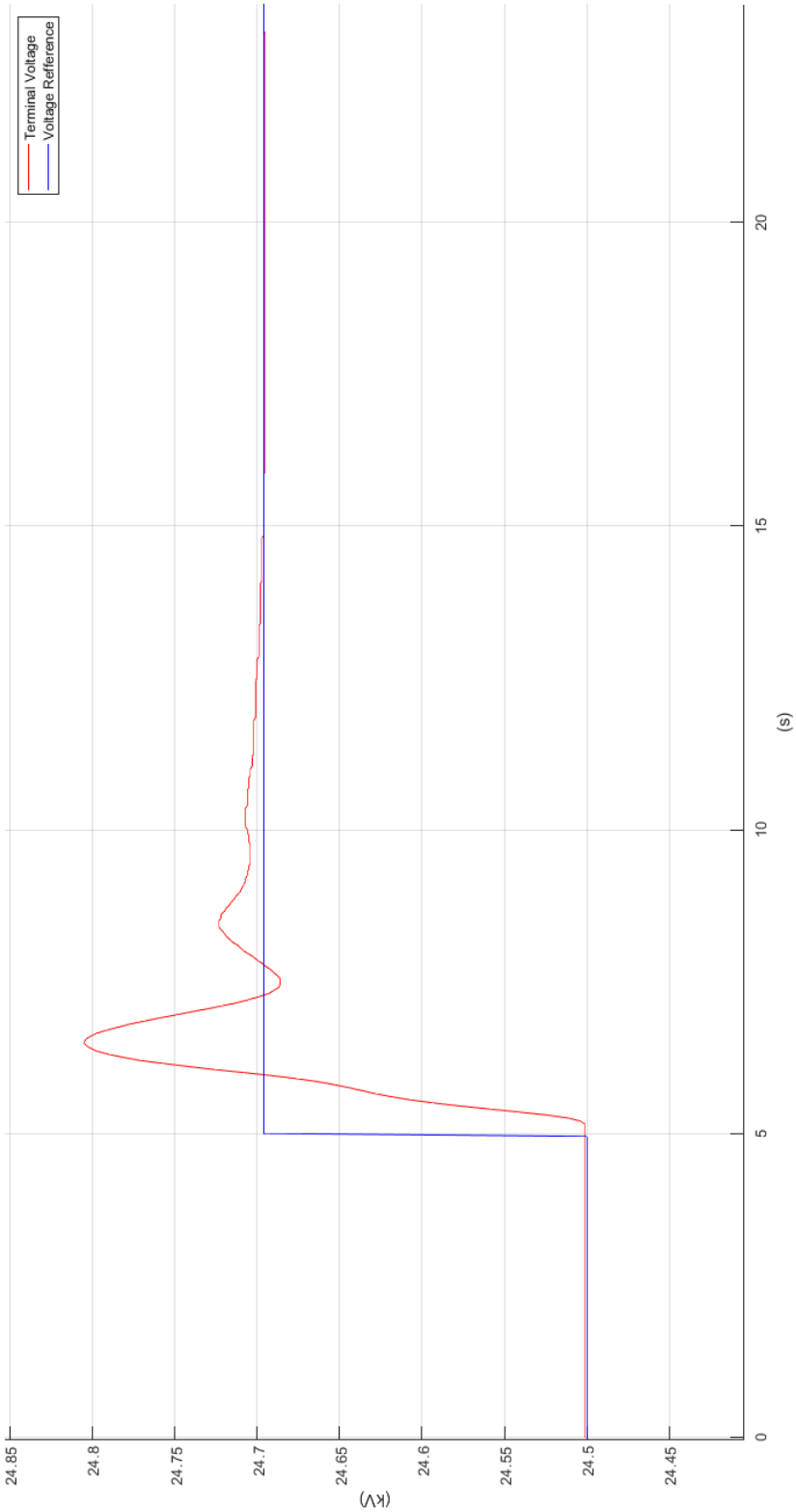

Figure 7.10: Terminal voltage response to 0.8% reference step change (no load)

Figure 7.11: Excitation system response to 0.8% reference step change (no load)

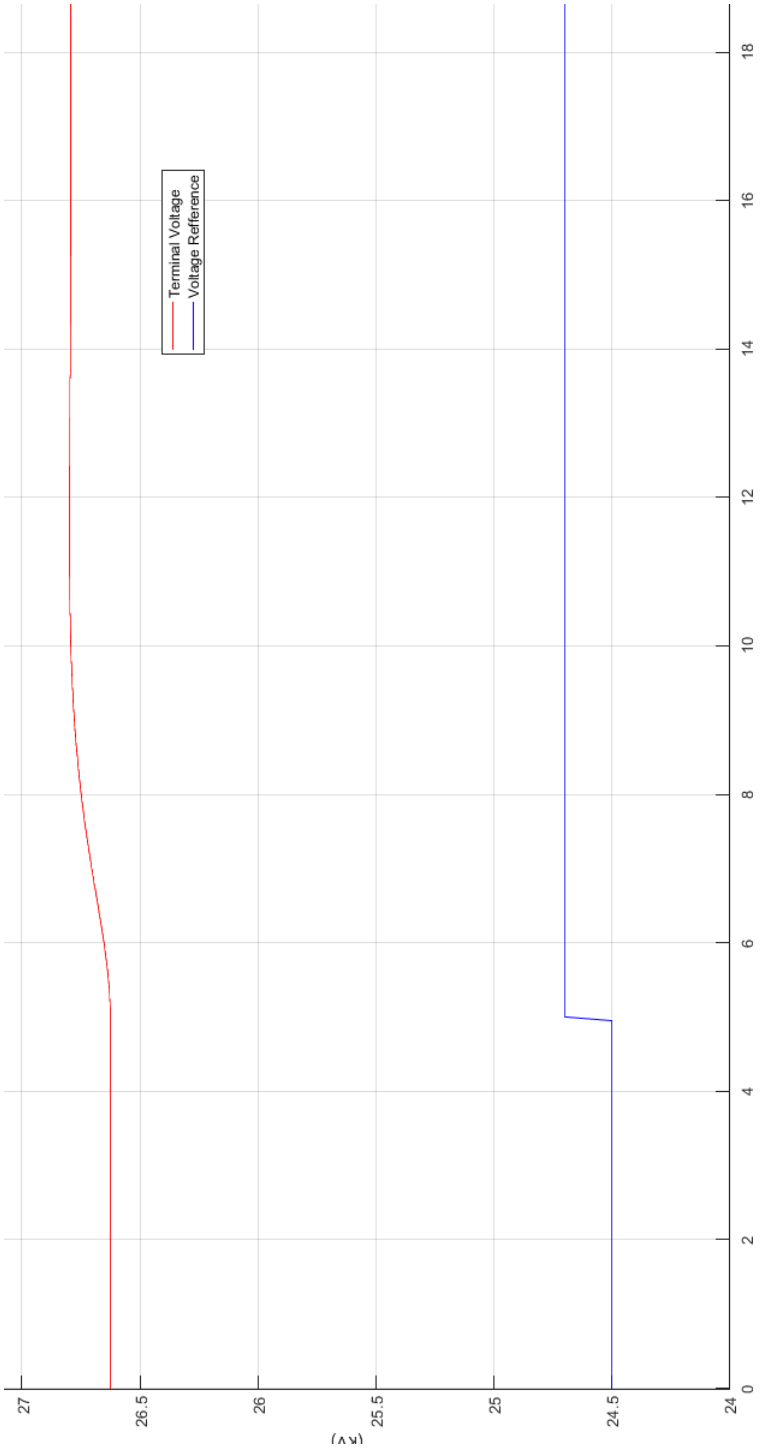

Figure 7.12: Terminal voltage response to 0.8% reference step change (no load)

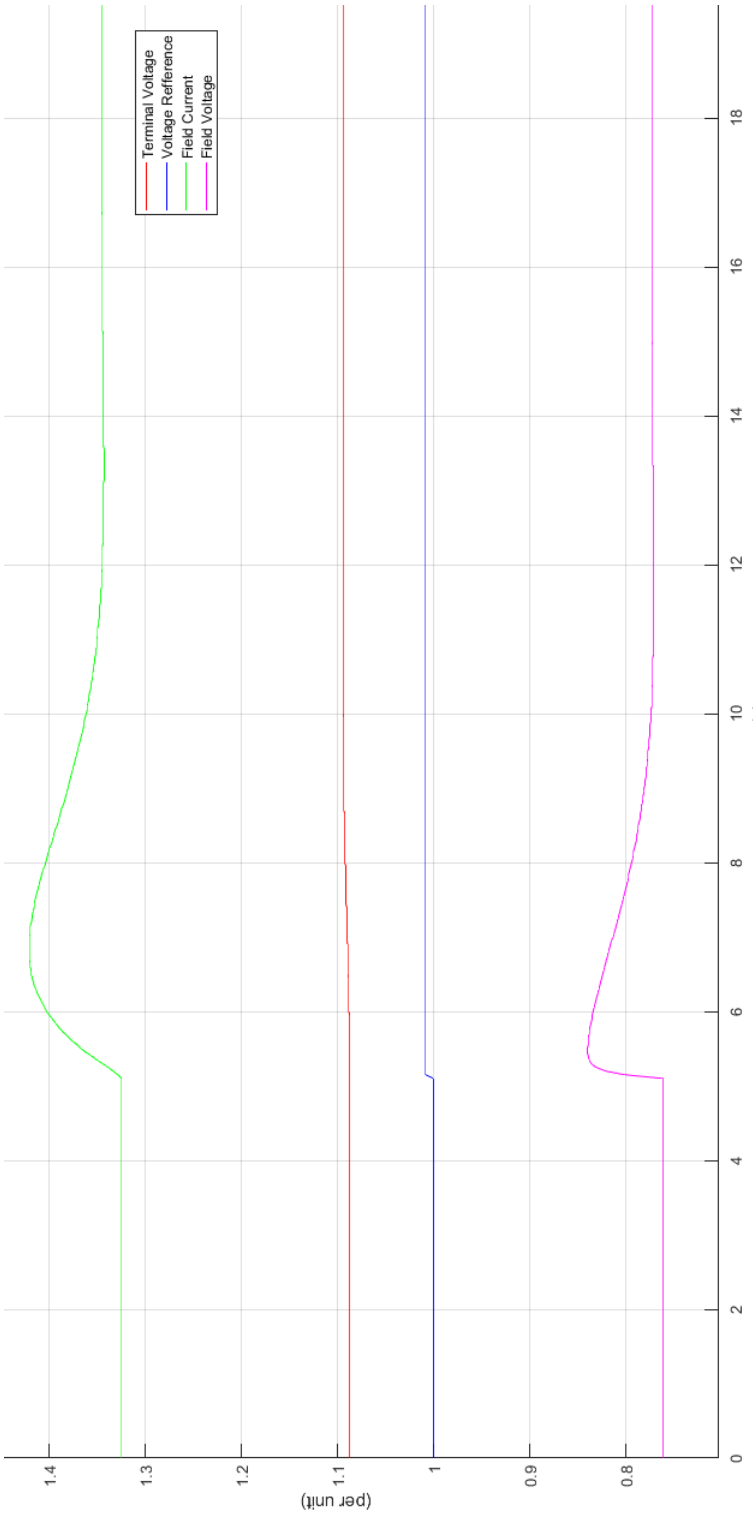

Figure 7.13: Excitation system response to 0.8% reference step change (no load)

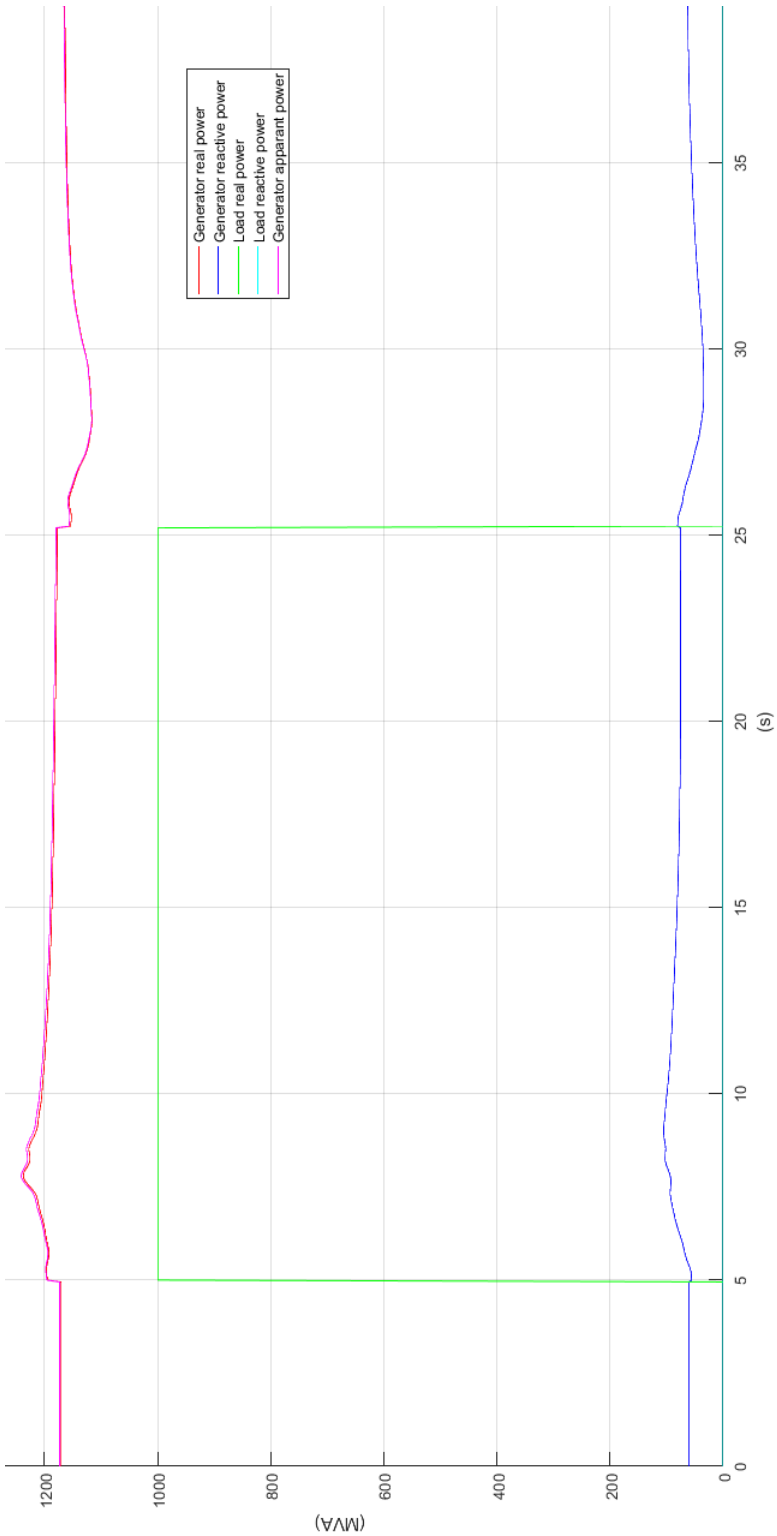

Figure 7.14: Generator output response to load changes with MBO AVR (active, $\pm$1000MW)

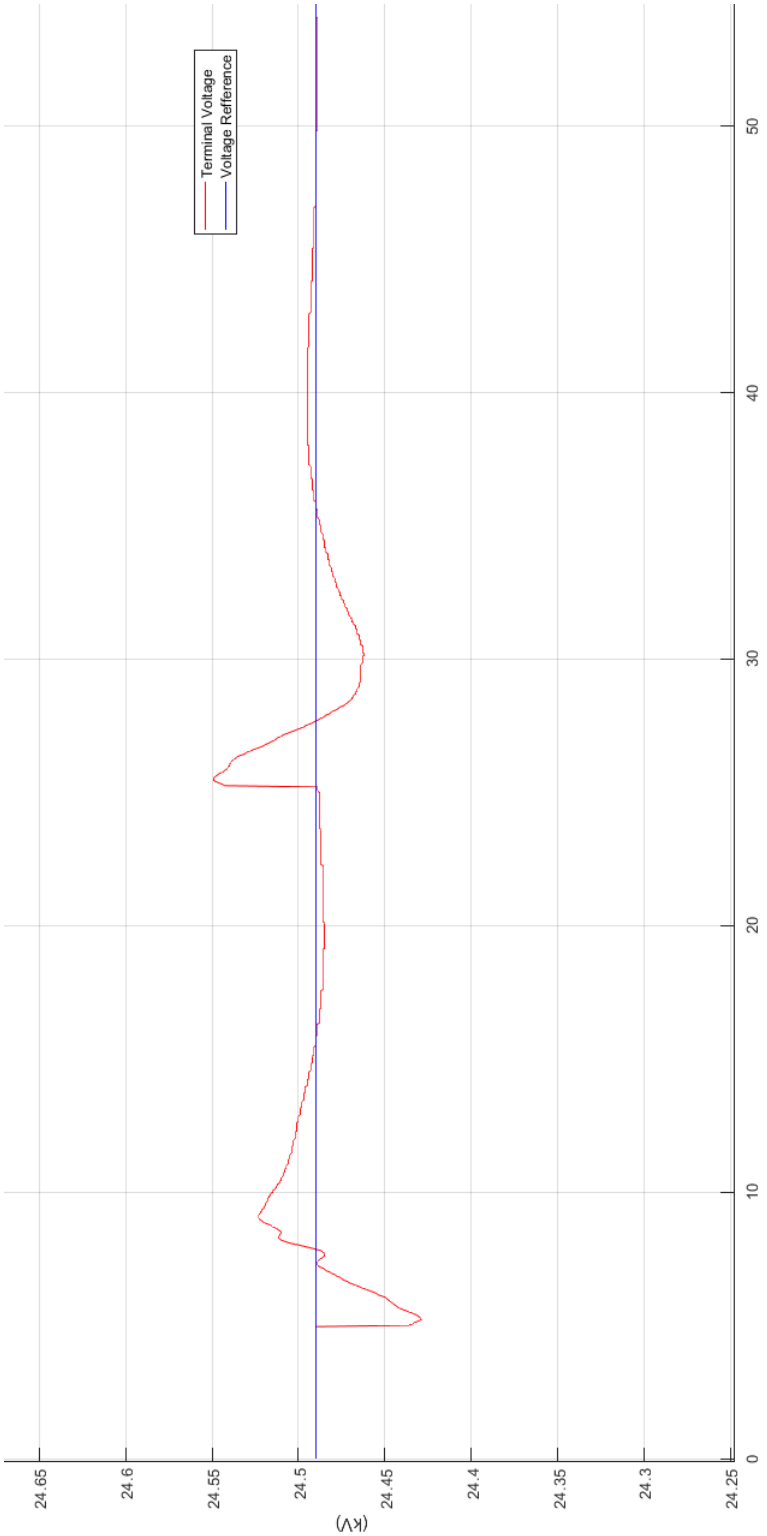

Figure 7.15: Terminal voltage response to load changes with MBO AVR (active, ±1000MW)

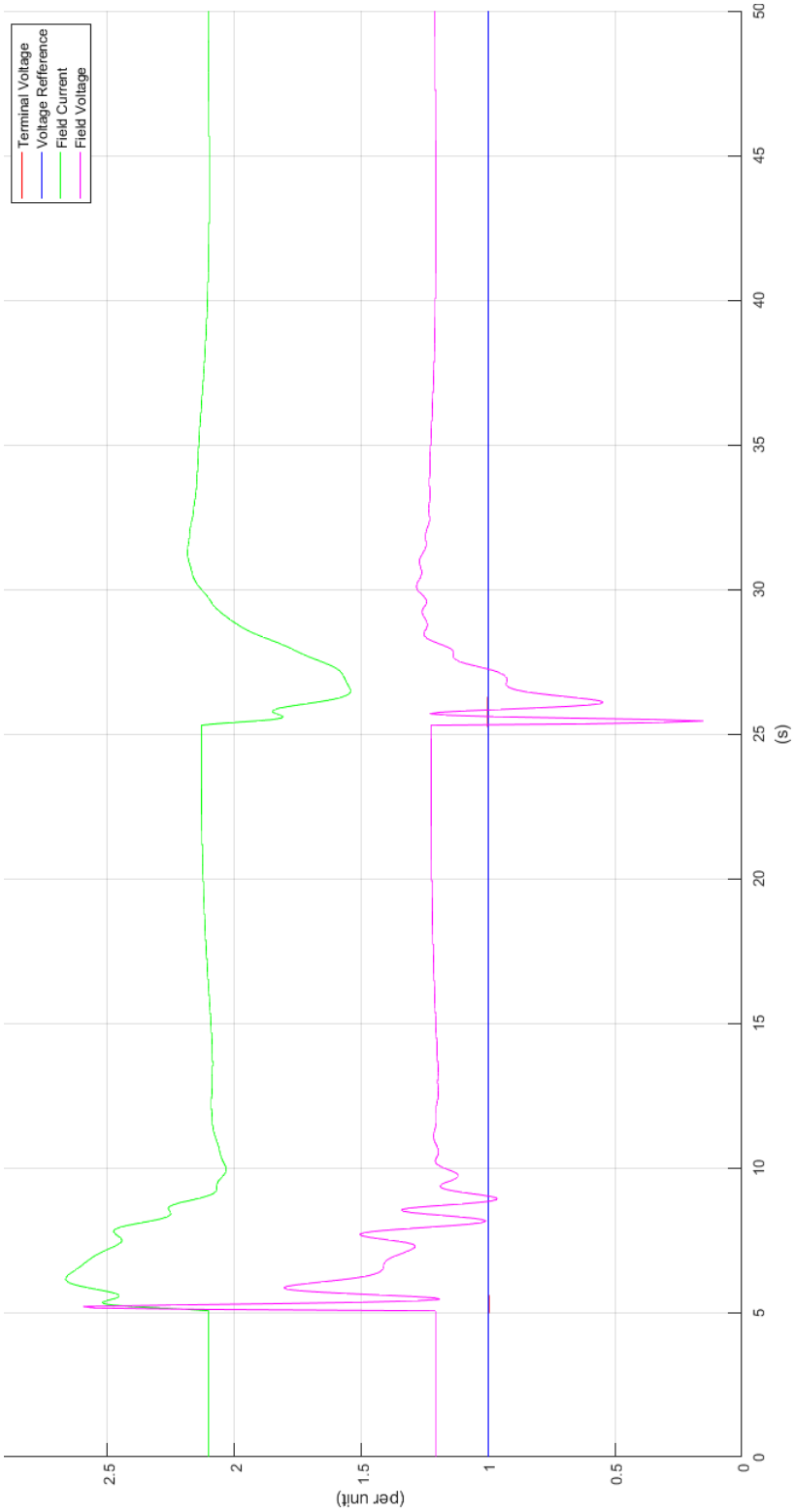

Figure 7.16: Excitation system response to load changes with MBO AVR (active, ±1000MW)

For comparison, the response of the unmodified system is also tested. The generator power output is given by Figure 7.17. The terminal voltage characteristics are given by Figure 7.18. The exciter response is characterized by Figure 7.19.

While active power switching events are fairly regular during power system operation, the changing of reactive loads usually has a more significant impact on power system voltage. This is because the system frequency is related to the flow of active power between rotating machines whereas the system voltage is more closely related to the flow of reactive power [1]. Events which can trigger a sudden change in the demand for reactive power include: 1) the loss of long transmission lines due to the action of protective devices, 2) the starting or stopping of large industrial motors, and 3) the switching of large capacitor banks. Again, these events can be modelled by a sudden change in the demand for reactive power at the generation substation bus. As above, the system response was evaluated by testing the insertion and removal of reactive loads ranging from 10MVAR to 1000MVAR. The terminal voltage response to the more extreme case of 1000MVAR is given by Figure 7.20. The generator power output is given by Figure 7.21. The excitation system response is described by Figure 7.22

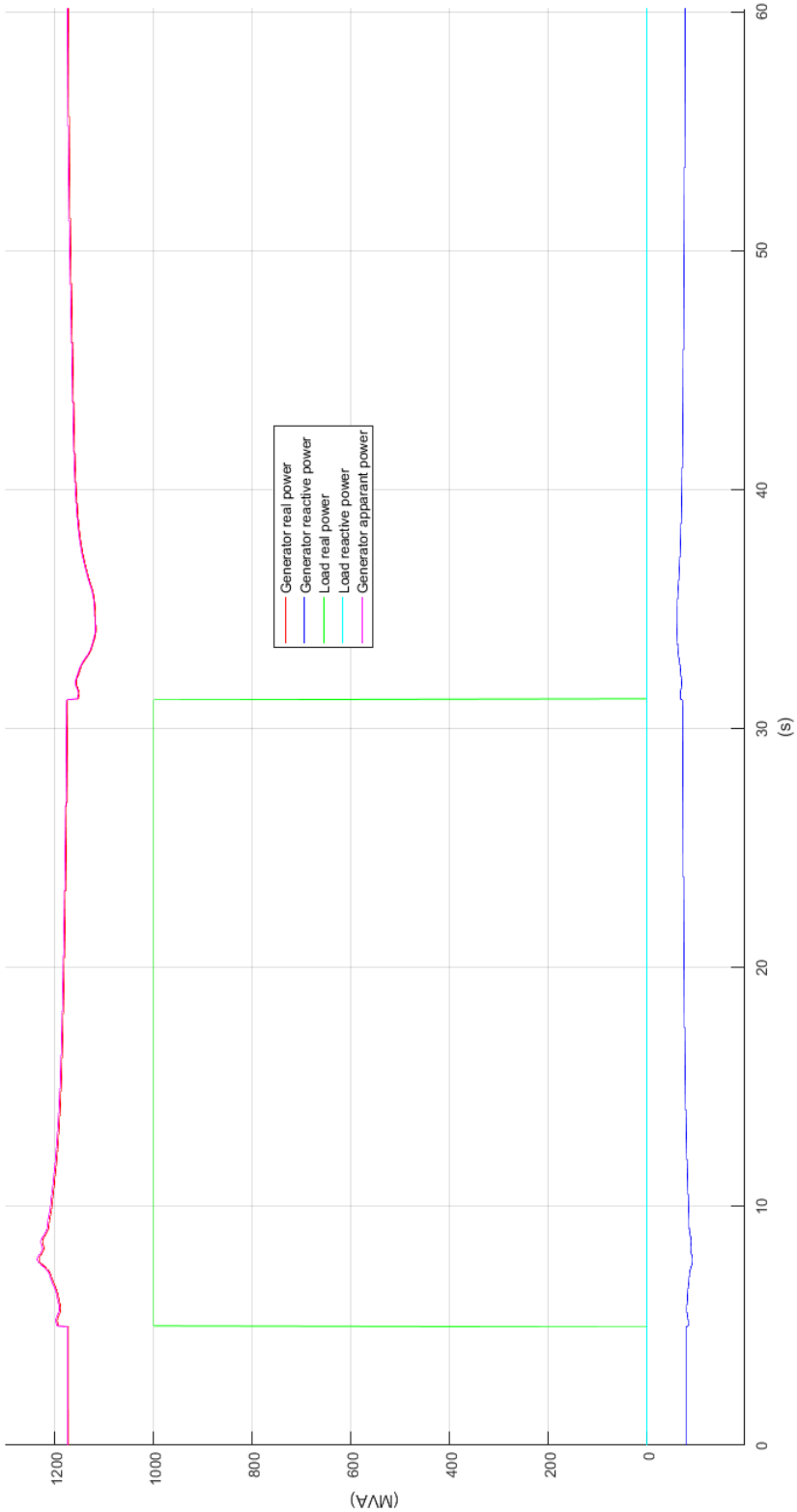

Figure 7.17: Generator output response to load changes with default AVR (active, ±1000MW)

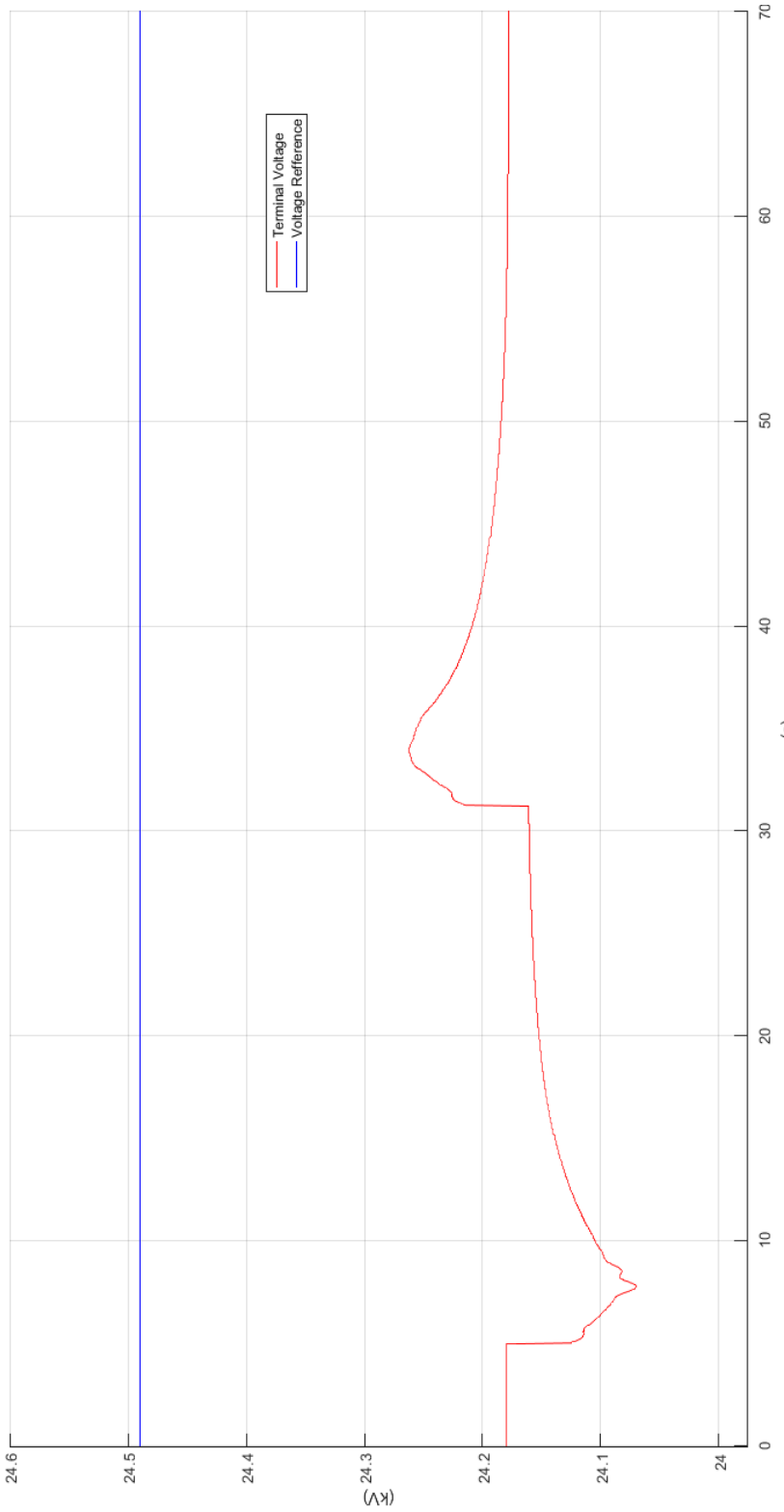

Figure 7.18: Terminal voltage response to load changes with default AVR (active, $\pm$1000MW)

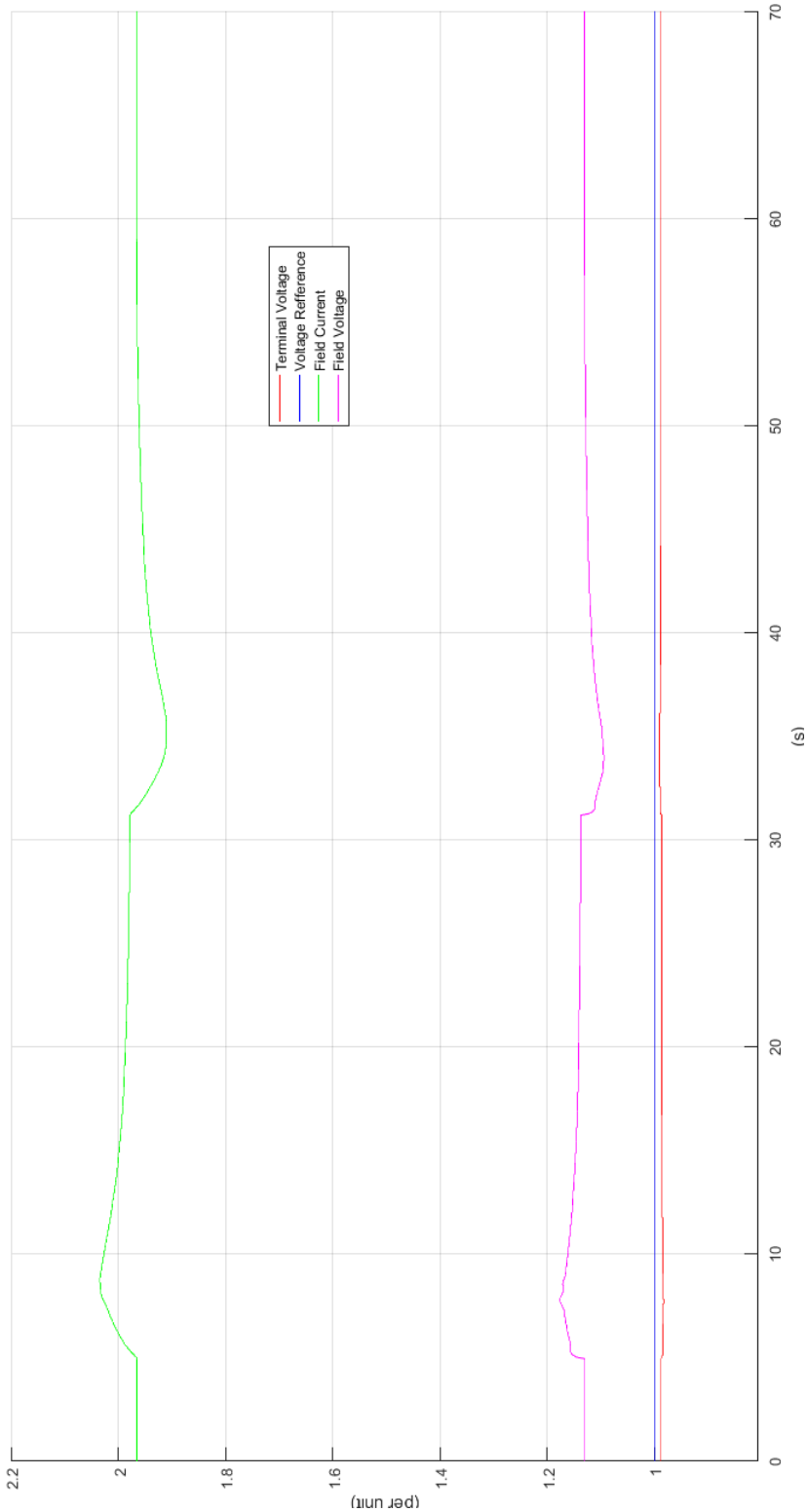

Figure 7.19: Excitation system response to load changes with default AVR (active, $\pm$1000MW)

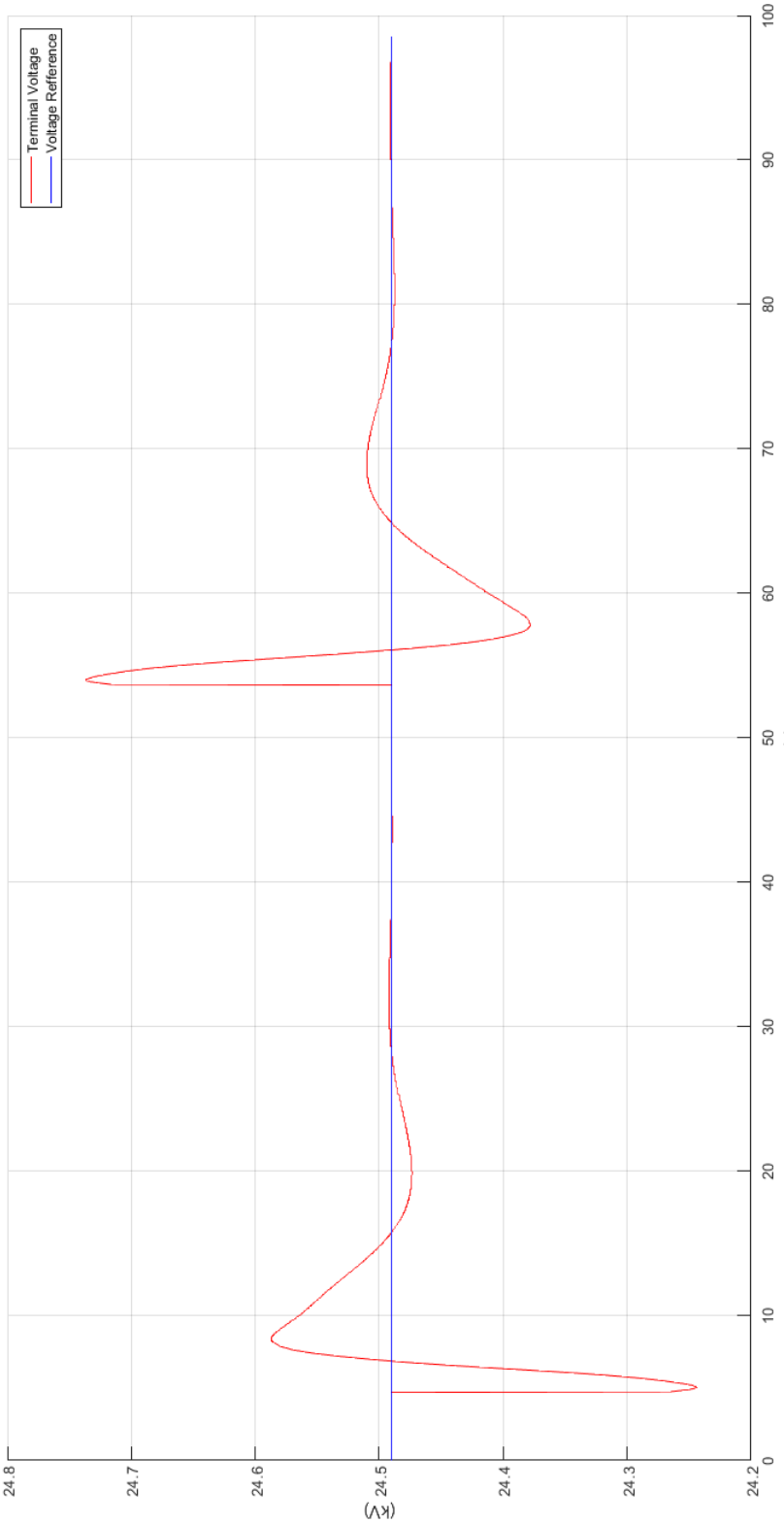

Figure 7.20: Terminal voltage response to load changes with MBO AVR (active, ±1000VAR)

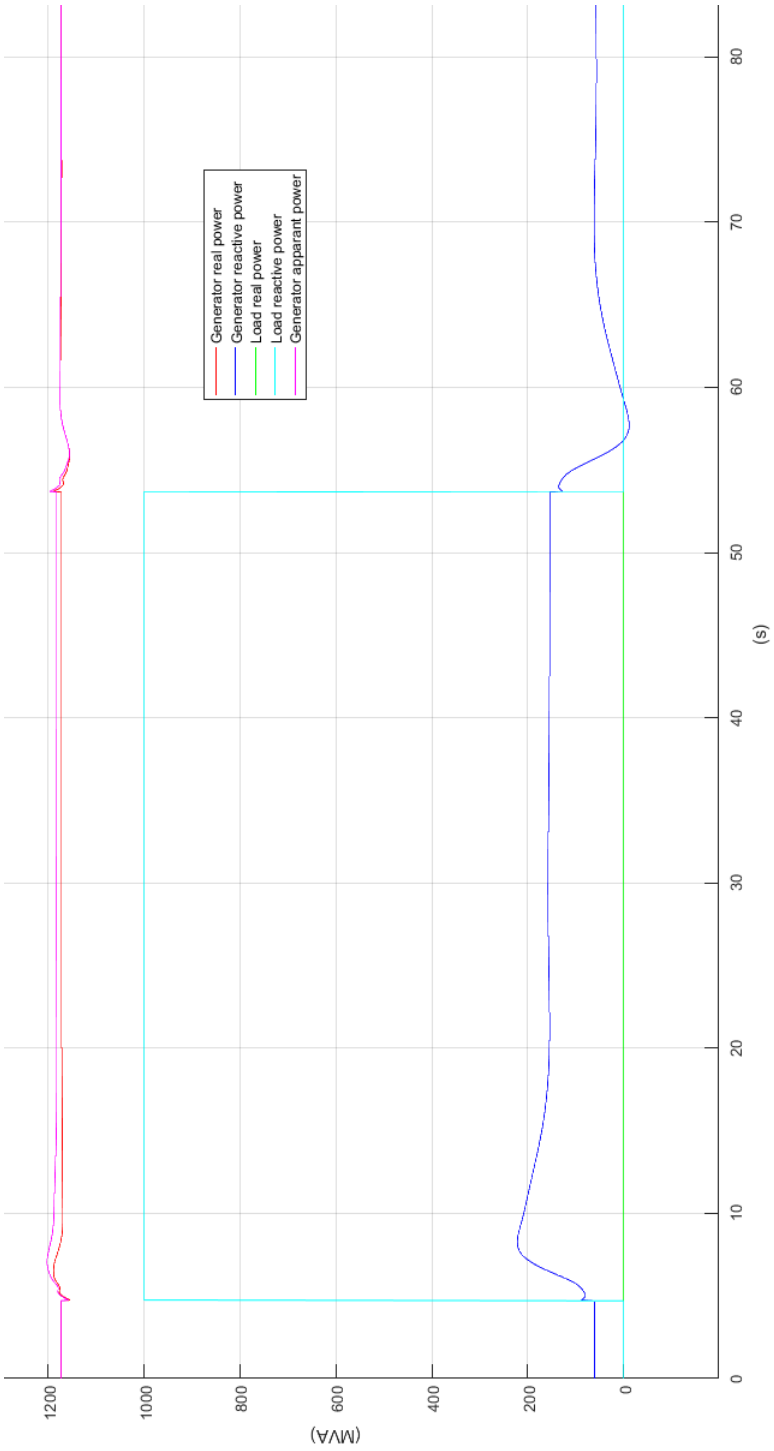

Figure 7.21: Generator output response to load changes with MBO AVR (active, $\pm$1000VAR)

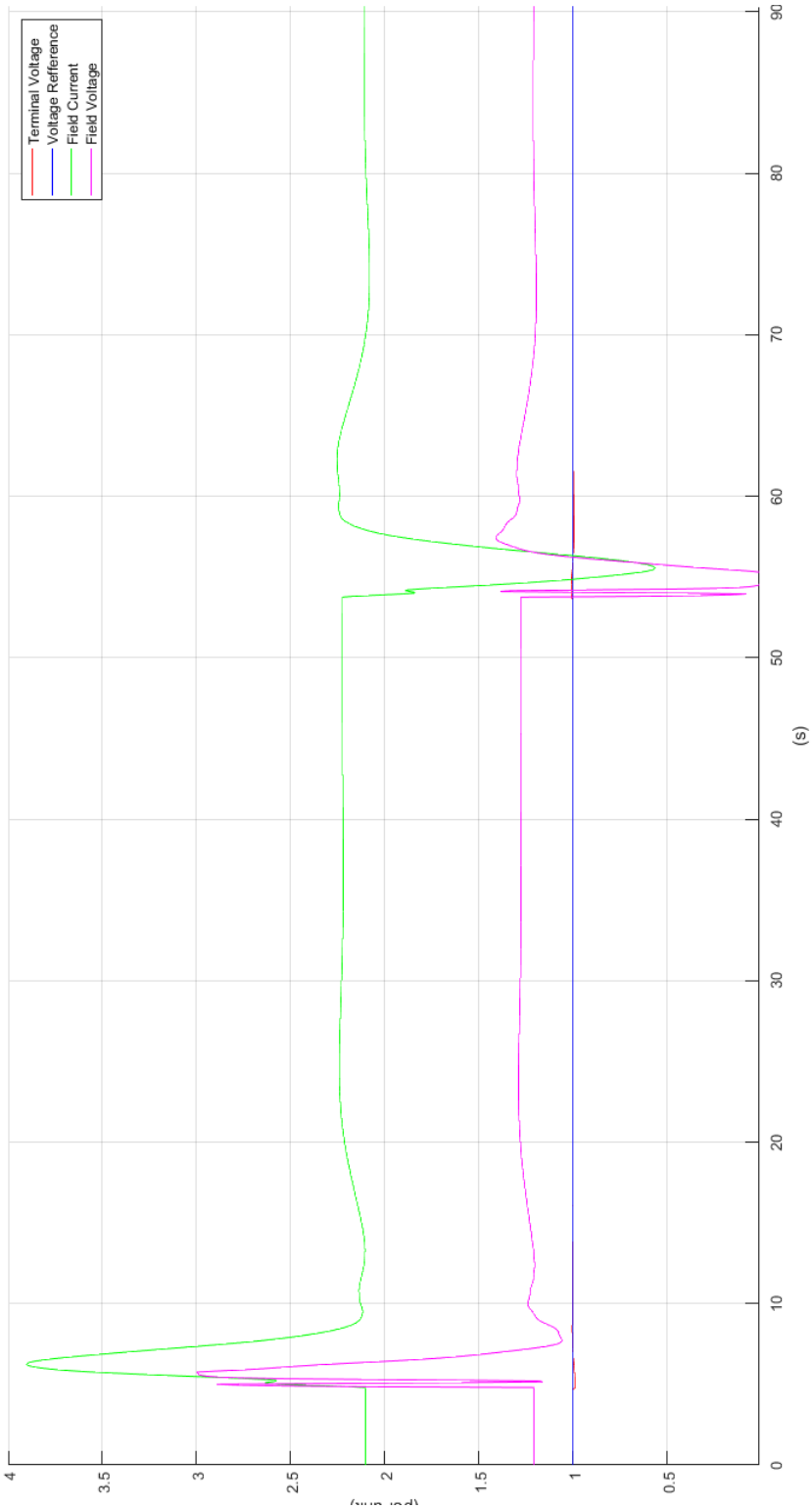

Figure 7.22: Excitation system response to load changes with MBO AVR (active, $\pm$1000VAR)

Once again, the system response for the uncompensated system is given for comparison. The Terminal voltage characteristic is described by Figure 7.23. The generator power output is given by Figure 7.24. The response of the excitation system is given in Figure 7.25

It is worth noting again that the examples presented here are extreme cases. It would be quite rare for the generator to experience a sudden unexpected load change on the order of 1000MW. These events stress the excitation system to its limit, and are presented to show subtleties in the response profile which are otherwise lost in smaller contingencies. In practice, such experimental data may be impractical or impossible to obtain. Additionally, most real loads consume both active and reactive power to some degree. Therefore, system response to true contingency events will be somewhat of a combination of the profiles presented here. For the purpose of this workM such considerations were ignored to present only the system behavior as a result of active and reactive power changes independently.

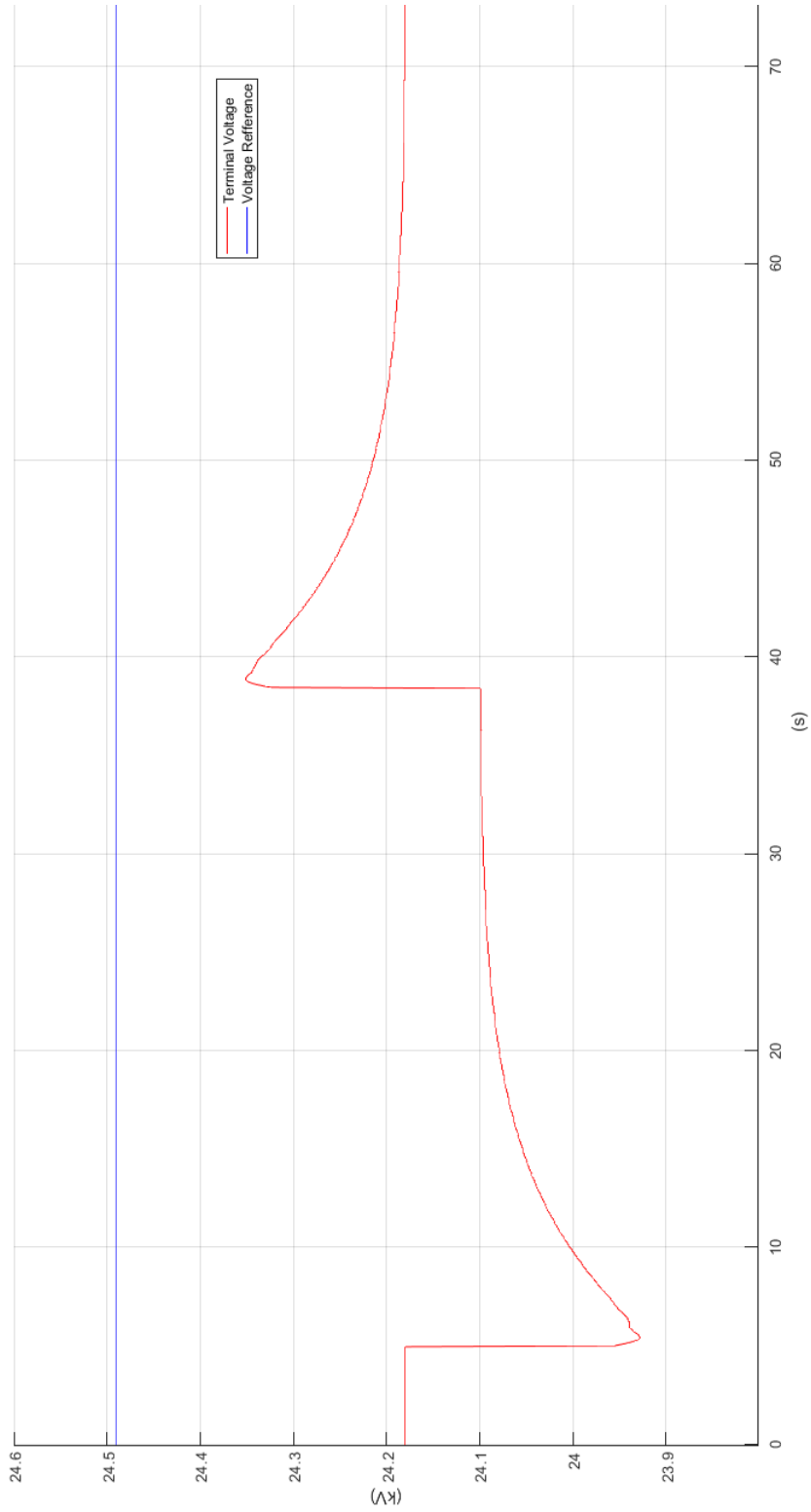

Figure 7.23: Terminal voltage response to load changes with default AVR ($\pm$1000VAR)

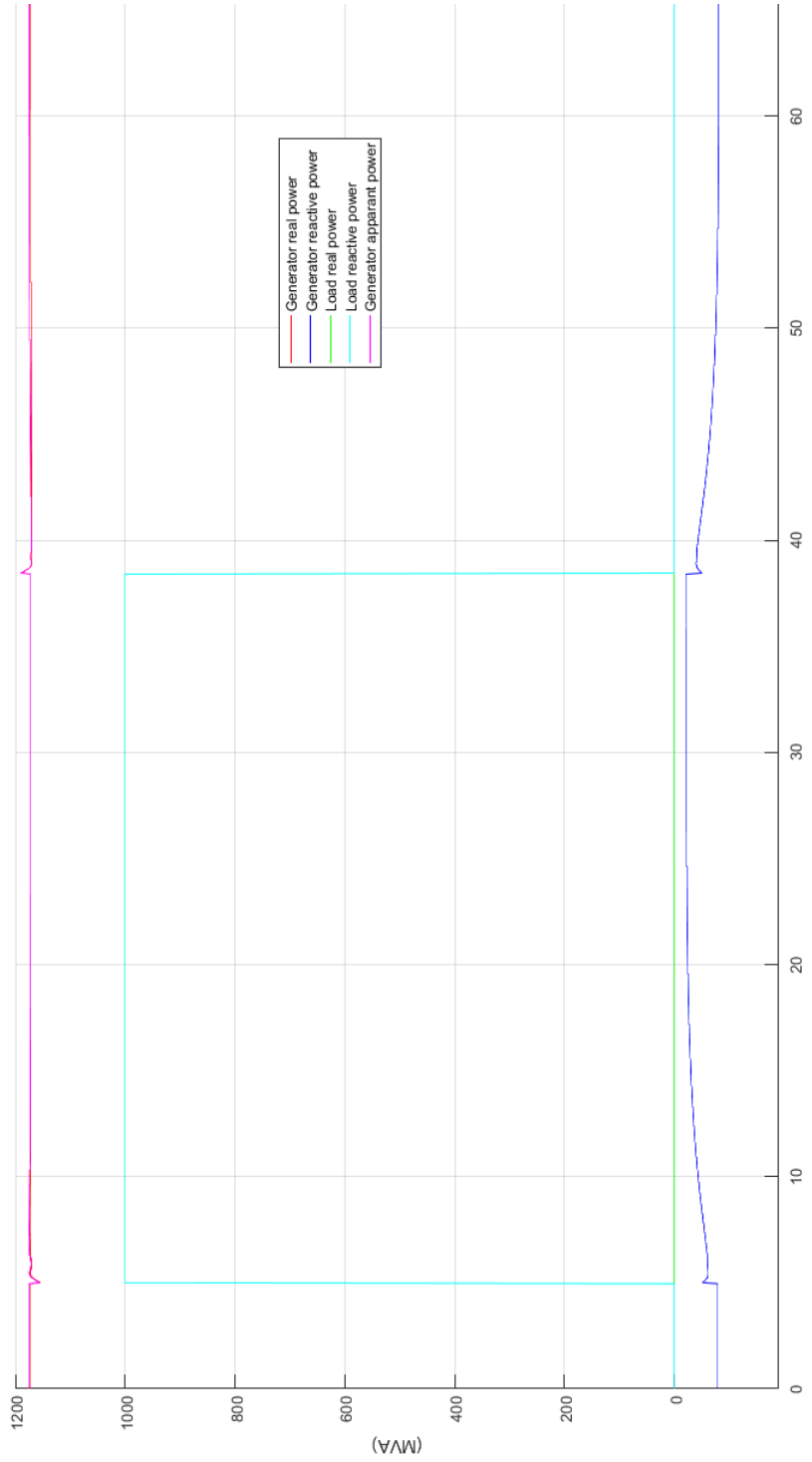

Figure 7.24: Generator power response to load changes with default AVR ($\pm$1000VAR)

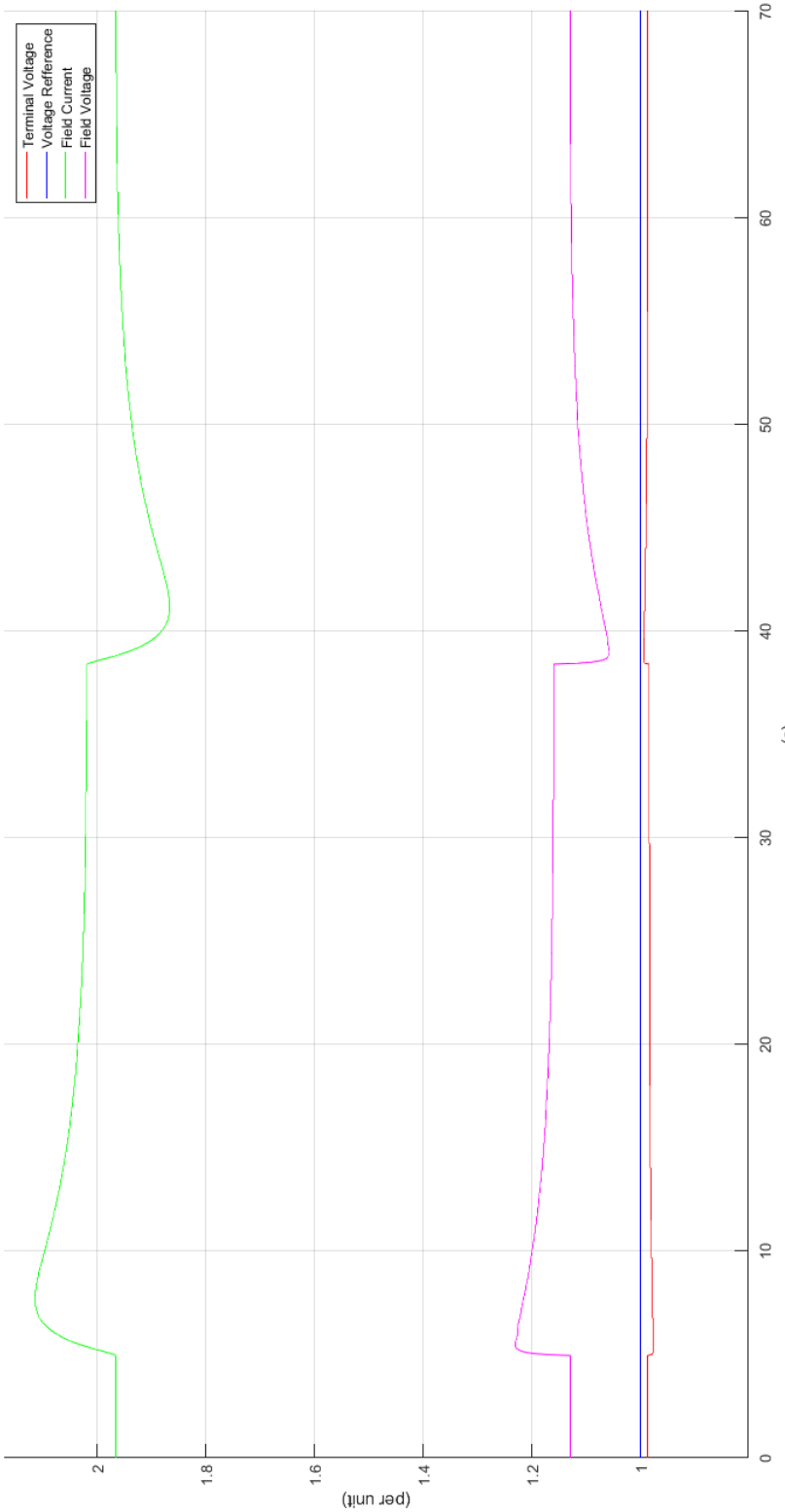

Figure 7.25: Excitation system response to load changes with default AVR ($\pm$1000MVAR)

Chapter 8: Summary, Conclusions, and Future Work

8.1 Summary

In this work a novel technique for the development of high performance compensators is applied to the development of an Automatic Voltage Regulator (AVR) for the generator excitation control system in a high fidelity model of a commercial nuclear generating station. The work begins with an introduction to the problem and a brief summary of the current state of AVR research.

Next, the theory behind excitation control systems, their history, and techniques for describing them is presented. Then, the theory behind frequency domain control design is presented as well as a brief discussion of Proportional Integral Derivative (PID) control systems. This in turn leads into a discussion of the development of the Modified Bode Optimal (MBO) compensator. Next, a detailed description of the Western Services Corporation (WSC) simulator is presented and the appropriate model adjustments necessary for the study of the excitation system is given. A MBO compensator is then developed for the simulator in accordance with the method presented by [3] and based on justifiable assumptions about the system. This compensator is then implemented using the simulation software. This is followed by a brief discussion of excitation system performance standards as presented in industry and literature. Finally, the compensator is tested under practical conditions. Modifications are then made to the design based on simulation results and justified by [3] and general frequency domain control theory.

Lastly, the final compensator is tested in accordance with methods presented in industry and literature. In this chapter, the performance of the compensator is described quantitatively. Additionally, an assessment of the MBO design technique and it's applicability to the WSC simulator and excitation systems in general is provided. Finally, implications of this work and suggestions for future avenues of research are discussed.

8.2 Conclusions

To quantify controller performance mathematically the standard performance metrics used in IEEE 421.2 for small signal performance were used [26]. These parameters include parameters such as rise

time, settling time, and overshoot. The definitions for these metrics as defined in [26] are summarized by Figure 8.1. For every case the reference step command is recieved at $t = 5$ s which corresponds to $t = 0$

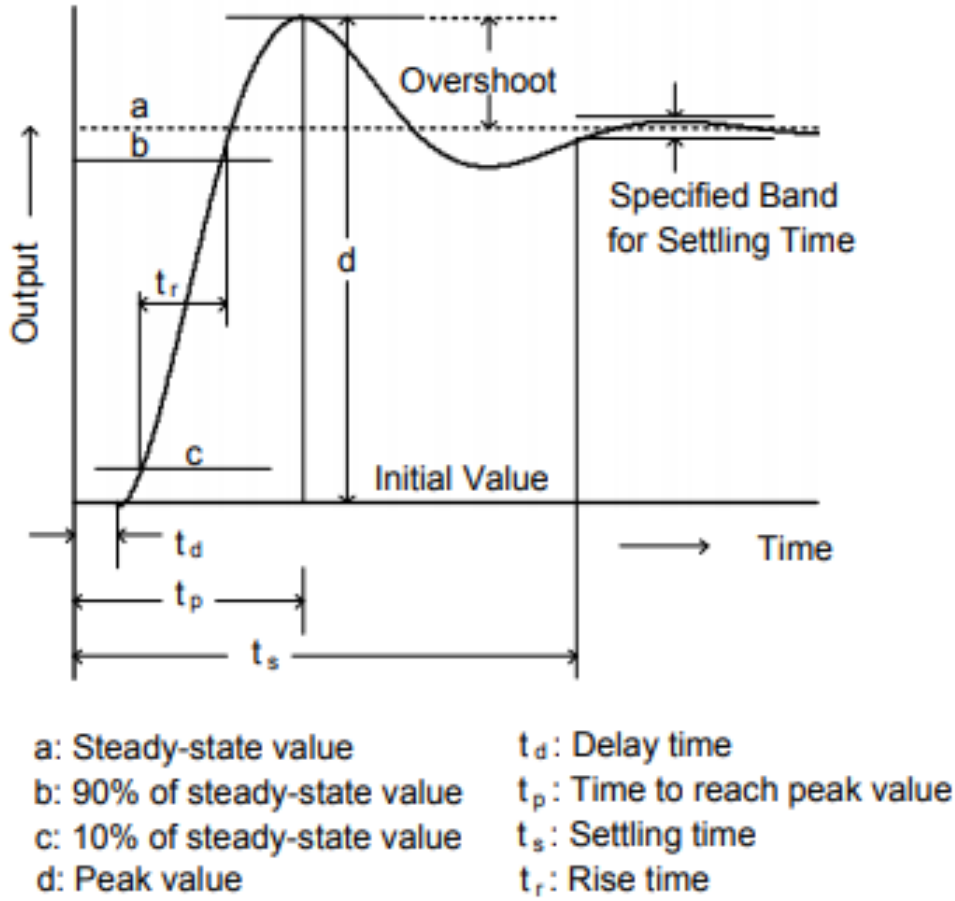

Figure 8.1: Small signal performance definitions

s in Figure 8.1. The value of the step command is 0.8% of the rated terminal voltage.

Figure 8.2 shows the terminal voltage response for the default excitation system to a reference step command under no load condition. In this figure various points corresponding to important time domain performance metrics have been highlighted. From this figure it can be seen that this configuration results in a delay time of 0.15 seconds. The final value for the terminal voltage is 26.793 kV which corresponds to a steady state error of 8.49%. The rise time is 3.15 seconds with a settling time of 4.35 seconds. The peak value is 26.798 kV which gives an overshoot of 2.994%.

For the MBO compensator the no load step response performance is given by Figure 8.3. For this configuration the system delay time is 0.2 seconds. The rise time is 0.65 seconds with a settling time of

5.65 seconds. The peak value is 24.805 kV which corresponds to an overshoot of 56.18 percent. The final value is 24.6956 kV which corresponds to a steady state error of 0.0014%

Under rated load the terminal voltage step response performance for the default excitation system is given in Figure 8.4. From this figure it is seen that the delay time is 0.4 seconds. The rise time is 18.15 seconds with a settling time of 25.55 seconds. The final value is 24.304 kV which leads to a steady state error of 1.5474%. The final value is also the peak value, therefore there is no overshoot for this system.

The performance of the MBO compensator for a reference step command in the loaded condition is given by Figure 8.5. The delay time is seen to be 0.2 seconds. The rise time is 1.25 seconds with a settling time of 17.55 seconds. The peak value is 24.759 kV which gives an overshoot of 37.2449%. the final value is 24.686 kV which gives a steady state error of 0%.

Overall the relative performance of the MBO compensator is summarized by the table of performance metrics given in Figure 8.6. IEEE standards do not specify a range of terminal values for defining settling time. In power quality studies, the accepted range of system voltage variations is $\pm 1\%$. However, This number is not suitable for use here, because, the magnitude of the oscillations varies based on the magnitude of the reference step. This means that the settling time would be different for different step commands and may be misleading. For a given control system the rate at which the system oscillations decay depends only on the design of the compensator and the characteristics of the plant. For this work, the settling time was defined as the time required for oscillation magnitudes to decay below 5% of the reference step change. This choice is arbitrary and is made only to provide a metric of relative performance between the different compensator/plant configurations.

From the above results it can be seen that there are a number of stark constrasts between the MBO compensator and the default system. One of the most significant observations is the presence of a persistent steady state error in the uncompensated system. This is because simple proportional gain compensators possess no memory and so require the presence of an error in steady state to generate a command signal. During initial exploration of the WSC simulator it was observed that the voltage reference is set at less than 100% to achieve rated terminal voltage as a way of compensating for the error during normal operation. This in turn lead to some uncertainty regarding the appropriate method for testing the default system. Ultimately, it was decided to conduct testing with the default reference signal set to 100%. This approach allows for a direct comparison of the error between the default system and that of the system with the MBO compensator. It also maintains consistency in the command signals

being recieved by the different compensators. As a result any differences in performance can be directly attributed to the differences in compensator behavior.

Another significant difference is the rise time between the compensators. In the unloaded condition the MBO compensator outperforms the default system by a factor of five and in the rated condition it exceeds the default system by a factor of ten. The MBO compensator also exhibits slightly less initial delay than the default system when connected to the Bulk Power System (BPS). In the unloaded condition the systems have comparable settling time however, under load the MBO is significantly faster. The only metric where the MBO compensator suffers is in overshoot. This is simply an unavoidable characteristic of aggressive compensator designs. So long as the duration of the overvoltage is not excessive, this is an acceptable trade-off for the otherwise superior compensator performance.

In conclusion it is apparent that the Cloud technique for developing high performance compensators can be successfully applied to the application of developing AVR compensators for excitation systems. Due to the limitations of the simulation model, additions needed to be made to accurately model a real excitation system. However these model additions had no impact on the compensator development and no other information about the generator or power system was assumed. The only assumptions made during model development were in regards to design criteria not specified by industry standards and consistent with information which would be available to a design engineer developing an AVR for a real excitation control system. One key advantage of the Cloud technique over other compensator design techniques is that it does not employ a computationally demanding learning algorithm.

Unfortunately, the response data presented here is only accurate so far as the model itself is accurate. While the simulator is of tremendously high fidelitym many simplifications were made for the sake of implementing the model in software. While the model additions were consistent with values found in literature a truly accurate reporting of the compensator performance could only be achieved by developing the compensator for an accurate system model. Including parameters for the actual equipment upon which the model is based would greatly improve the validity of the performance data. Given the proprietary nature of the simulatior it is unlikely that such an exercise may ever be performed. Regardless, this work demonstrates a successful application of the MBO tuning algorithm developed by Cloud. Additionally, this work highlights many of the deficiencies found in excitation system studies and modeling as well as bringing attention to the lack of standardization between industry and academia.

8.3 Future work

While this work shows great promise for the application of high performance compensation in power system applications there is considerable additional work to be done in this field. Specifically it is noted that the results presented here are only applicable for small signal analysis. Real Excitation control systems possess significant nonlinearities which affect control system performance for large signals. This is in addition to the nonlinearities present in the BPS. For simple compensators, nonlinearities are not a significant risk. High performance compensators, however, can become unstable in the presence of actuator saturations and other nonlinear dynamics. To account for such effects high performance compensators are typically implemented along with nonlinear dynamic compensation. The development of nonlinear dynamic compensators requires detailed plant knowledge. Therefore work should be conducted into the development of nonlinear dynamic compensation without plant information to accompany the development of MBO compensators.

Additionally, most modern excitation control systems include an additional compensator known as a power system stabilizer. This compensator acts to reduce the severity of frequency variations within the power system. Signals from the power system stabilizer can often be contradictory to those from the AVR and can affect overall excitation system performance. Therefore, additonal work should be done to determine the application of high performance compensation in systems possessing a power system stabilizer. Also, overall power system stability is affected by a wide range of systems beyond simply excitation system control. The general applicability of high performance control to other control loops within both the generating station itself and the wider BPS should be explored.

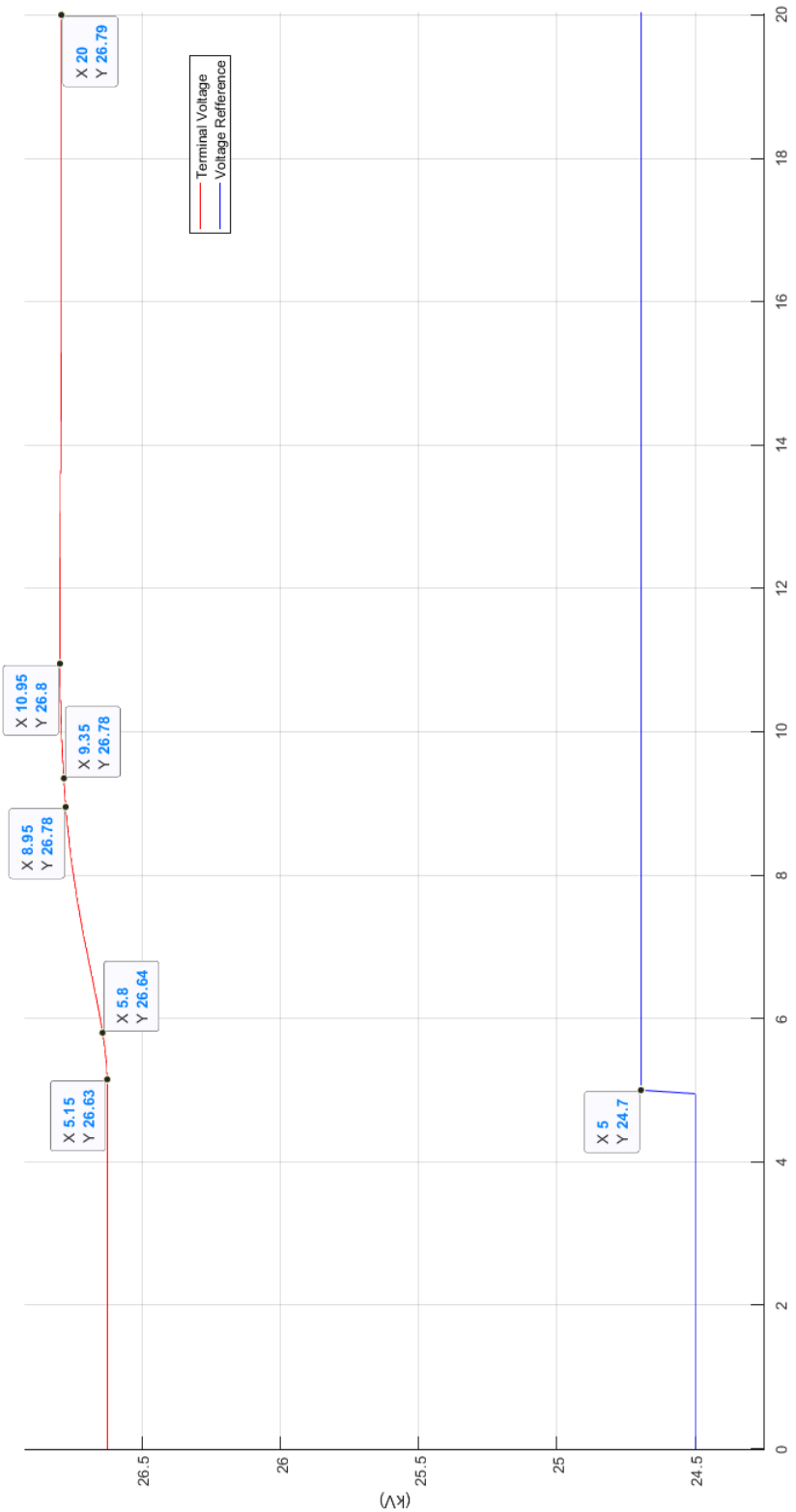

Figure 8.2: Small signal performance (default AVR, no load)

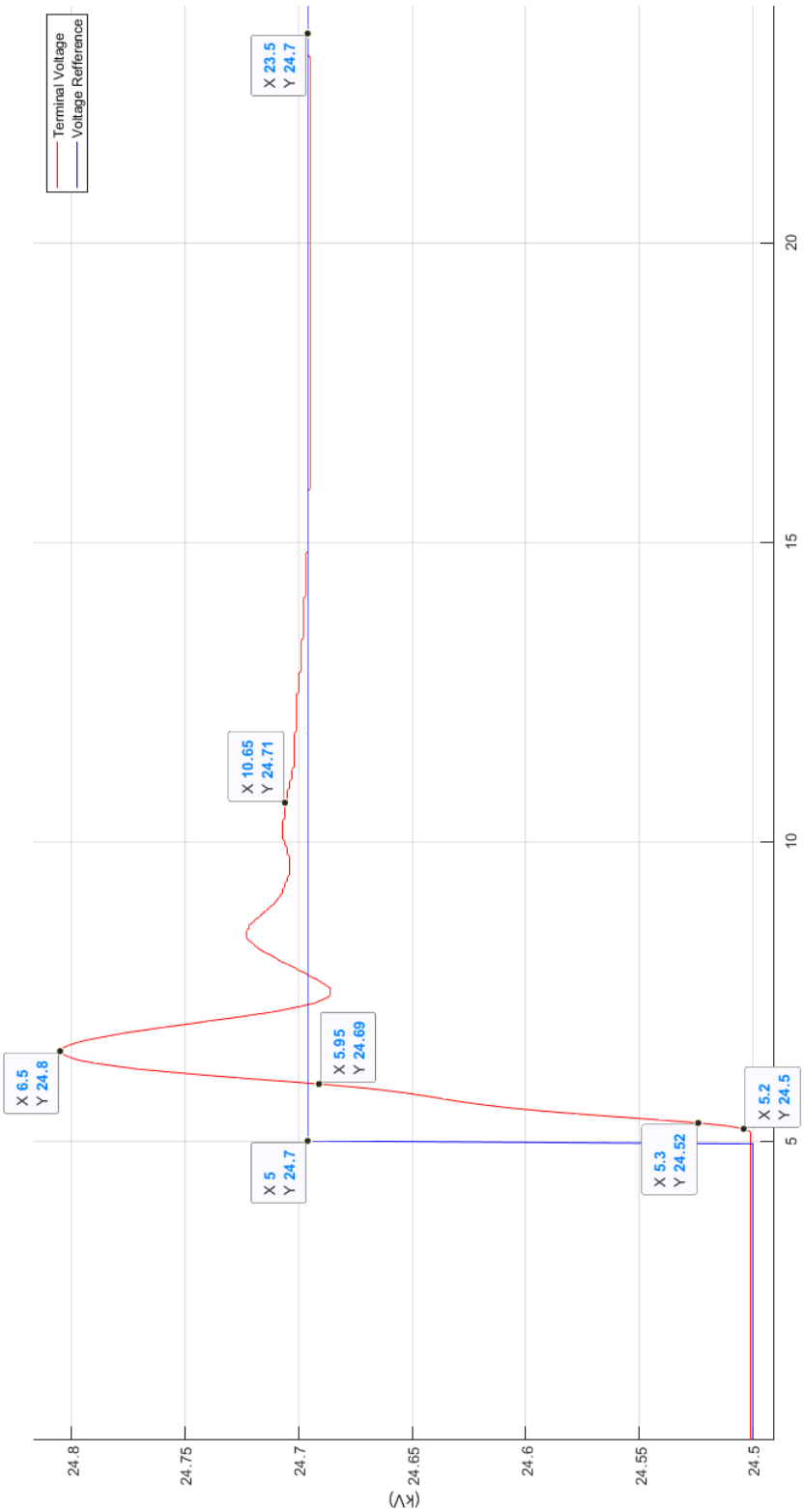

Figure 8.3: Small signal performance (MBO AVR, no load)

Figure 8.4: Small signal performance (default AVR, rated load)

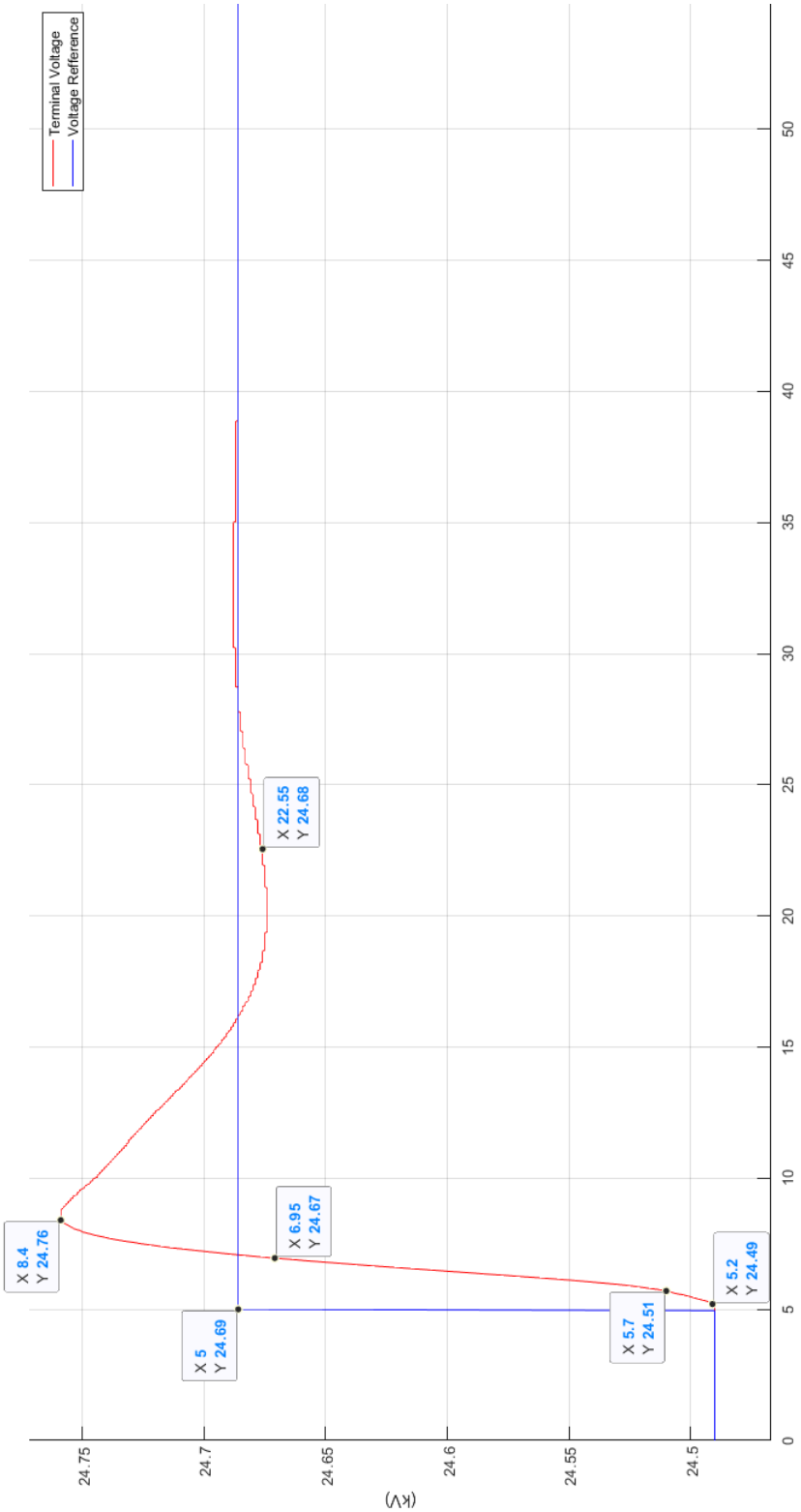

Figure 8.5: Small signal performance (MBO AVR, rated load)

AVR	Final value (kV)	Steady state error (%)	Delay time (s)	Rise time (s)	Peak time (s)	Settling time* (s)	Overshoot (%)
Default (no load)	26.7930	8.4913	0.1500	3.1500	5.9500	4.3500	2.9940
MBO (no load)	24.6950	0.0014	0.2000	0.6500	1.5000	5.6500	56.1801
Default (rated load)	24.3040	1.5474	0.4000	18.1500	-	25.5500	0.0000
MBO (rated load)	24.6860	0.0000	0.2000	1.2500	3.4000	17.5500	37.3449

Figure 8.6: Performance summary of MBO versus default AVR for no load and nominal load conditions

References

[1] P. Kundur., *POWER SYSTEM STABILITY AND CONTROL*, 1st ed. McGraw-Hill Inc, 1994.

[2] J. G. Ziegler and N. B. Nichols, "Optimum settings for automatic controllers," 1942.

[3] R. L. Cloud and J. F. O'Brien, "Large feedback control design with limited plant information," *Control Engineering Practice*, vol. 72, pp. 219 – 229, 2018. [Online]. Available: http://www.sciencedirect.com/science/article/pii/S0967066117302824

[4] H. Gozde and M. Taplamacioglu, "Comparative performance analysis of artificial bee colony algorithm for automatic voltage regulator (avr) system," *Journal of the Franklin Institute*, vol. 348, no. 8, pp. 1927–1946, 10 2011.

[5] B. Selvabala and D. Devaraj, "Co-ordinated tuning of avr-pss using differential evolution algorithm," pp. 439–444, 10 2010.

[6] S. Panda, B. Sahu, and P. Mohanty, "Design and performance analysis of pid controller for an automatic voltage regulator system using simplified particle swarm optimization," *Journal of the Franklin Institute*, vol. 349, no. 8, pp. 2609 – 2625, 2012. [Online]. Available: http://www.sciencedirect.com/science/article/pii/S0016003212001573

[7] S. Kansit and W. Assawinchaichote, "Optimization of pid controller based on psogsa for an automatic voltage regulator system," *Procedia Computer Science*, vol. 86, pp. 87 – 90, 2016, 2016 International Electrical Engineering Congress, iEECON2016, 2-4 March 2016, Chiang Mai, Thailand. [Online]. Available: http://www.sciencedirect.com/science/article/pii/S1877050916303581

[8] E. Ãelik and R. Durgut, "Performance enhancement of automatic voltage regulator by modified cost function and symbiotic organisms search algorithm," *Engineering Science and Technology, an International Journal*, vol. 21, no. 5, pp. 1104 – 1111, 2018. [Online]. Available: http://www.sciencedirect.com/science/article/pii/S2215098618309261

[9] L. B. Prasad, H. O. Gupta, and B. Tyagi, "Application of policy iteration technique based adaptive optimal control design for automatic voltage regulator of power system," *International Journal of Electrical Power Energy Systems*, vol. 63, pp. 940 – 949, 2014. [Online]. Available: http://www.sciencedirect.com/science/article/pii/S0142061514004153

[10] H. Shayeghi, A. Younesi, and Y. Hashemi, "Optimal design of a robust discrete parallel fp+fi+fd controller for the automatic voltage regulator system," *International Journal of*

Electrical Power Energy Systems, vol. 67, pp. 66 – 75, 2015. [Online]. Available: http://www.sciencedirect.com/science/article/pii/S0142061514006954

[11] V. J. Å til and M. MehmedoviÄ, "Interconnection and damping assignment automatic voltage regulator for synchronous generators," *International Journal of Electrical Power Energy Systems*, vol. 101, pp. 204 – 212, 2018. [Online]. Available: http://www.sciencedirect.com/science/article/pii/S0142061517325218

[12] V. Rajinikanth and S. C. Satapathy, "Design of controller for automatic voltage regulator using teaching learning based optimization," *Procedia Technology*, vol. 21, pp. 295 – 302, 2015, sMART GRID TECHNOLOGIES. [Online]. Available: http://www.sciencedirect.com/science/article/pii/S2212017315002601

[13] S. Chatterjee and V. Mukherjee, "Pid controller for automatic voltage regulator using teachingâlearning based optimization technique," *International Journal of Electrical Power Energy Systems*, vol. 77, pp. 418 – 429, 2016. [Online]. Available: http://www.sciencedirect.com/science/article/pii/S0142061515004305

[14] M. Blondin, P. Sicard, and P. Pardalos, "Controller tuning approach with robustness, stability and dynamic criteria for the original avr system," *Mathematics and Computers in Simulation*, vol. 163, 03 2019.

[15] M. Sahib, "A novel optimal pid plus second order derivative controller for avr system," *Engineering Science and Technology, an International Journal*, vol. 13, 01 2015.

[16] B. HekimoÄlu, "Sine-cosine algorithm-based optimization for automatic voltage regulator system," *Transactions of the Institute of Measurement and Control*, p. 014233121881145, 11 2018.

[17] N. Aguila-Camacho and M. A. Duarte-Mermoud, "Fractional adaptive control for an automatic voltage regulator," *ISA Transactions*, vol. 52, no. 6, pp. 807 – 815, 2013. [Online]. Available: http://www.sciencedirect.com/science/article/pii/S0019057813000888

[18] F. A. S. babu and S. B. Chiranjeevi, "Implementation of fractional order pid controller for an avr system using ga and aco optimization techniques," *IFAC-PapersOnLine*, vol. 49, no. 1, pp. 456 – 461, 2016, 4th IFAC Conference on Advances in Control and Optimization of Dynamical Systems ACODS 2016. [Online]. Available: http://www.sciencedirect.com/science/article/pii/S2405896316300969

[19] I. Pan and S. Das, "Chaotic multi-objective optimization based design of fractional order (pid mu)-d-lambda controller in avr system," *International Journal of Electrical Power Energy Systems*, vol. 43, 05 2012.

[20] ——, "Frequency domain design of fractional order pid controller for avr system using chaotic multi-objective optimization," *International Journal of Electrical Power Energy Systems*, vol. 51, pp. 106 – 118, 2013. [Online]. Available: http://www.sciencedirect.com/science/article/pii/S0142061513000811

[21] A. Sikander, P. Thakur, R. Bansal, and S. Rajasekar, "A novel technique to design cuckoo search based fopid controller for avr in power systems," *Computers Electrical Engineering*, 07 2017.

[22] T. Yinggan, M. a, C. Hua, L. Li, and Y. b, "Optimum design of fractional order (pid mu)-d-lambda controller for avr system using chaotic ant swarm," *Expert Systems with Applications*, vol. 39, pp. 6887–6896, 02 2012.

[23] M. Zamani, M. Karimi, N. Sadati, and M. Parniani, "Design of a fractional order pid controller for an avr using particle swarm optimization," *Control Engineering Practice*, vol. 17, pp. 1380–1387, 12 2009.

[24] G.-Q. Zeng, J. Chen, Y.-X. Dai, L.-M. Li, C.-W. Zheng, and M.-R. Chen, "Design of fractional order pid controller for automatic regulator voltage system based on multi-objective extremal optimization," *Neurocomputing*, vol. 160, pp. 173 – 184, 2015. [Online]. Available: http://www.sciencedirect.com/science/article/pii/S0925231215002210

[25] J. OBrien., *Frequency-Domain Control Design for High-Performance systems*, 1st ed. The Institution of Engineering and Technology, 2012.

[26] "Ieee guide for identification, testing, and evaluation of the dynamic performance of excitation control systems," *IEEE Std 421.2-2014 (Revision of IEEE Std 421.2-1990)*, pp. 1–63, June 2014.

[27] "Nerc requirements for power system stabilizer: Var-501-wecc-3.1," 01 2019.

[28] D. L. V. Frank L. Lewis and V. L. Syrmos., *Optimal Control*, 3rd ed. John Wiley & Sons, inc., 2012.

[29] "Nerc requirements for verification of models and data for generator excitation control system or plant volt/var control functions: Mod-026-1," 01 2019.

[30] *Reliability Guideline Power Plant Model Verification and Testing for Synchronous Machines.* North American Electric Reliability Corporation, 2018.

[31] "Ieee recommended practice for excitation system models for power system stability studies," *IEEE Std 421.5-2016 (Revision of IEEE Std 421.5-2005)*, pp. 1–207, Aug 2016.

[32] C. Mozina, "Nerc requirements for setting load-dependent power plant protection: Prc-025-1," 03 2014, pp. 430–449.

[33] "Ieee standard definitions for excitation systems for synchronous machines," *IEEE Std 421.1-2007 (Revision of IEEE Std 421.1-1986)*, pp. 1–33, July 2007.

[34] R. C. Dorf and R. H. Bishop, *Modern Control Systems.* Pearson Education Inc, 2017.

[35] "Ieee guide for synchronous generator modeling practices in stability analyses," *IEEE Std 1110-1991*, pp. 1–96, Nov 1991.

[36] MATLAB, *9.5.0.1067069 (R2018b).* Natick, Massachusetts: The MathWorks Inc., 2020.

[37] *Keymaster Logic Tool Modeling Guide*, v. 2.0-1 ed., Western Services Corporation, 7196 Crestwood Boulevard, suite 300, 9 2009.

Appendix A: MBO Synthesis Code

To facilitate in the iterative design of the MBO compensator a program was developed using Matlab to automatically compute the compensator polynomial coefficients from known parameters. This code is given below:

```
clear
clc
close all

%z_n technique
Ku= 26      %26 AVR
%input('Ku=')
Tu=  1.9598 %1.9598AVR
%input('Tu=')

%compute PID gains
Kp = .6*Ku
Ki = 1.2*Ku/Tu
Kd = .6*Ku*Tu/8
PIDcomp = tf([Kp],[1])+tf([Ki],[1 0])+tf(Kd.*[1 0],[1]);
%sanity checks
[PIDnum,PIDden]=tfdata(PIDcomp,'v')
Kp = PIDnum(2)
Ki = PIDnum(3)
Kd = PIDnum(1)
%pid closed loop period
tb= 2.6667 %MBO(22.8-7.7)/4;
%.869

%input('tb=')

wb= 2*pi/tb
pidcross = freqresp(PIDcomp, j*wb)
pidcrossmag=abs(pidcross)
pidcrossphase= 180/pi*phase(pidcross)
figure(2)
bode(PIDcomp)
figure(1)
magP =pidcrossmag^-1; %estimate plant magnitude
if pidcrossphase >0 %estimate plant phase
    Porder = 2;
else
    Porder = 1;
end

%design for -10db rolloff to step
b=2;
a=1;
q=b/(a+b);
```

```
n=3;


NMP=0; %non minimum phase
L0=.4; %break freq damping
Ls1=.4; %fractional order transition damping
Ld=.4; %bode step transition coefficient
Lc=.4; %high order roll off transition coefficient
x=-10; %step depth
wd=2*wb;
wc= wd*((n+pi/2*NMP)/(1+q))
m=0;
while m<=0
w0=0;
% input('w0= (0 for undefined)')
if w0==0
    m=2; %3m octaves of pole/zero spacing to produce 30degree phase
    ↪ margin at crossover
    ws1=wb/(2^(3*m+1));
    w0=ws1/4; %for undefined bandwidth give 2 octaves of 3rd order slope
else
    m=floor((log2(wb/w0)-1)/3);
    ws1=wb/(2^(3*(m+1)));
    if m==0 || ws1<=w0
        disp('error, bandwidth too large for plant')
        m=0;
    end
end
end
hold on

cp=[1];
for j=1:m+1
    p = wb/(2^(3*(j-1)));
    cp=conv(cp,[1,p]);
end
bode(tf(1,cp))

c0= conv([1,w0],[1,2*L0*w0,w0^2]); %high order low frequency roll-off
%c0=[1,ws1]; %shift functional bandwidth to just before bode optimal
    ↪ slope
bode(tf(1,c0))
%
cbsc=[1, 2*Lc*wc, wc^2];

bode(tf(1,cbsc))
cz=[1];
for i=1:m
    z = wb/(2*2^(3*(i-1)));
    cz=conv(cz,[1,z]);
end
bode(tf(cz,1))
```

```
cbsd=[1,2*Ld*wd,wd^2];
bode(tf(cbsd,1))

network=tf(cz,cp)

zs1=conv([1,2*Ls1*ws1,ws1^2],[1]); %poles to transition from high order
% roll-off to bode optimal shape
%zs1=1;

bode(tf(zs1,1))
if Porder==2
    zs2=[1,1.2*(wb/8),(wb/8)^2];
else
    zs2=[1,wb/2]
end

bode(tf(zs2,1))
compnum=conv(conv(zs1,zs2),conv(cz,cbsd));
compden=conv(conv(c0,cp),cbsc);

MBOcomp=tf(compnum,compden)
MBOcross = freqresp(MBOcomp, i*wb);
MBOcrossmag=abs(MBOcross);
MBOcrossphase= phase(MBOcross);
MBOgain = pidcrossmag/MBOcrossmag
MBOcomp=MBOgain*MBOcomp*2;
roots(compden);
bode(MBOcomp)
hold on
% bode(PIDcomp)
hold off
grid on
%sanity check
% [compnum,compden]=tfdata(MBOcomp,'v')
```

Listing A.1: vsphere-info script

Appendix B: Complex Pole Modelling

To accurately model the high order compensator the development framework itself needed to be modified to include functionality for modeling higher order transfer functions. To this end a new model object was created consistent with the existing model objects used to describe the system. The Lag block used by the simulator models first order differential equations using the euler method [37]. Therefore to maintain consistency a second order lag block was developed using the euler method for approximating second order differential equations. This section includes a brief explanation of the euler method as well as a listing of the code used for it's implementation.

Consider the general first order differential equation given by:

$$\frac{dy}{dt} = f(y(t), t) \tag{B.1}$$

If $y(t_0) = y_0$ then values of y(t) near y_0 can be approximated by the following linear equation:

$$y = y_0 + f(y_0, t_0)(t - t_0) \tag{B.2}$$

For a point t_1 sufficiently close to t_0 an accurate approximation for the slope of $y(t)$ can be found:

$$\frac{dy}{dt} \approx f(y_1, t_1) \tag{B.3}$$

where:

$$y_1 = y_0 + f(y_0, t_0)(t_1 - t_0) \tag{B.4}$$

This then allows for an approximation of a new value of $y(t_2)$, y_2 at a point sufficiently close to t_1 but not necessarily close to t_0:

$$y_2 = y_1 + f(y_1, t_1)(t_2 - t_1) \tag{B.5}$$

This is the euler method, a well known method for approximating differential equations. The method can be extrapolated to n points as follows:

$$y_n = y_{n-1} + f(y_{n-1}, t_{n-1})(t_n - t_{n-1}) \tag{B.6}$$

Consider again the Lag object described in Chapter 6. The output Y of the block to an input X is given by the solution to the differential equation [37]:

$$lag\_time * dY/dT + Y = X \tag{B.7}$$

The WSC simulator generates a solution to this equation using the euler method as in Equation B.6:

$$Y_{new} = Y_{old} + f(Y_{old}, X)(dT) \tag{B.8}$$

The simulator computes the states of every object in discrete time steps of dT. The derivative is calculated for each new input as follows:

$$dY/dT = (X - Y_{old}) * \frac{1}{lag\_time} \tag{B.9}$$

Which leads to a final form of the equation as:

$$Y_{new} = Y_{old} + (X - Y_{old}) * \frac{1}{lag\_time}(\Delta t) \tag{B.10}$$

The C++ source code for the Lag object is given by Figure B.1:

```
void  Lag_calc( void *PP )
{
 lgLag *pLag;
 pLag = (lgLag*) PP ;
 if( fabs(pLag->Kref) < 1e-6 )
   {
    if (messages) {
       char *Name = GetVarName(PP);
       printf( "Zero Kref const in object %s (number=%d), ", Name, pLag->number);
       printf( "output set to default value.\n");
    }
     pLag->State_r = pLag->PresState;
   }
 else
   {
    pLag->Klag= 1/(pLag->Kref  ) ;
    pLag->Integral  = pLag->Integral +
                          ( pLag->Input1_r  - pLag->Integral ) *pLag->Klag * dT ;
    pLag->State_r = pLag->Integral;

   }
 pLag->Output_r = pLag->State_r ;
}
```

Figure B.1: Source code of Lag block

In order to implement the complex poles used by the MBO compensator design a method for implementing second order differential equations was needed. To maintain consistency with the other model objects in the simulation it was desired to find a method analogous to Equation B.10. Consider the transfer function of a pair of lightly damped poles:

$$\frac{Y(s)}{X(s)} = \frac{1}{s^2 + 2\zeta f_0 s + f_0^2} \tag{B.11}$$

This transfer function can be rewritten as a second order differential equation as follows:

$$X(t) = \frac{d^2Y}{dt^2} + 2\zeta f_0 \frac{dY}{dt} + f_0^2 \tag{B.12}$$

$$\frac{d^2Y}{dt^2} = X(t) - 2\zeta f_0 \frac{dY}{dt} - f_0^2 \tag{B.13}$$

To approximate this equation using the euler method the key is to separate it into two first order equations:

$$\frac{dY}{dT} = V(t) \tag{B.14}$$

$$\frac{dV}{dt} = X(t) - 2\zeta f_0 V(t) - f_0^2 \tag{B.15}$$

The solution to $Y(t)$ is found in terms of the approximation of V:

$$Y_{new} = Y_{old} + V * dT \tag{B.16}$$

where $V(t)$ is found in terms X:

$$V_{new} = V_{old} + \frac{dV}{dt} * dT \tag{B.17}$$

$$V_{new} = V_{old} + (X - 2\zeta f_0 V_{old} - f_0^2) * dT \tag{B.18}$$

Equations B.16 and B.18 can be implemented directly into code thus generating a reasonable approximation for the second order differential equation. The source code used in the simulation is given by Figure B.2:

```
void  Lag2_calc( void *PP )
{
 lgLag2 *pLag2;
 pLag2 = (lgLag2*) PP ;
 if( fabs(pLag2->f0) < 1e-6 )
   {
    if (messages) {
       char *Name = GetVarName(PP);
       printf( "Zero Kref const in object %s (number=%d), ", Name, pLag2->number);
       printf( "output set to default value.\n");
    }
     pLag2->State_r = pLag2->PresState;
   }
 else
   {
    pLag2->Klag= 1/(pLag2->f0  ) ;
    pLag2->Integral  = pLag2->Integral + dT*pLag2->Integral2;
    pLag2->Integral2  = pLag2->Integral2 +
                              ( pLag2->Input1_r  - 2*pLag2->f0*pLag2->sigma*pLag2->Integral2
                              - pLag2->f0*pLag2->f0*pLag2->Integral )  * dT ;
    pLag2->State_r = pLag2->Integral;

   }
 pLag2->Output_r = pLag2->State_r ;
}
/*****************************************************************/
```

Figure B.2: Source code of second order Lag block